CFD Analysis of a Bubbling Fluidized Bed Combustor Based on Co-firing Biomass & Coal

A Thesis
submitted in fulfillment of the requirements
for the award of degree of

Doctor of Philosophy
in
Mechanical Engineering

Submitted By

Hemant Kumar

(Registration no. 951008001)

Under the guidance of

Prof. S.K. MOHAPATRA
Sr. Professor & Head
Department of Mechanical Engineering
Thapar University, Patiala

Dr. RAVI INDER SINGH
Assistant Professor
Department of Mechanical Engineering
Birla Institute of Technology & Science, Pilani

Department of Mechanical Engineering
Thapar University, Patiala – 147004
INDIA

CERTIFICATE

It is certified that the thesis entitled, **"CFD Analysis of a Bubbling Fluidized Bed Combustor Based on Co-firing Biomass & Coal"** which is being submitted by **Er. Hemant Kumar** to Thapar University, Patiala for fulfillment of the award of degree of Doctor of Philosophy in Mechanical Engineering is a record of bonafide research work carried out by him under our guidance and supervision. The matter presented in this thesis has not been submitted either partially or fully to any other University or Institution for the award of any other degree.

Prof. S.K. MOHAPATRA
Sr. Professor & Head
Department of Mechanical Engineering
Thapar University, Patiala

Dr. RAVI INDER SINGH
Assistant Professor
Department of Mechanical Engineering
Birla Institute of Technology & Science
Pilani

Acknowledgement

It gives me immense pleasure to express my sincere and whole hearted gratitude to my esteemed guide ***Dr. S.K Mohapatra*** *for his dexterous guidance, invaluable and untiring help, ever encouraging attitude and supervision throughout my study, to device benefit of his enormous experience. It is a matter of great privilege to me. I am also thankful to* ***Dr. Ravi Inder Singh,*** *who contributed so much for the successful completion of my research work by his positive thoughtful reviews and valuable suggestions.*

Much appreciation and many thanks are expressed to the authorities of Ambuja Cement Limited for collection of data and samples along with providing information and facts about the plant. In special, authors would like to thank to Mr. RC Kothari, Senior President, Ambuja Cement Limited, Mr. BS Rana, GM (CPP) and Er. Vijay Verma. I owe my sincere gratitude to my colleagues Dr. V.K Gupta, Dr. Amit Arora and Dr. Gurpreet Singh for their encouragement and unfailing interest and sincere suggestions, from time to time in this work.

I find no words to acknowledge in so formal manner the sacrifice, love, help and inspiration rendered by my parents (mother Lt. Smt. Kamla Devi and father Sh. Raj Kamal Dhiman) to take up this study. I give full appreciation to my wife Dipti and my loving daughters Shreya and Navya for their ever willing cooperation, moral support and best wishes for successfully completing this study.

Last but not least, I express my indebtedness to the ***"ALMIGHTY"*** *for his showers of blessings and kindness throughout my research work to complete the research successfully.*

All cannot be mentioned but none is forgotten.

Hemant Kumar

ABSTRACT

Coal is one of the greatest sources of energy used for power generation across the world, providing almost 40% of the total energy produced. However, coal burning is a major source of CO_2 emission, which adversely affects the climate. As a result, techniques such as co-firing coal with biomass have become increasingly popular as an alternative. Through the utilization of biomass, in the form of agricultural residues such as cotton stalks, wheat straw, rice straw, sugarcane bagasse and rice husks, not only can heat and power be produced efficiently, but there is also the potential to improve rural income and energy security through the substitution of coal, oil and natural gas. The global demand for electric energy is expected to increase from about 14 billion tonnes per coal equivalent (TCE) to19 billion TCE by 2020. In India too, the demand for electric energy is expected to rise dramatically. Power generation based on biomass holds considerable promise in agricultural states such as Punjab, which has huge biomass resources from the crop production system and agricultural industries. With the availability of 15million tonnes of paddy straw and 5 million tonnes of other agricultural residues such as cotton and mustard stalk, the state has the potential to generate 2000 MW of power through biomass. Fluidized bed combustion (FBC) is considered an established technology for burning coal, biomass and waste fuels for power generation.

The present study was performed in two stages. In first stage operational and monitoring data were collected from a real power plant FBC boiler of 45TPH capacity. In the next stage three dimensional computational fluid dynamics (CFD) analysis was performed using Fluent 6.3 CFD code on this large scale commercial FBC boiler. The boiler was fuelled by both coal and biomass. Coal was fed from the bottom through 16 ports, uniformly distributed in the four zones of the bed and biomass was fed from four ports from a height of 1·8 m above the bed. Discrete phase modeling (DPM) approach has

been used to determine particle residence time to predict the flow behaviour of fuel particles. Discrete phase modeling of char burnout and devolatilization has been also performed to study the effect on combustion efficiency by using both of the fuels. The standard k–ε two-phase turbulence model was used to describe the gas–solids flow in the fluidized bed combustor and the combustion analysis was done through a non-premixed (NPM) approach in a species model. Temperature profiles and mass fractions of CO_2 and O_2 were obtained over the entire combustion domain and validated with experimental data.

INDEX

LIST OF FIGURES

LIST OF TABLES

NOMENCLATURE

P_g, P_s	gas, solid phase pressure [Nm^{-2}]
v_g, v_s	gas, solid phase velocity vector [ms^{-1}]
$\varepsilon_g, \varepsilon_s,$	gas, solid phase volume fraction
ρ_g, ρ_s	gas, solid phase density [kgm^{-3}]
μ_g, μ_s	gas, solid phase shear viscosity [Nsm^{-2}]
τ_g, τ_s	gas, solid phase shear stress [Nm^{-2}]
h_g, h_s	gas, solid phase enthalpy [Jkg^{-1}]
q	heat flux, W
σ	solid-phase shear stress, [Nm^{-2}]
$\vec{r}$, $\vec{s}$	Directions
Θ	Granular temperature [K]
c_p	specific heat [Jkg^{-1} K^{-1}]
k	Thermal conductivity [$Wm^{-1}K^{-1}$]
α	volumetric interphase heat-transfer coefficient [$Wm^{-}K^{-1}$]
H	Enthalpy [J]
I	Radiant intensity

Abbreviations

BFB	Bubbling fluidized bed
CPP	Captive Power Plant
FBC	Fluidized bed combustion
LES	Large eddy simulation
NPM	Non-Pre Mixed
ODE	Ordinary differential equation
PDE	Partial differential equation
PDF	Probability density function
PSH	Primary superheater
RANS	Reynolds average Navier Stokes
RNG	Re-normalization group
RTE	Radiative transfer equation
TFM	Two fluid model
TPH	Tons per hour

Subscripts

b	Bubble
g	Gas phase
s	Solid phase
m_f	Minimum fluidization
w	Wall

CHAPTER 1

INTRODUCTION

There is no doubt that energy is the basis for our development. Energy trends across the world such as higher energy demand and prices, big geographical differences across the regions, structural changes in power industry increasingly dominated by national companies, the affect of adverse climate change, as well as demand for energy security, all highlight the need for a transition to a low-carbon, efficient and environment friendly energy system. The search for energy alternatives involving locally available and renewable resources is one of the main concerns of governments, engineers and business people worldwide [1].

Coal is one of the greatest sources of energy used for power generation, cross over the world, which is almost 40% of the total energy produced [2]. But due to limited reserves of coal the use of techniques such as co-firing coal with renewable energy resources have become increasingly popular [3,4]. Also with the present major worldwide agenda to reduce greenhouse gas emissions, the emphasis is on conventional coal-fired utilities to burn renewable fuels such as biomass residues or energy crop-derived biomass fuels as a low-cost option for reducing gas emissions. However, the emissions of oxides of nitrogen and sulphur from coal combustion plants have been greatly reduced in the last two decades but the emissions of carbon dioxide remained a problem [5]. The need for finding new renewable sources of energy together with the necessity of searching new technologies to reduce the negative impact of waste accumulation has led to the possibility of using biomass as an alternate fuel. As a result, techniques of co-firing coal with biomass are being primarily used instead of waiting for the development of carbon capture techniques [6]. Also, the ratification of the Kyoto Protocol would need countries to implement measures to meet Kyoto standards by 2008 [7]. Co-firing is the

simultaneous combustion of a supplementary fuel with a base fuel. It is a low-cost option for efficiently and cleanly converting biomass to electricity by adding biomass as a partial substitute fuel in high-efficiency coal boilers. It has been demonstrated, tested, and proved in all boiler types commonly used by electric utilities. There is little or no loss in total boiler efficiency after adjusting combustion output for the new fuel mixture. This implies that biomass combustion efficiency to electricity would be close to 33% - 37% when co-fired with coal [8]. Different biomass forms are shown in Fig. 1.1.

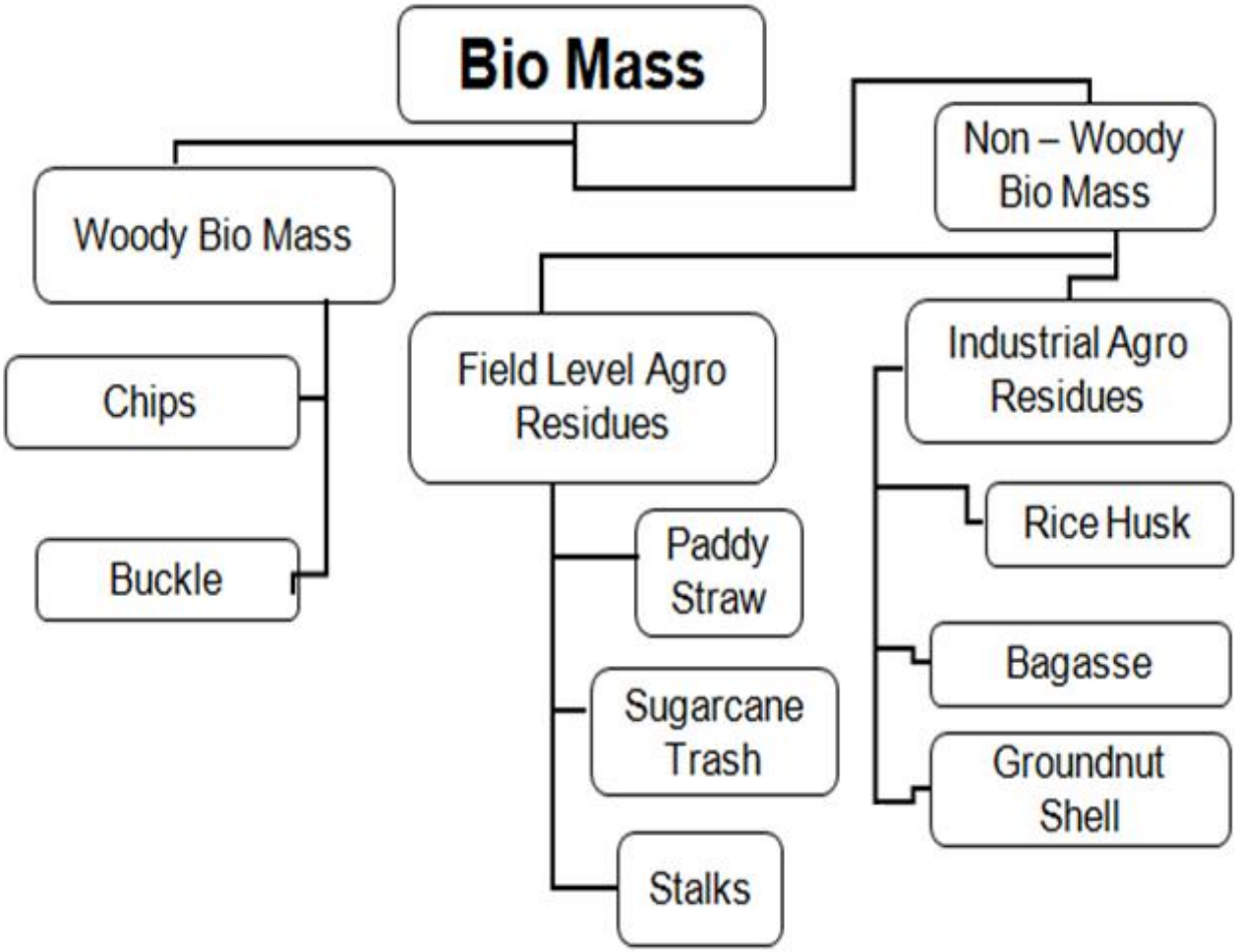

Fig. 1.1: Various biomass forms [1]

Extensive demonstrations and tests also confirmed that biomass energy can provide as much as 15% of the total energy input with only feed intake system and burner modifications. The opportunities for biomass co-firing are great because large scale coal-

powered boilers represent 310 GW of generating capacity [8].Various utilities and independent power producers have used biofuels, to generate electricity in small generating stations with less than 50 MW capacity [9]. In recent years, utilities have become interested in co-firing biofuels with coal and other fossil fuels, applying wood wastes, crop residues and other solid forms of biomass to high efficiency, higher capacity generating plants [10–14]. Initially, co-firing was seen as a means for reducing greenhouse gas emissions from fossil energy generation. Later on biomass co-firing with coal was proved to be the cheapest method for generating green power in utility plant and power generation sector [10,15–20]. Those savings come not only from replacement of coal, but also from displacement of materials being sent to landfill, that ultimately decompose and form both CO_2 and another more powerful greenhouse gas: namely methane. Co-firing is generally viewed as the most cost effective approach to biomass utilization by the electric utility industry. Co-firing was introduced as a means for utilities to accomplish the following objectives: To alter the use of fossil fuels, with renewable fuel, initially with sharing and completely in later stages for promoting sustainable development, support economic development among wood products and agricultural wastes; reduce fossil CO_2 emissions as part of the global climate challenge program; also reduce other emissions including oxides of nitrogen (NOx) and metal traces etc [21].

1.1 Global Scenario of Biomass

Biomass is a major source of energy throughout the world. Biomass is the primary source of energy for nearly 50% of the world's population [22] and wood biomass is a major renewable energy source in the developing world, representing a significant proportion of the rural energy supply [23]. In the past decade, the number of countries exploiting biomass opportunities for the provision of energy has increased rapidly, and has helped make biomass an attractive and promising option in comparison to other renewable

energy sources. The global use of biomass for energy increased continuously and has doubled in the last 10 to 11 years as shown in Fig. 1.2 [24].

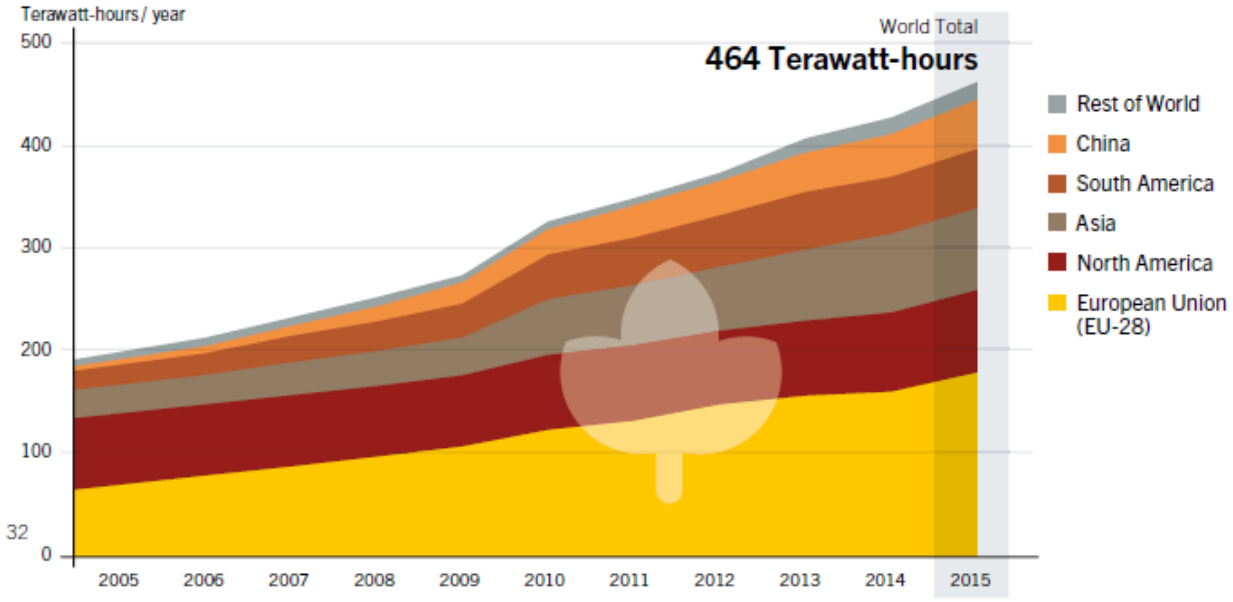

Fig. 1.2: Bio-power global generation [24]

Biomass is the third largest primary energy resource in the world, after coal and oil [25]. In all its forms, biomass currently provides about 1250 million tones of energy which is about 14% of the world's annual energy consumption [26]. Biomass is a major source of energy in developing countries, where it provides 35% of all the energy requirements. In developed countries, biomass energy use is also substantial. The annual global primary production of biomass is equivalent to the 4500 EJ of solar energy captured each year [27]. About 5% of this energy, or 225 EJ, would have covered almost 50% of the world's total primary energy demand as shown in Fig. 1.3. These 225 EJ along with other estimates based on models which assume an annual sustainable bioenergy of 270 EJ [28].

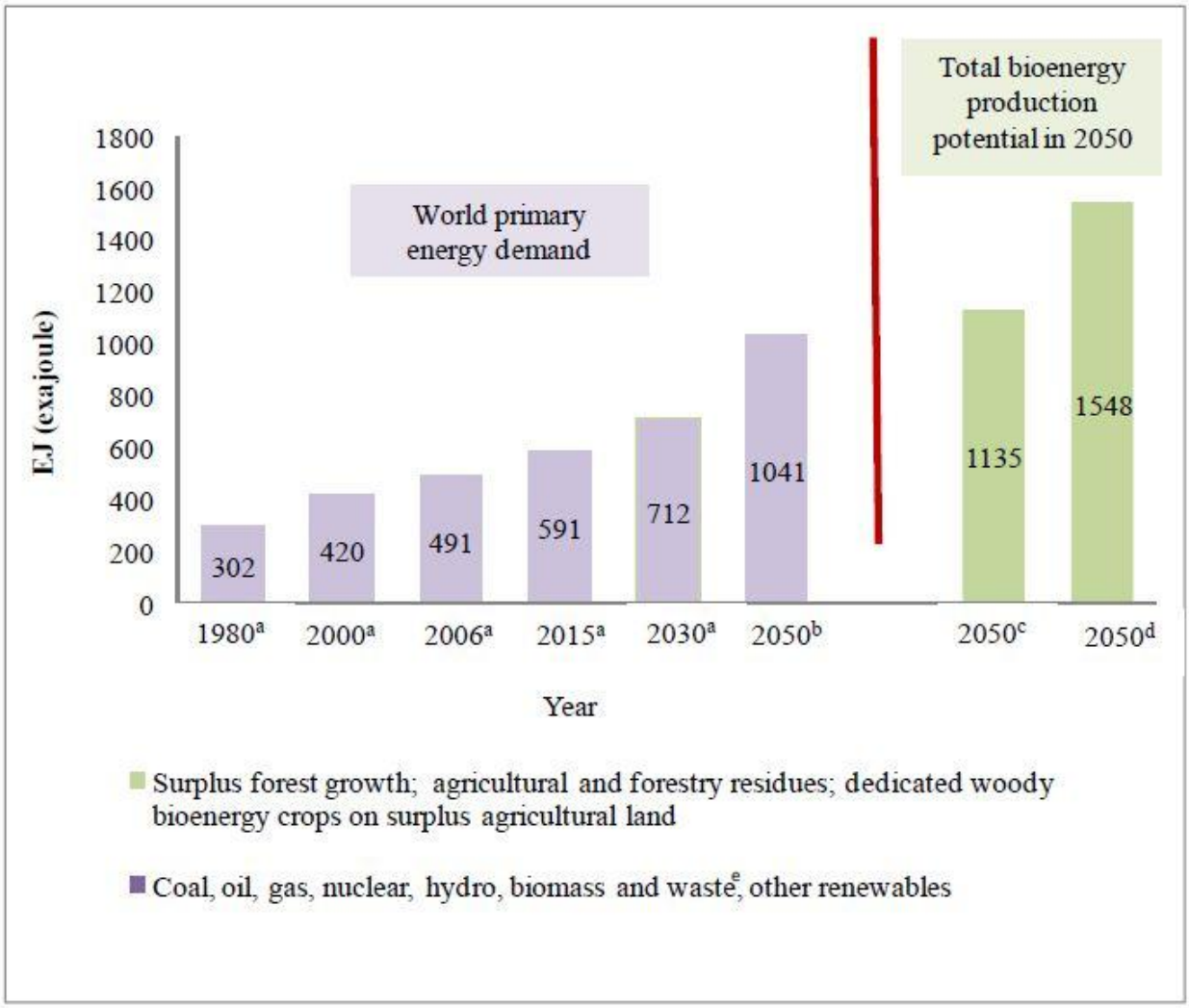

Note: [a] IEA
[b] Highest consumption scenario (Smeets et al.)
[c] Based upon biomass yield available for power production without any effect on food crop yield (Hoogwijk et al.)
[d] (Smeets et al.)

Fig. 1.3: World primary energy demand and forecasts for years 2015, 2030 and 2050 and estimates for total global bioenergy production outcomes in 2050 [1]

There are many scenarios that predict a future potential in biomass. There are also many studies performed during the past decades which attempt to estimate the future demand and supply of bioenergy [29-36]. For a detailed analysis and comparison of studies on global biomass production potentials see Berndes et al. [37]. However, published estimates of the total global bioenergy production potential in 2050 ranged from 33 to 1,135 EJ annually [38,39], from which 0 to 358 EJ annually came from woody

biomass [40,41]. Energy crops from surplus agricultural land have the largest power potential contribution of 0-988 EJ/year [42].

1.2 Energy Potential of Biomass in Asia and India

Biomass remains the primary energy source in the developing countries in Asia. Share of biomass in energy varies - from a very high over three quarters in percent in Nepal Laos, Bhutan, Cambodia, Sri Lanka and Myanmar; nearly half in Vietnam, Pakistan and Philippines; nearly a third in India and Indonesia, to a low 10 percent in China and 7 percent in Malaysia [43]. The absolute consumption of biomass energy has however risen undoubtedly during past two decades, growing at an annual rate of over 2% (FAO, 1997). India is well cherished with renewable energy resources. Coal, oil, and natural gas are the three primary commercial sources of energy. Over the years, there has been a significant change in the pattern of supply and consumption of energy. The share of commercial fuels in the total energy supply in India has risen from 41% to approximately 70% in [44], despite the dominance of the traditional fuels in the energy sector in India. The total domestic primary commercial energy supply in India has risen from 147.05 MTOE (Million tons of oil equivalent) in to 248 MTOE [45]. There exists a potential for generating about 1500MW of power from the urban and municipal wastes and about 1000MW from industrial wastes in the country [46,47]. The potential for expanding the use of biomass energy technologies (BETs) for energy generation is vast in India and awaits further exploitation. In this context, biomass co-firing and its applicability to Indian power production will be a great boost to the power producers, environmentalists and all concerned.

In India 64% of the nation’s workforce is engaged in agriculture and it contributes 29.4% of nation’s GDP [48,49]. Wood, crop residue and animal manure are the major biomass fuels which are used in rural areas at very low efficiencies [50]. Total

potential of energy from all these sources was estimated equivalent to be 5.14 EJ, which amounts to a little more a third of the total fossil fuel used in India. The energy potential in 2010 was estimated to be about 8.26 EJ. Today biomass is the world's fourth largest source of energy, contributing 15% of the world's primary energy needs [51]. According to one estimate, it is possible that India will be able to produce 35,000 MW of electric energy, by the year 2035, using biomass. At this level of production it would not only be able to meet 9% of India's power needs, but would also replace 8 million tons of coal, and prevent 40 million tons of carbon emission annually [52]. Biomass generation and power potential in various states of India is shown in Table 1.1 [53] which shows the present power potential of India is 33290 MW from agricultural residues, forest and wasteland. And state Punjab is having 3200 MW of power potential.

Table 1.1: Biomass generation and power potential in various states of India [53]

State	Agro-residues			Forest & wasteland residue		
	Biomass generation kT/yr	Biomass surplus kT/yr	Power potential MW	Biomass generation kT/yr	Biomass surplus kT/yr	Power potential MW
Andhra Pradesh	24871.7	4259.4	520.8	3601.0	2435.5	341.1
Arunachal Pradesh	400.4	74.5	9.2	8313.1	6045.4	846.3
Assam	11443.6	2436.7	283.7	3674.0	2424.4	339.4
Bihar	25756.9	5147.2	640.9	1248.3	831.9	116.3
Chhattisgarh	11272.8	2127.9	248.3	13592.3	9066.0	1269.2
Goa	668.5	161.4	20.9	180.7	119.2	16.7
Gujarat	29001.0	9058.3	1224.8	12196.3	8251.9	1150.0
Haryana	29034.7	11343.0	1456.9	393.3	259.5	36.3
Himachal Pradesh	2896.9	1034.7	132.6	3054.6	2016.1	282.2
Jammu and Kashmir	1591.3	279.5	37.1	11461.7	7564.6	1059.1
Jharkhand	3644.9	890.0	106.7	4876.6	3249.8	455.0
Karnataka	34167.3	9027.3	1195.9	10001.3	6601.0	924.3
Kerala	11644.3	6351.9	864.4	2122.1	1429.2	200.0
Madhya Pradesh	33344.8	10329.2	1373.3	18398.2	12271.2	1718.0
Maharashtra	47624.8	14789.9	1983.7	18407.1	12440.1	1741.6
Manipur	909.4	114.4	14.3	1264.0	834.3	116.7
Meghalaya	61.1	91.6	11.3	1705.9	1125.7	157.5
Mizoram	511.1	8.5	1.1	1590.9	1050.1	147.0
Nagaland	492.2	85.2	10.0	843.8	556.9	77.9
Odisha	20069.5	3676.7	429.1	9370.2	6084.6	851.8
Punjab	**50847.6**	**24843.0**	**3172.1**	**398.5**	**263.0**	**36.9**
Rajasthan	29851.3	8645.6	1126.7	9541.6	6297.4	881.6

Sikkim	149.5	17.8	2.3	531.5	350.7	49.1
Tamil Nadu	22507.6	8899.9	1159.8	4652.4	3070.6	429.9
Telangana	19021.5	2697.2	342.5	1550.7	1048.9	147.0
Tripura	40.9	21.3	3.0	1035.5	683.4	95.7
Uttar Pradesh	60322.2	13753.7	1748.3	5478.4	3672.1	514.1
Uttarakhand	2903.2	638.4	81.0	4559.2	3055.5	427.8
West Bengal	35989.9	4301.5	529.2	1430.7	949.1	133.0
Total	**511040.9**	**145105.7**	**18729.9**	**155473.9**	**104048.1**	**14561.5**

1.3 Biomass Potential in Punjab

Through the utilisation of biomass, in the form of agricultural residues such as cotton stalks, wheat straw, rice straw, sugarcane bagasse and rice husks, not only can heat and power be produced efficiently, but there is also the potential to improve rural income and energy security through the substitution of coal, oil and natural gas. The global demand for electric energy is expected to increase from about 14 billion tons per coal equivalent (TCE) to 19 billion TCE by 2020 [54]. In India too, the demand for electric energy is expected to rise dramatically. Power generation based on biomass holds considerable promise in agriculture states such as Punjab, which has huge biomass resources from the crop production system and agricultural industries. With the availability of 20 million tons of paddy straw and 10 million tons of other agricultural residues such as cotton and mustard stalk, the state has the potential to generate 3200 MW of power through biomass as shown in Table 1.1 [53,55].

With only 1.5% of the geographical area of India, the Punjab state produced 22.5% wheat, 55% rice and 25% of cotton of annual productions presently as per the latest survey of Punjab Energy Development Agency (PEDA), thus producing a large amount of crop residue [56, 57]. Crop residues in the mechanized farms in Punjab are burned to minimize residue management cost [58]. Burning of residues, results in loss of organic matter and nutrients thus increasing pollution. The increase in pollution is evident from the fact that one ton of straw burning releases 3 kg of particulate matter, 60 kg of

CO, 1460 kg of CO_2, 199 kg of ash and 2 kg of sulphur if burned in open [59]. In order to motivate the disposal of agro waste in an eco-friendly way the state government implemented new energy policy in year 2006. This policy offered financial and fiscal incentives to add power generation capacity of 3200 MW bringing the share of New and Renewable Sources of Energy (NRSE) to the level of 10% of conventional power [60-61].

1.4 Hydrodynamics of Fluidization

When a fluid is passed upwards through a bed of solid particles at a very low flow rate the fluid percolates through the void space without disturbing the bed. This condition represents a fixed bed. If the upward flow rate is very high the bed mobilizes pneumatically and may be swept out of the vessel. At an intermediate flow rate, the bed expands: the particles are separated by a mean free distance and are supported by the drag force of the fluid. The expanded bed, having some of a fluid's properties, is called a fluidized bed. Typical results of a gas-fluidized bed of particles are shown in Fig. 1.4 where the pressure drop across the bed and its height are plotted as a function of the superficial gas velocity [63]: starting from line A, for slowly increasing flow, the overall pressure drop is slightly more than enough to support the weight of the particles. Above point B, a slight increase in flow velocity frees the particles: the pressure drop becomes just enough to support their weight and, consequently, point C is commonly defined as a point of incipient fluidization, characterized by the minimum fluidization velocity U_{mf} and the voidage fraction ε_{mf}. If the flow rate is decreased from point C, the particles are more loosely packed so the bed height is greater and the pressure drop smaller (point D).

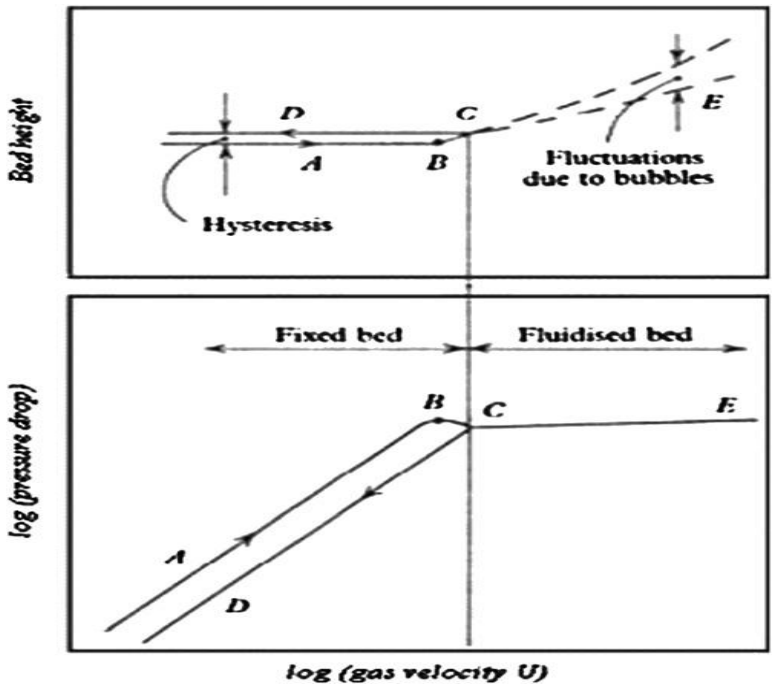

Fig. 1.4: Typical curves for gas fluidized bed of particles [63]

For a gas fluidized bed in which the gas velocity is greater than U_{mf}, some of the gas may pass through the bed as bubbles: these agitate the bed and consequently its height fluctuates as indicated in region E. The formation of bubbles characterizes the bubbling fluidized bed; with still greater flows the bubbles grow and appear more frequently, until the bed becomes slugging. A further increase in flow carries particles out of the combustor according to the phenomena of pneumatic transport. After the gas reaches the minimum fluidization velocity, bubbles form and during their rise to the surface of the bed, not only do they increase in size and coalesce, they are also divided.

In general, fluidized bed models consider the division between the bubble phase and the particulate phase, also called emulsion or dense phase, the degree of mixing in the particulate phase and the transfer of gas between the two phases. The reason for developing a conceptual model for the bubbling bed is to estimate its main features, such as velocities of gas and solid, volume fractions and contacting regimes, from very little information about the solid particles in the bed. The first significant breakthrough was made by Davidson [63] who proposed a straight forward, simple model for single rising

bubbles, based on the following postulates: a gas bubble is solid-free and circular in shape; as a bubble rises, particles move aside. The emulsion behaves like an incompressible fluid through which the gas flows as an incompressible viscous fluid. Pressure in the bubble is assumed to be constant. One of the most appreciable results of this model is the pressure distribution near a 3-D bubble: the pressure in the lower part of the bubble is lower than that of the surrounding bed, whereas in the upper part it is higher. Hence, gas flows into the bubble from below and leaves at the top. Although the circular shape of the bubble is not a realistic hypothesis, the Davidson model fits the data quite well.

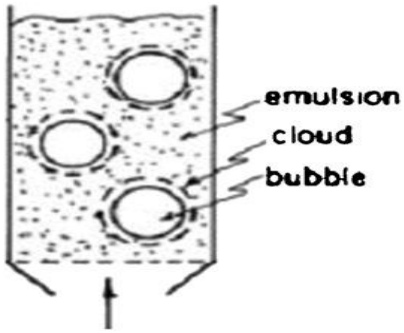

Fig. 1.5: Representation of the three phases in a fluidized bed [64]

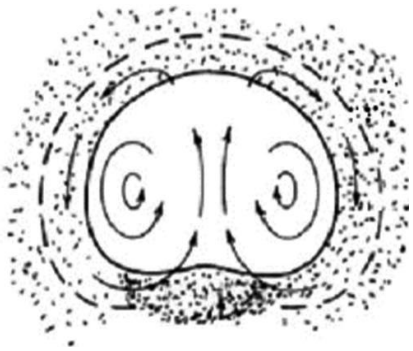

Fig. 1.6: Gas flow pattern around and within the bubble [64]

A significant attempt to understand the behavior of a bubbling bed as a whole was made by Toomey and Johnstone [65], the fathers of the two-phase theory of fluidization. Since experiments in bubbling beds indicate roughly that all gas in excess of that needed to fluidize the bed passes through the bed as bubbles and the emulsion phase remains close to minimum fluidizing conditions, they considered the bubbling bed to be composed of two phases: the bubbling phase and the emulsion phase. The emulsion flow rate is equal to the flow rate for incipient fluidization (U_{mf}) while the bubble phase carries the additional flow of fluidizing fluid (U - U_{mf}). Comparison between predicted and experimental data makes it clear that the two-phase theory overestimates the volume of

gas passing through the bed as bubbles. Besides, evaluation of solids movement in the bed is not considered.

A more detailed description of the bubbling bed was proposed by Kunii and Levenspiel [66]. They introduced a new phase called ‘‘cloud’’ thus their contribution is also known as the three-phase theory (Fig. 1.5). Consider the following flow patterns: if the emulsion gas rises faster than the bubble, it enters the bottom of the bubble and leaves at the top; this generates an annular ring of gas that circulates within the bubble. On the contrary, if the bubble rises faster than the emulsion, the gas leaving the top of the bubble is swept around and returns to the base of the bubble. The region around the bubble covered by this circulating gas is the cloud: slow bubbles are cloudless whereas, in the case of fast bubbles, cloud cannot be neglected. In addition, this model is the first to show that solids are dragged up the bed behind bubbles and drift downwards in the emulsion. Although, the volume fraction of particles dispersed in rising bubbles might be less than 0.1%, these could enormously affect processes in which rapid kinetics occurs. Unlike the previous theory, bubbles are not spherical but have a flattish or even concave base (Fig. 1.6). The region just below the bubble is the wake: this leaks the solid matter that a rising bubble drags up, assuring an interchange with the emulsion. This model hypothesizes that all the fluid passes through the bubble phase (the gas flow through the emulsion is negligible) and solid matter mixes perfectly with the gas in the emulsion phase.

The three-phase theory has been the object of controversies for some time since its complexity cannot often assure better results than the simpler two-phase theory. However, investigations by many researchers demonstrated that, among others models, it adapts better to different operating conditions. In order of rising complexity, the last fluidization model was developed by Werther [67]. He adopted known mass-transfer phenomena with concentration profiles around the bubbles. The key assumption is

concerned with defining a height below which bubble size does not change. Additional hypotheses include that the gas flow through the emulsion phase is negligible whereas the one in the bubble phase is a plug flow; the coefficient of mass transfer and the interfacial film between bubble and emulsion are considered independent of the height in the bed. The conservation of mass in the bubble, cloud and emulsion phase is the core of the model. Because of high complexity in process, it is used only if necessary: chemical reactions occurring at the bubble–emulsion interface represent one of the most suitable cases for Werther's model application.

1.4.1 Incineration of solid fuel

Fluidized bed combustion involves the analysis of several phenomena: firstly, when a fuel particle is injected into a hot fluidized bed it begins to dry. Drying, which usually takes a few seconds, can be followed by shrinkage. Then, the heating process is responsible for devolatilization that consists of the detachment of the volatile matter from the solid fuel. Average devolatilization time varies between 10 and 100s depending on the fuel, on the particle size and on the bed temperature. Volatiles burn in a homogeneous phase; the remaining char particles, mainly composed of carbon and ash, ignite and burn by heterogeneous reaction with oxygen. The time in which char complete combustion takes place is of the order of hundreds or even thousands of seconds therefore it determines fuel particle residence time in the bed.

1.4.2 Drying process

The physicochemical transformation of a solid organic fuel due to fluidized bed combustion starts with drying, characterized by moisture evaporation from the bulk of the fuel particle. The evaporation front moves inside the particle under the influence of an increase in the temperature of the drying surface. It is a heat transfer limited process influenced by the furnace temperature, fuel particle size and porosity. Drying and heating

may cause particle shrinkage, a reduction in the pore size, internal cracking or particle break up.

1.4.3 Combusting volatile materials

When the temperature exceeds 250^0C, the fuel particle organic matter starts to thermally degrade, with the release of volatiles. These gaseous compounds react with oxygen partly inside the bed and partly above the bed. Since the reaction is rapid, it has a negligible effect on the overall combustion time. Nevertheless, the location of volatile combustion significantly affects the heat release profiles throughout the combustor. Many different works deal with the modeling of volatiles combustion [68]. If the furnace is fed from below, volatiles form an oxygen-starving plume rising through the bed. Combustion of gases involves the boundary between volatiles and the surrounding oxygen rich gas: the result is a diffusion flame at the plume boundary. This model was further modified with the introduction of the ‘‘meandering’’ plume that gives relevance to radial dispersion of gases [69]. Subsequently, model calculations showed that the hypothesis of instantaneous devolatilization was unrealistic; in fact devolatilization time is comparable to particle mixing time in the bed. For finding the reason why volatiles burn both in the bed and in the freeboard, Stubington and Chan [70] proposed the multiple discrete diffusion flame model according to which devolatilizing particles are transported to the top of the bed by the ascending fluidized bed bubbles. Consequently, a significant fraction of the volatiles can reach the freeboard. All these models share the same defect: they neglect the hydrodynamic interaction between the volatile stream and the surrounding suspension of fluidized bed particles. This issue has been analyzed in conditions of incipient fluidization by Fiorentino et al. [71,72]

1.4.4 Fixed carbon combustion

The residual of devolatilization is made up of char. The combustion of fixed carbon is governed by several complex phenomena: mass transfer of oxygen from the bubble phase to the solid one; boundary layer and intra-particle transport of the mass (oxygen and combustion products) and heat; heterogeneous reaction on the fuel particle external and internal surfaces. Their importance varies according to fuel properties and combustor operating conditions. In general, the boundary layer oxygen diffusion increases with the bed temperature and char particle size while a decrease in the bed temperature and in the char particle size increases the intra-particle mass transport.

Char oxidation has been investigated with different techniques: observation of flame formation [73,74]; analysis of solid combustion residual [75]; measurements of flue gas concentrations [76]. The main aim is to predict the char burning time since it governs the fuel particle residence time in the bed. The combustion of solid matter can follow one of the following extreme types of behavior: the diffusion of gaseous reactant into a particle is rapid enough compared to chemical reaction for fuel to be consumed more or less uniformly throughout the particle or the opposite may happen, diffusion into the fuel particle is so slow that the reaction zone is restricted to a thin front that advances from the outer surface into the particle. Each of these hypotheses is the basis for a char combustion model: the former is the core of the uniform-reaction model; the latter is the starting point for the shrinking-core model.

Laboratory examinations of relatively large coal particles in bubbling fluidized beds [77] confirm that the boundary between the central core of fuel and the char is sharp and distinguishable and the velocity of the boundary was found to be constant. A model for the process involves heat transfer from the fluidized bed to coal particle, followed by heat conduction through the outer layer of char to provide the enthalpy required for

thermal decomposition in the moving reaction zone. Also the prediction of the temperature reached by burning char particles is one of the most important issues in fluidized bed combustion [78]. On the one hand, experimental measurements are restricted by the presence of inert bed particles and the circulation of char particles [79–81]; on the other hand, theoretical models, based on energy balance around the burning particle [82,83], are weakened by the lack of a complete understanding of the primary CO/CO_2 production ratio. However, different works lead to the same conclusion: the particle temperature increase due to char burning varies from 10 to 500^0C beyond the bed temperature. Heat generated by carbon combustion is transferred both to percolating gas and to inert bed particles. These highly enhance heat transfer by an additional particle convective flux and, at the same time, reduce mass transfer, lowering the volume available for gas diffusion around the particle.

As mentioned before, the right calculation of the primary CO/CO_2 production ratio is very difficult. This parameter has a strong influence on the combustion rate because the heat of CO combustion accounts for approximately two-thirds of the total heat release during the complete oxidation of carbon. Published information proposes a single or double film model for the prediction of CO and CO_2 concentration profile around burning particles [84–86]. According to Hayhurst and Parmar's theory [87] experimental observations can be explained considering only the CO as a product of carbon oxidation while Biggs and Agarwal [88] support the idea that both CO and CO_2 are primary combustion products.

1.4.5 Comparison between conventional and non-conventional fuels

Combustion of alternative solid fuels in fluidized beds includes a wide variety of non-fossil solid materials, ranging from biomass and peat to municipal, agricultural and industrial waste. Although there is a certain amount of operating experience in connection

with this topic [89,90], a complete comprehension of the phenomena occurring during incineration of these fuels is still lacking, probably due to the great difference in physical and chemical features from conventional ones. In fact, alternative fuels are characterized by high moisture and volatile content, a low density and high reactivity. The presence of a large quantity of water in fuel particles amplifies drying time and postpones devolatilization. The high volatile content leads to longer devolatilization times and larger quantities of volatiles evolved: as a result, a larger contribution to the overall heat release is associated with homogeneous volatile combustion. Devolatilization is completed at (or close to) the bed surface and a large fraction of the volatile matter is released directly in the freeboard: a direct consequence of bypassing the bed is that the post-combustion of volatiles in the splashing region leads to significant local overheating with respect to the bed. Besides, fine carbon particles are significantly formed by attrition and fragmentation of coarse particles. As a result, the conversion of fixed carbon occurs as much through the generation of fines, followed by their combustion over their residence time in the bed, as through direct combustion of coarse char particles. Because of high reactivity, the fine char particles are mostly burned in the bed [91]. Whereas conventional fuels like coal undergo moderate primary fragmentation: after devolatilization about 99% of the fixed carbon can be found in coarse char particles. Consequently, coal conversion occurs primarily in the bed, mostly via coarse char particle direct combustion.

1.4.6 Fluidized bed interaction with internal components

The channeling of the rising bubbles causes the circulation of solids in a fluidized bed while the intermixing of particles taking place within the wakes is a small-scale phenomenon. When solids of wide size distribution are fluidized, the heavier particles tend to settle to the bottom of the bed but this is countered by the solid circulation. However, they slowly settle at the bottom of the bed. In bubbling fluidized beds, mixing

and segregation of different solids is an equilibrium process influenced by bed operating conditions. This equilibrium is actually broken by the presence of internal components. Vertical or horizontal tubes are often fitted in fluidized bed reactors for temperature control and their presence reduces bubble size, increases the emulsion voidage and the overall residence time of gas in the bed.

The heat transfer coefficient h (defined by $h = Q/A\Delta T$, where Q is the heat transfer rate, A is the area of the heat exchanger and ΔT is the mean temperature difference between the bed and the surface) in a gas-fluidized bed has been found to be one or two orders of magnitude larger than that for gases alone. This is mainly due to the thorough mixing of the solid phase assured by bubble motion and entrainment. Many factors influence the value of h such as particle size, gas velocity, bed temperature and pressure, thermal conductivity and heat capacity. It was discovered that h becomes maximum at some intermediate gas velocities: the decreasing of the heat transfer coefficient at higher velocities can be due to an increase in contact time with the bubbles. Other experimental studies showed that h increases with temperature and pressure. Botterill et al. [92] concluded that the bed-to surface heat transfer coefficient is influenced by the relative heat capacities of bed particle and the surface; also the relative temperatures affect the heat transfer coefficient. On the contrary, the tube diameter of the heat exchanger has only a small influence on the coefficient h. Because of the extreme variability of h, the numerous correlations reported in published material are limited to a narrow range of conditions [93,94].

1.5 Advantages of Fluidized Bed Combustors

- **High efficiency**: FBC boilers can burn fuel with a combustion efficiency of over 95% irrespective of ash content. FBC boilers can operate with overall efficiency of 84% (±2%).

- **Reduction in boiler size:** High heat transfer rate over a small heat transfer area immersed in the bed results in overall size reduction for the boiler.
- **Fuel flexibility:** FBC boilers can be operated efficiently with a variety of fuels. Even fuels like flotation slimes, washer rejects, agro waste can be burnt efficiently. These can be fed either independently or in combination with coal into the same furnace.
- **Ability to burn low grade fuel:** FBC boilers would give the rated output even with an inferior quality fuel. The boilers can fire coals with ash content as high as 62% and having calorific value as low as 2500 kcal/kg. Even carbon content of only 1% by weight can sustain the fluidized bed combustion.
- **Ability to burn fines:** Coal containing fines below 6 mm can be burnt efficiently in FBC boiler, which is very difficult to achieve in conventional firing system.
- **Pollution control:** SO_2 formation can be greatly minimized by addition of limestone or dolomite for high sulphur coals (3% limestone is required for every 1% sulphur in the coal feed). Low combustion temperature eliminates NOx formation.
- **Low corrosion and erosion:** The corrosion and erosion effects are less due to lower combustion temperature, softness of ash and low particle velocity (around 100 cm/s).
- **Easier ash removal – No clinker formation:** Since the temperature of the furnace is in the range of 850 – 900°C in FBC boilers, even coal of low ash fusion temperature can be burnt without clinker formation. Ash removal is easier as the ash flows like liquid from the combustion chamber. Hence less manpower is required for ash handling.
- **Simple operation, quick start-up:** High turbulence of the bed facilitates quick start up and shut down. Full automation of start up and operation using reliable equipment is possible.

- **Fast response to load fluctuations:** Inherent high thermal storage characteristics can easily absorb fluctuation in fuel feed rates. Response to changing load is comparable to that of oil fired boilers.
- **Provision of automatic ignition system:** Control systems using micro-processors and automatic ignition equipment give excellent control with minimum supervision.
- **High reliability:** The absence of moving parts in the combustion zone results in a high degree of reliability and low maintenance costs.
- **Reduced maintenance:** Routine overhauls are infrequent and high efficiency is maintained for long periods.
- **Quick responses to changing demand:** FBC can respond to changing heat demands more easily than stoker fired systems. This makes it very suitable for applications such as thermal fluid heaters, which require rapid responses.
- **High efficiency of power generation:** By operating the fluidized bed at elevated pressures, it can be used to generate hot pressurized gases to power a gas turbine. This can be combined with a conventional steam turbine to improve the efficiency of electricity generation resulting in a potential fuel savings of at least 4%.

1.6 Scope of Study and Problem Formulation

Coal is one of the greatest sources of energy used for power generation, cross over the world, which is almost 40% of the total energy produced. But due to limited reserves of coal the use of techniques such as co-firing coal with renewable energy resources have become increasingly popular. Among the energy sources that can substitute fossil fuels, biomass fuels appear as the option with a higher worldwide potential. Power generation based on biomass holds a considerable promise in Punjab, which has huge biomass resources from the crop production system and agro industries. The total biomass production in Punjab was estimated at about 76350 kilo tons. In Punjab, there is a total potential of 3200MW of power that can be generated from the agri-residue and forest biomass.

Keeping in mind the biomass potential in the agricultural state like Punjab, India, various corporate sectors initiated the use of these renewable energy sources such as rice husk, paddy rejects and sugarcane baggase etc. in sharing with conventional fuels such as coal. For present study Captive Power Plant (CPP) of Ambuja Cement Limited (ACL), Ropar in Punjab province of India is opted for performing CFD analysis of real plant boiler and validating the results with actual monitoring data. The research is performed in two stages. In first stage the experimental observations at the plant and data collection were performed. The data collection included types of fuel used i,e coal and biomass. Ultimate and proximate analysis of fuels, various input parameters and geometrical details required for simulation of CPP boiler, experimental observations included bed temperatures, exit temperature of flue gas, O_2 and CO_2 values at the exit of boiler.

In second stage CFD analysis was performed using Fluent 6.3 code and then the validation of results with plant data. The information available from this study includes temperature distributions, species concentration, velocity profiles, particle trajectories, heat fluxes and particle burnout.

1.7 Objectives of Research

The aim of the proposed research work is to carryout CFD analysis of a real plant bubbling fluidized bed combustor based on co-firing coal and biomass. Following are the objectives of proposed study:

1. To obtain the temperature contours inside the combustor.
2. To obtain contours of CO_2, and O_2 mass fraction.
3. Contours of heat flux.
4. Trajectories and residence time of biomass and coal particles.

The results of the study will be validated with the actual plant data and reported literature.

1.8 Organization of Thesis

The dissertation is primarily divided in to six chapters. **Chapter 1** deals with the extensive role of agricultural wastes and another biomass fuels in present power generation scenario. It provides information of biomass potential throughout the world, in

India and in Punjab. It also explains FBC technology which is proved to be a prevalent technology for combustion of low density fuels, basics of fluidization and different types of FBC systems.

In Chapter 2 a detailed study of extensive literature available on modeling and CFD analysis of Fluidized bed combustors derived by biomass fuels alone and based on Co-firing (biomass and coal) is done. At the end problem formulation and objectives of study are defined.

In Chapter 3 the detailed description of CPP, Ambuja cement limited, Ropar is provided. It includes the technical specifications of plant, the usage of different biomass forms used in plant, the technologies evolved for the implementation of biomass derived combustion system and relevant data required for CFD analysis of CPP boiler.

Chapter 4 deals with the CFD analysis of CPP combustor. It explains the need of CFD in combustion systems, methodology to be used for performing CFD analysis, different approaches used in CFD and different models applied in the present study.

Chapter 5 explains results obtained and explanations rose during discussion. Here the different objectives of study (temperature contours, mass fractions of species of interest, particle trajectories of coal and biomass, char burn out and devolatilization, heat flux on the internal components) obtained from simulation were validated with real monitoring data and reported literature.

Chapter 6 provides information on conclusions and future scope of the study. List of references and appendix section are given at the end of the report.

CHAPTER 2

LITERATURE REVIEWED

2.1 Fluidized Bed Combustion Modeling

Fluidized bed combustors are being used successfully due to flexible technology evolvement which may use even low quality fuel in terms of its calorific value. These low-heating value fuels can be easily used in FBC due to the high mixing rate of solids and the absence of temperature gradients in the bed. Also the reduction in pollutants emitted with flue gas is one of the most relevant advantages of fluidized bed combustion. The low combustion temperature guarantees the NOx control while sulphur capture is achieved by limestone or dolomite injection in the bed. Limestone not only reacts with SO_2 to form calcium sulphite and calcium sulphate, but also captures hydrogen chloride to form liquid- or solid-phase calcium chloride.

The first significant effort was made by Davidson [63] who proposed a simple model for single rising bubbles based on the assumptions that gas bubbles are solid-free and circular in shape, as they rise, particles move aside. The particulate or emulsion behaves like an incompressible fluid through which the gas flows as an incompressible viscous fluid. Pressure inside the bubble remains constant. The most accepted results of this model are the pressure distribution near the bubble region. The pressure in the lower part of the bubble is lower than that of the surrounding bed, whereas in the upper part it is higher. Hence, gas flows into the bubble from below and leaves at the top.

Another attempt to understand the behavior of a bubbling bed was made by Toomey and Johnstone [65], the originators of the two-phase theory of fluidization. The experiments conducted in the field of bubbling beds indicated that all gas needed to fluidize the bed passed through the bed as bubbles and the emulsion phase remained close to minimum fluidizing conditions. In view of that Toomey and Johnstone considered the

bubbling bed to be composed of two phases: the bubbling phase and the emulsion phase. The emulsion flow rate is equal to the flow rate for incipient fluidization (U_{mf}) while the bubble phase carries the additional flow of fluidizing fluid (U-U_{mf}). It was further observed that the two-phase theory does not explain the evaluation of solids movement in the bed.

Finally a more detailed description of the bubbling bed was proposed by Kunii and Levenspiel [66]. They introduced a new phase called 'cloud', thus their contribution is known as the three-phase theory (Fig. 1.11). This model suggests that if the gas in emulsion phase rises faster than the bubble velocity, then it enters from the bottom of the bubble and leaves it at the top. This generates an annular ring of gas that circulates within the bubble. On the other hand, if the bubble rises faster than the emulsion, the gas leaving the top of the bubble is swept around and returns to the base of the bubble. The region around the bubble covered by this circulating gas is in the form of cloud. Slow bubbles are usually cloudless whereas, in the case of fast bubbles, cloud cannot be neglected.

Fuel particles during combustion inside fluidized bed undergo several phenomena. Firstly, when a fuel particle is injected into a hot fluidized bed it begins to dry. Drying, which usually takes a few seconds, can be followed by shrinkage. Then, further heating at temperature more than 250^0C the organic matter of fuel decomposes in to volatiles. The process is known as devolatilization that consists of the detachment of the volatile matter from the solid fuel matrix. Average devolatilization time depends on the fuel, on the particle size and on the bed temperature. The residual of devolatilization is made up of char particles which composed of carbon and ash. They burn by reaction with oxygen on the bed. The time in which complete char combustion takes place determines fuel particle residence time in the bed.

Char oxidation may be investigated by different methods, Firstly, by observation of flame formation [73,74]. Secondly, by analysis of residual product after combustion [75] and by the measurements of flue gas concentrations [76].The prediction of char burning time is very useful investigation as it governs the fuel particle residence time in the bed.

Biomass fuels have different chemical and physical composition from those of fossil fuels. They contain higher moisture and volatile content, a lower density and a higher reactivity. Consequently, the behavior of each of the two kinds of fuel in the bed is very different. Coal conversion occurs primarily in the bed, mostly through direct combustion of coarse char particles whereas, for biomass, a large amount of the fixed carbon conversion occurs through the generation of fine particles followed by their post-combustion in the bed as shown in Fig 2.1. Further, a small fraction of the volatile matter burns in the splashing region above the bed [95].

Making use of commercial fluidized bed processes to recover energy from biomass is becoming more frequent. As a result, need for models simulating commercial equipment are becoming urgent. In view of this comment, an overview of solid fuel combustion models has provided with reference to FBCs (Table 2.1).

Table 2.1: Review of solid fuel models in fluidized bed

Author/Theoretical issue	**Modeling**	**Plant/Experimentation**	**Remarks**
S. Bittani et al.[96] Two phase theory	Non linear lumped parameter model to estimate the carbon load on temperature variation	ENEL (Italian electricity board) with department of electronics & information (DEI), Milano	
A. Schmidt et al.[97] Kinetic theory of granular flow	Eulerian formulation of the particulate enthalpy equation	RWTH, Germany	Very few of them worked on real plant data using biomass fuels.
L. Armesto et al.[98] Combustion	Combustion of rice husk and characteristics of the ash formed during	30kW pilot plant of CIEMAT	

	combustion process.	
S.K. Mohapatra et al.[99,100] Three phase theory	Solid population balance and exit gas composition.	10 MW power plant, TISCO, India
T. Kataza et al.	Dynamic model of air flue gas through splashing region & secondary zone.	Research project with Mestro power inc.
H. Zhou et al.[101] Coal combustion	DEM – LES simulation of coal combustion.	Simulated bed
Campbell & Davidson[102]	Different bed operating conditions and model parameters	Small scale experimental unit

The fluidized furnace is divided primarily into three segments according to the different combustion zones: the bed, the splashing region and the freeboard. The structure of the furnace is shown in Fig 2.1. The fluidized bed is modeled according to the two-phase theory. In the theory the flow rate through the emulsion phase is equal to the flow rate for the minimum fluidization. Any flow in excess of that required for minimum fluidization appears as bubbles in the separate bubble phase [103,104]. The bed is considered isothermal where two phases have uniform temperature. Minimum fluidization velocity is adopted from Wen et al. [105]. An average bubble size is assumed throughout the bed and calculated according to Kato and Wen [106].

It is assumed that fuel is fed above the bed and it will spread uniformly and immediately across the cross-section of the bed. In the bed section, according to the two-phase theory, combustion takes place in the emulsion phase. Coarse char and fine char particles are burnt there. In the model the coarse char particles can also burst to the secondary zone of the furnace and drop back into the bed. The fine particles can elutriate out from the furnace [107].

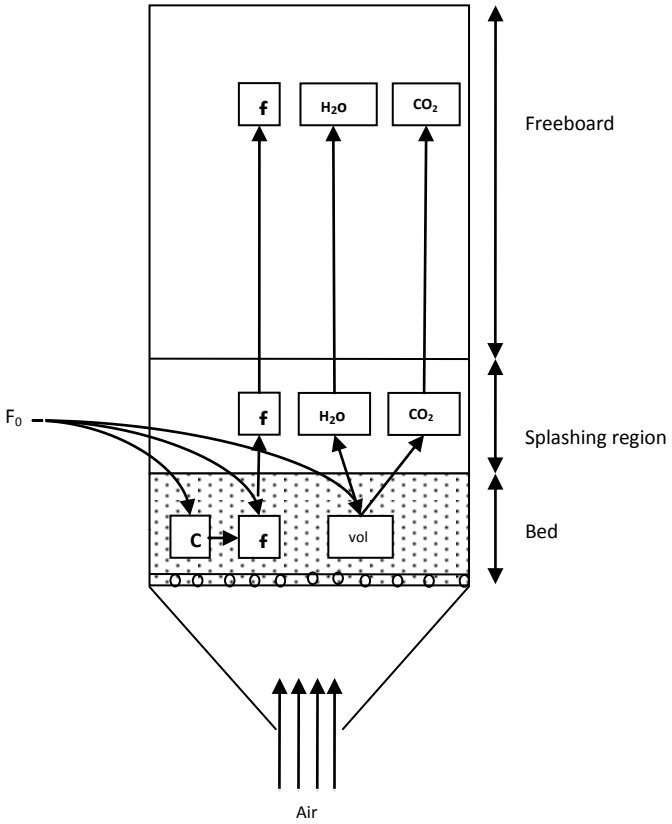

Fig 2.1: Framework of the fluidized bed boiler

Where **C** = coarse char particles, **f** = fine char particles, **vol** = volatile matter.

Elutriation rate

Elutriation refers to the selective removal of fines by entrainment from a bed consisting of a mixture of particle sizes. Elutriation rate constant K*(*dp*) and elutriation constant K(*dp*) are two important features in fluidized-bed combustors. K*(*dp*) varies with size of solids, a large value corresponds to a rapid removal rate and K*(*dp*) = 0 means that the particular size of solid is not removed at all by entrainment, whereas K(*dp*) varies proportionately with bed cross-section and inversely with bed height, but K*(*dp*) is unaffected by these changes as long as quality of fluidization remains same. Since the generation of fines in the bed may be due to chemical, mechanical and hydrodynamic breakdown of the solids, it becomes difficult to predict the actual concentration of any particular size fraction in the bed. Many a correlation are available in the literature for the prediction of elutriation

rate constant K*(*dp*) viz., Yagi and Aochi [108], Zenz and Weil [109], Wen and Harshinger [110] and Geldart et al. [111]. etc. Geldart et al. have shown that high accuracy should not be expected from any of these correlation and agreement between experimental and prediction is unlikely to be better than ±100%. For low density solids such as coal char, cracking catalyst, etc. and well mixed beds at velocities up to 1.2 m/s, Zenz and Weil correlation probably gives the most consistent values of K*(*dp*). The Zenz and Weil correlation [112] has been used in this model to predict the elutriation rate of solids from the fluidized bed which is given below:

$$\frac{K^*(d_p)}{\rho_g . U_0} = \left[1.26\ x\ 10^7 \left(\frac{U_0^2}{g\ .d_p\ .\rho_p^2} \right)^{1.88} \right] \quad when \quad \frac{U_0^2}{g\ .d_p\ .\rho_p^2} < 3\ X\ 10^{-4}\ m^6/kg^2 \tag{2.1}$$

$$\frac{K^*(d_p)}{\rho_g . U_0} = \left[4.31\ x\ 10^4 \left(\frac{U_0^2}{g\ .d_p\ .\rho_p^2} \right)^{1.88} \right] \quad when \quad \frac{U_0^2}{g\ .d_p\ .\rho_p^2} > 3\ X\ 10^{-4}\ m^6/kg^2 \tag{2.2}$$

The elutriation constant K(dp) is calculated from the elutriation rate constant K*(*dp*) as follows:

$$K(d_p) = \frac{K^*(d_p)}{H_{mf}\,(1-\varepsilon_{mf}).\ \rho_p} \tag{2.3}$$

Carbon utilization efficiency

The carryover rate, i.e. total particles/fines generated from the bed will be

Carry over rate = F_1 = elutriation rate $*$ total area of bed = [(g/cm^2 s) $*$ (cm^2)] = (gm/s)

$F_1 = K^*(d_p) *$ area of bed (gm/s) (2.4)

and the carbon carry over rate from the boiler = $F_3 = F_1$ x (percentage of carbon in fly ash)

Carbon utilization efficiency = $\frac{F_0 - F_3}{F_0}$ x 100 (2.5)

2.2 Modeling and Numerical Simulation

Natarajan et al. [113] in this study provided an overview of previous works on combustion and gasification of rice husk in atmospheric bubbling fluidized bed reactors.

He explained how low bulk density, poor flow characteristics and low ash melting point made the other types of reactors like grate furnaces and downdraft gasifiers either inefficient or unsuitable for rice husk conversion to energy, the fluidized bed reactor seemed to be the promising choice. The overview shows that the reported results are from only small or lab scale units. It is also found technically feasible to gasify rice husk in a fluidized bed reactor to yield combustible producer gas, even with sufficient heating value for application in internal combustion engines. A combustible gas with heating value of 4–6 MJ/Nm at a rate of 2.8–4.6 MW/m^2 has been found possible. Only very little information is available on the pollutant emissions in combustion and tar emissions from gasification. The major conclusion is that the results reported in the literature are limited and vary widely, emphasizing the need for further research to establish suitable and optimum operating conditions for commercial implementations.

Bittanti et al. [114] presented a nonlinear lumped parameter model of a bubbling fluidized bed in this study. Furthermore, it has been found that the model can be successfully used to estimate the total carbon load based on an easily accessible plant variable, namely the bed temperature.

Armesto et al. [98**]** performed an experimental combustion work using the rice husk as fuel in a 30 kW atmospheric bubbling fluidized bed pilot plant of CIEMAT. The influence of different variables such as temperature, fluidization velocity on the combustion efficiency and CO emissions has been investigated in this study. Combustion efficiency in all test runs has been found higher than 97%. The characteristics of ash removed from the bed, cyclones and bag house have been also studied which showed that in the bed ashes, the potassium content increased along the operation hours.

Dixon et al. [115**]** in this study summarized a wide range of ongoing applications of CFD in the sugar industry. Principal among these have been the development of

bagasse combustion technologies and understanding the processes involved in bagasse combustion and steam generation. Typical areas of application have included particle erosion, corrosion and heat transfer in tube bundle units, particle drying, ignition and burnout dynamics, the development of advanced boiler designs and CO and NOx pollutant generation and reduction. Another applications of CFD that have been summarized include the modeling and design upgrading of evaporators, capacity and design improvements including stirrer retrofits to vacuum pans used in sugar crystallization and the development of bagasse gasification technology for advanced power generation.

Pennisi et al. [116] presented a numerical model for the single-phase fluid flow of a sugar mill evaporator vessel. The model incorporated the effect of temperature and sugar concentration on the fluid properties. The evaporator including vertical heating tubes have been modeled through a momentum source term in three directions. The predictions showed reasonable agreement with the measurements taken from the actual vessel.

Ghenai and Janajreh [117] performed CFD analysis of the effects of co-firing biomass in this study. Coal/biomass co-firing is a complex problem that involves gas and particle phases, along with the effect of the turbulence on the chemical reactions. The CFD analysis included the prediction of volatile evolution and char burnout from the co-pulverized coal/biomass particles along with the simulation of the combustion chemistry occurring in the gas phase. The mathematical models consisted of models for turbulent flow (RNG k–e model); gas phase combustion (two-mixture fractions/PDF model); particles dispersion by turbulent flow (stochastic tracking model); coal/biomass particles devolatilization (two competing rates Kobayashi model); heterogeneous char reaction (kinetics/diffusion-limited rate model); and radiation (P-1 radiation model). The coal used

is a Canadian high sulfur bituminous coal. The coal was blended with 5–20% wheat straw (thermal basis) for co-firing. The effect of the percentage of biomass blended with coal on the flow field, gas and particle temperature distribution, particles trajectories and gas emissions (CO_2 and NOx) are presented. The coal used in this study is a Canadian high sulfur bituminous coal. The wheat straw was blended with the coal with a proportion of 10% and 20% thermal basis. The velocity vectors showed the presence of four re-circulation zones produced by the four tabs placed inside the furnace. These vortices helped to mix efficiently the coal or coal/biomass particles and consequently to increased the combustion efficiency. The results showed a reduction of NO and CO_2 emissions when using co-combustion of biomass with coal. The reduction of the pollutants emission depends on the proportion of biomass (wheat straw) blended with coal. An increase of the mass fraction of wheat straw blended with coal will result in a net decrease of the concentration of NO and CO_2 at the exit of the furnace. The results obtained in this study show the benefit of co-combustion of biomass with coal in reducing traditional pollutant (NOx) and net greenhouse gases (CO_2) emissions.

Zhou et al. [118] used the discrete element method-large eddy simulation (DEM-LES) to model coal combustion at the particle level in a bubbling fluidized bed. The gas phase has been modelled as a continuum and the solid phase has been modeled by DEM. Chemical reactions consist in the heterogeneous reactions of char with O_2, CO, CO_2, NO, and N_2O, and in the homogeneous reactions involving CO, O_2, NO, and N_2O. The colliding particle–particle heat transfer is based on the analysis of the elastic deformation of the spheres during their contact. The model predicted the effects of the particle heterogeneous flow structure on the thermal characteristics of coal particles when heating and burning, and the gaseous emissions from a fluidized sand–coal binary mixture. The instantaneous contribution of the collision heat transfer has been found less than 5% of

the total power exchanges (coal combustion, radiation, convection and collision) during the heating and 1.5% during the combustion. The temperature of the coal particles exceeded the bed temperature, which was in qualitative agreement with experimental data from literature. The effects of the diameter of coal particles, of the bed temperature, and of the inlet gas velocity on the thermal characteristics have been also studied. Singh et al. [119] studied environmental assessment, a model for exit gas composition, agglomeration problem and another model for solid population balance of 10 MW power plant at Jalkheri, Distt. Fatehgarh Sahib, Punjab, India based on rice husk. Three phase multistage mathematical model for exit gas composition of rice husk in fluidized bed has been derived. The model is based on three-phase theory of fluidization and material balance for shrinking rice husk particles and it is similar to model developed by Kunii and Levenspiel. The burning of rice husk is assumed to take place according to single film theory. The model has been used to predict the exit gas composition particularly O_2, CO_2 and N_2. The agglomeration problem of above plant which is main reason for defluidization of bed has also been discussed. SEM of ash agglomerates has been done. Ash samples taken from the above 10 MW power plant at Jalkheri has been quantitatively analyzed. Finally solid population model has been formed to calculate bed carbon load and carbon utilization efficiency. Above mentioned models have been experimentally correlated with the data collected from the above 10 MW power plant at Jalkheri, Distt. Fatehgarh Sahib, Punjab, India. All the results from the model for rice husk have been found within the permissible limits.

Ravelli et al. [120] described the (CFD) modeling as an effective means of analysis and optimization of energy-conversion processes, even to fluidized bed combustion of refuse-derived fuel (RDF). This overview has been divided into three main parts. In the first one, after a brief introduction to the fluidized bed hydrodynamics, the

phenomena taking place during fluidized bed combustion of solid fuels have been explained, with particular interest in drying, devolatilization and char oxidation. Differences in combustion between conventional and alternative fuels have been highlighted so as to fully characterize the RDF behavior in the bed. In the second part, a review of one-dimensional and multidimensional models, applied to the fluidized bed and conventional combustors, have been analyzed in order to emphasize what has already been done and what remains to be done.

In the last section, a numerical model of a bubbling FBC fed by RDF has been presented. The calculation of mass and energy fluxes entering from the bed into the freeboard provided the boundary conditions for the subsequent CFD analysis. In the freeboard model, implemented by means of the commercial code Fluent 6.1, the two mixture-fraction-pdf approach has been employed to track both the gases coming from the bed and the solid fuel particles that do not burn in the bed but above it. The freeboard operation has been simulated consistent with two conditions representing the combustor minimum and maximum load. The comparison between the predicted and the experimental data were found in agreement.

Wankhede and Adgulkar [121] presented an Eulerian CFD model of heat transfer from the immersed body in a two dimensional fluidized bed varying the gas velocity in the range of u/u_{mf} from 5 to 15. The study provided a comparison for the groups A, B & C for the heat transfer in the fluidized bed varying the u/u_{mf} from 5 to 15. For group A material the heat transfer coefficient has been found drastically varying with the gas velocity. The variation of heat transfer coefficient for group B with u/u_{mf} has been found linear. Group C, because of cohesive nature showed increase in heat transfer coefficient between 5 to 10 u/u_{mf} and a decrease for upper position.

Singh et al. [122] divided the study in to into two parts; in first part review of CFD applied to the various types of boilers based on biomass fuels/alternative fuels has been presented. In second part CFD analysis of fluidized bed boilers based on rice husk considering the rice husk based furnace has been discussed. The Eulerian multiphase model has been used for fluidized bed. Fluidized bed has been modeled using Fluent 6.2 commercial code. The effect of numerical influence of bed superheater tubes has also been discussed.

Wang et al. [123] combined numerical simulation and experiment to study a self-making small-scale fluidized bed reactor. Different fluidized velocities have been selected to examine its uniformity; different packing heights have been set to examine the influence of critical fluidized velocity on particles; different particles have been filled to test its fluidized property, and then to select the best inert support; different parts of furnace have been installed with heating device to simulate its temperature field, all these numerical calculus and the experimental results have been matched. The results indicated that the Fluent software can be in good simulation to the mobility of particles in the small-scale fluidized bed reactor. The reactor can be used for the further thermal state experiment device.

Rozainee et al. [124] applied (CFD) modeling technique to determine the trajectories and residence time of burning rice husk particles in the fluidized bed combustor (FBC) at different secondary air flow rates. In FBC, the intra and extra-particle mass transfer resistance of the oxidizing agent plays a major role in determining the combustion rate because of high temperature processing. The factors such as turbulence and retention time which determine the reaction rate and difficult to find experimentally have been found with CFD analysis. The modeling results offered significant insights into

the trajectory and mass loss history of the rice husk particle combustion. The actual experimental results also showed agreement with the modeling results.

Hamzehei et al. [125] studied heat transfer and hydrodynamics of a two-dimensional nonreactive gas-solid fluidized bed reactor experimentally and computationally in this paper. A multifluid Eulerian computational model incorporating the kinetic theory for solid particles coupled with the *k-ε* turbulence model has been developed and used to simulate the heat conducting gas-solid flows in a fluidized bed configuration. Momentum exchange coefficients have been evaluated using the Syamlal-O'Brien, Gidaspow, and Cao-Ahmadi drag functions. Temperature distributions of different phases in the reactor have been also computed. Good agreement is found between the model predictions and the experimentally obtained data for the bed expansion ratio as well as the qualitative gas-solid flow patterns. The simulation and experimental results showed that the gas temperature decreased as it moves upward in the reactor, while the solid particle temperature increased. Pressure drop and temperature distribution predicted by the simulations were in good agreement with the experimental measurements at superficial gas velocities higher than the minimum fluidization velocity. Also, the predicted time-average local voidage profiles were in reasonable agreement with the experimental results. The study showed that the computational model was capable of predicting the heat-transfer and the hydrodynamic behavior of gas-solid fluidized bed with reasonable accuracy.

Guodong et al. [126] studied gas-particle two-phase turbulent flows in a 50 MW circulating fluidized bed combustor. The dense flow of particles has been modeled by the frictional stress models adopted from solid mechanics theory and the dilute flow in the so-called rapid granular flow regime has been modeled from the kinetic theory of granular flow. At low concentrations the viscosity due to the effect of the presence of particles was

modeled by means of a semi empirical viscosity for fluidized catalytic cracking particles. The distribution of the velocity and concentration of particles in a circulating fluidized bed combustor has been predicted. Simulations indicated that the dense regime with a high concentration of particles remained in the bottom part and the dilute regime with a low concentration in the upper part of the furnace.

The effect of secondary air on the flow behavior has been analyzed and the penetration length of the secondary air jet has been computed in a 50 MW circulating fluidized bed combustor.

Al-Abbas et al. [127] in this paper has performed a CFD modeling study of the Victorian brown coal combustion in a 550 MW utility boiler under the air-fired and three oxy-fuel-fired scenarios. The air-fired firing case was modelled based on the real life operating conditions of Loy Yang, A power plant located in the state of Victoria/Australia. This study of oxy-fuel combustion in a large-scale tangentially-fired boiler is important prior to its implementation in real-life power plant. The multi-step chemical reaction mechanisms were carried out on the pulverized lignite particles. The simplified approach of the chemical kinetics has been modelled to calculate the fuel and the thermal NO formation. The predicted results showed a reasonably good agreement against the measured data.

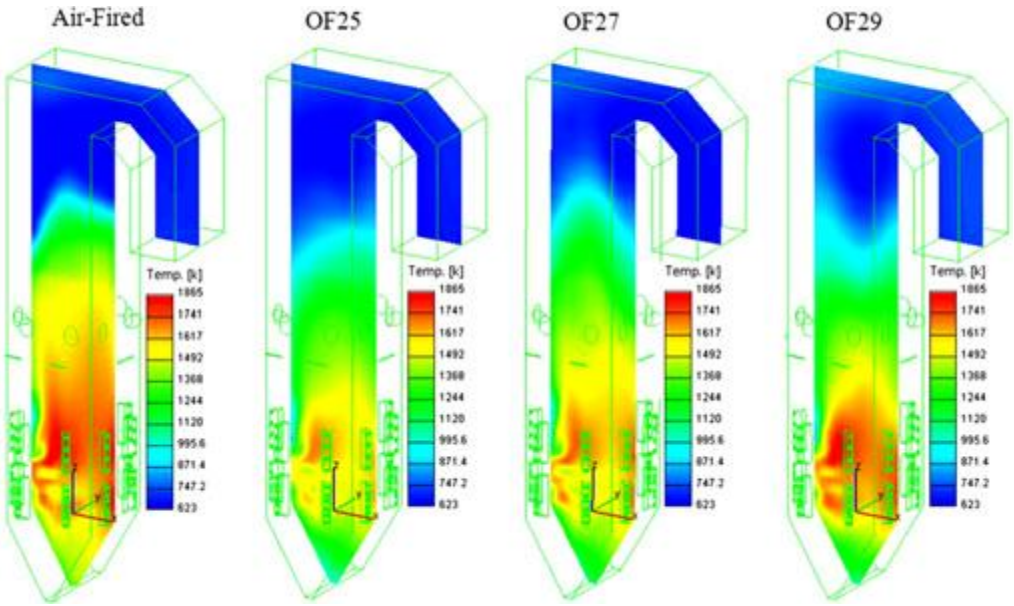

Fig. 2.2. Distributions of the flue gas temperature (K) along the height of the furnace at the mid cut (X–Z plane) for air-fired, OF25, OF27, and OF29 combustion cases.

Oxy-fuel combustion mode can potentially provide significant opportunities for near-zero emissions from the existing and new build power plants. In this study, a commercial CFD code, AVL Fire ver.2008.2, has been modified to investigate the Victorian brown coal combustion in a 550MW tangentially-fired boiler under different combustion media. Several mathematical models such as coal devolatilization, char burnout, combustion chemistry, convection and radiation heat transfer processes, carbon in fly-ash, and thermal and fuel nitric oxides models were developed through subroutines and added to the CFD calculations. The available experimental data [128] were used to validate the predicted results under air-fired condition, a good agreement is achieved. The oxyfuel combustion approach adopted in a 100 kW facility unit was applied to the present large-scale furnace in three O_2/CO_2 mixture conditions, namely OF25, OF27, and OF29. As the compositions of feed oxidizer gases are replaced from O_2/N_2 to O_2/CO_2 mixtures, significant changes in the combustion characteristics were observed. In the OF25 and OF27 combustion scenarios, a clear reduction in the gas temperatures was noticed compared to the reference firing case. In contrast, OF29 case showed similar gas

temperature levels and radiative heat transfer to that of the air-fired case. This is due to augmenting the residence time of coal particles and oxygen concentrations in the gas mixture.

For all oxy-fuel combustion cases examined, lower gas temperatures levels were observed in the hopper region compared to the air-fired case due to availability of O_2 in the latter combustion case, which also led to increased burning rate of residual char. The higher CO_2 concentrations in the oxy-fuel cases significantly affected the pyrolysis process of coal particles and thus resulted in an increase in the carbon in fly-ash. A remarkable decrease in the NOx formation was observed because of the elimination of thermal NO process from the oxy-fuel combustion scenarios, as well as low nitrogen content and higher H_2O concentrations in the raw brown coal. In the furnace zone, the CO concentrations in oxy-fuel cases gradually increased with oxygen concentrations, and made a chemical equilibrium with CO_2 based on the multi-step chemistry mechanism adopted in these investigations. Finally, the aerodynamic and thermodynamic conditions of OF29 combustion case are favorable, and closely matched the conventional combustion characteristics in several important areas in comparison with the other oxy-fuel-fired conditions.

Nikolopoulos et al. [129] in this paper presented a three-dimensional numerical investigation of a pulverized-fuel, tangentially fired utility boiler located at Florina/Greece under air, partial and full oxy-fuel conditions. The results for temperature distributions, wall heat flux and particle trajectories were obtained at different planes for different case.

The temperature distributions in the cross sections I, II and III for all cases are shown in Fig. 2.3. The temperature of the flue gas is relatively high in the central part of each section, where combustion mainly takes place. The temperatures of the primary and

secondary inlet gas injected from the burners and re-burners are equal to 493K and 578K and it increases up to a maximum average along the boiler's height temperature of 1527K for case A, 1577K for case B and 1604K for case C in the central part of the boiler. Section's I core is characterized by higher temperatures for cases B and C (case A: 1393K, case B: 1458K, case C: 1414K) in contrast to case A. Furthermore, in Case C, section I is characterized by lower temperatures in its central part against the periphery of the swirling flow, Fig. 2.3. The pattern of the flue gas temperature is changing along the height of the burner. Regarding section II, its mean temperature is higher than that of section I due to the additional burning of coal particles from the re-burners, whilst the core temperature is increasing for cases A and B in contrast to case C (Fig. 2.3).

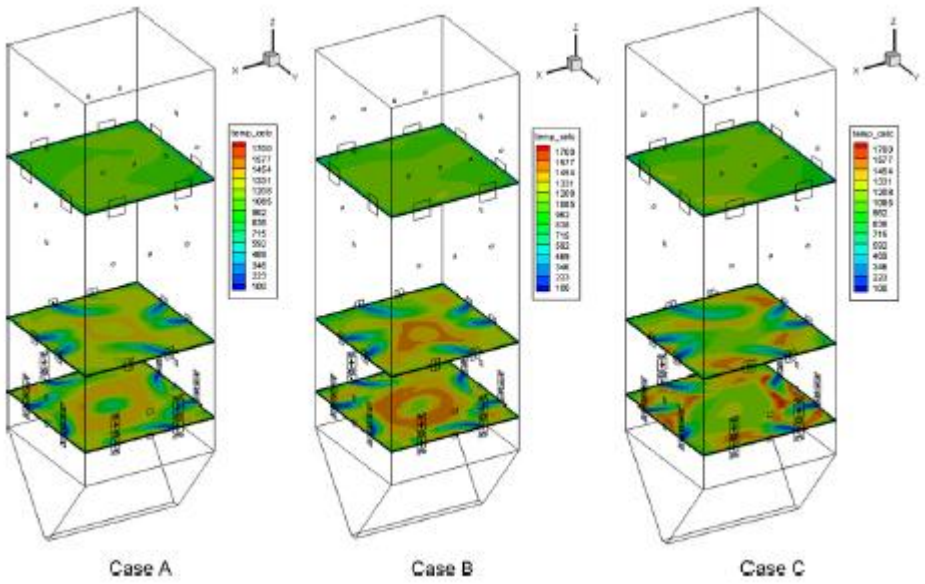

Fig. 2.3: Temperature distribution in different cross sections (a) passing from the main burners (1st row), (b) passing from the re-burners and (c) passing from the recycled flue gas stream

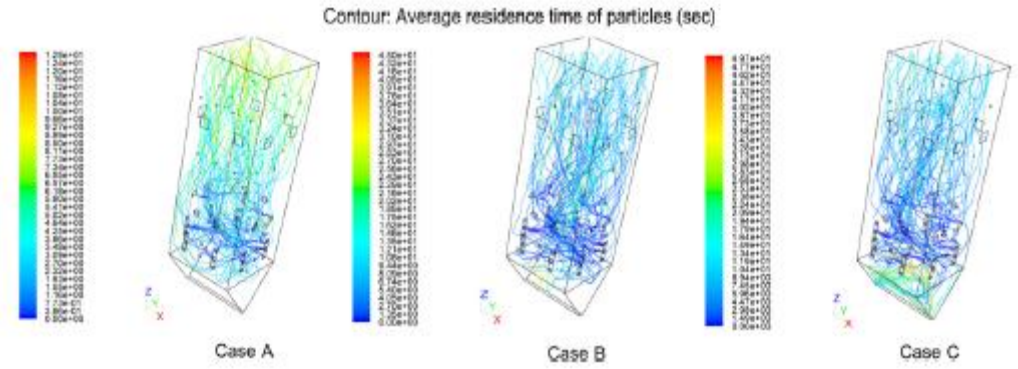

Fig. 2.4. Particle trajectories colored by its residence time inside the boiler for cases A, B and C

The streamlines of the lignite particles trajectories are shown in Fig. 2.4. These trajectories demonstrate a very complicated flow with a three-dimensional character, promoting the mixing of the gas with the lignite particles and increasing the residence time for the particles and thus enhancing the heat transfer via bulk motion. The fuel particles trajectories do not coincide with the corresponding gas streamlines, due to the large differences both in density and turbulent fluctuations. In case A, the lignite particles initially circulate clock wisely in sections I (main burners) and II (re-burners) and eventually travel up through the high-temperature and high swirling-flow region induced in the central region of the furnace, towards the boiler's exit. As a result, the residence time for all cases is shorter for the particles injected from the re-burners than from the main burners. For case A, the maximum mean residence time of the coal particles is equal to around 13s, for case B equal to 45s and for case C equal to around 50s. Overall, the mean maximum residence time is almost doubling from case A to case C.

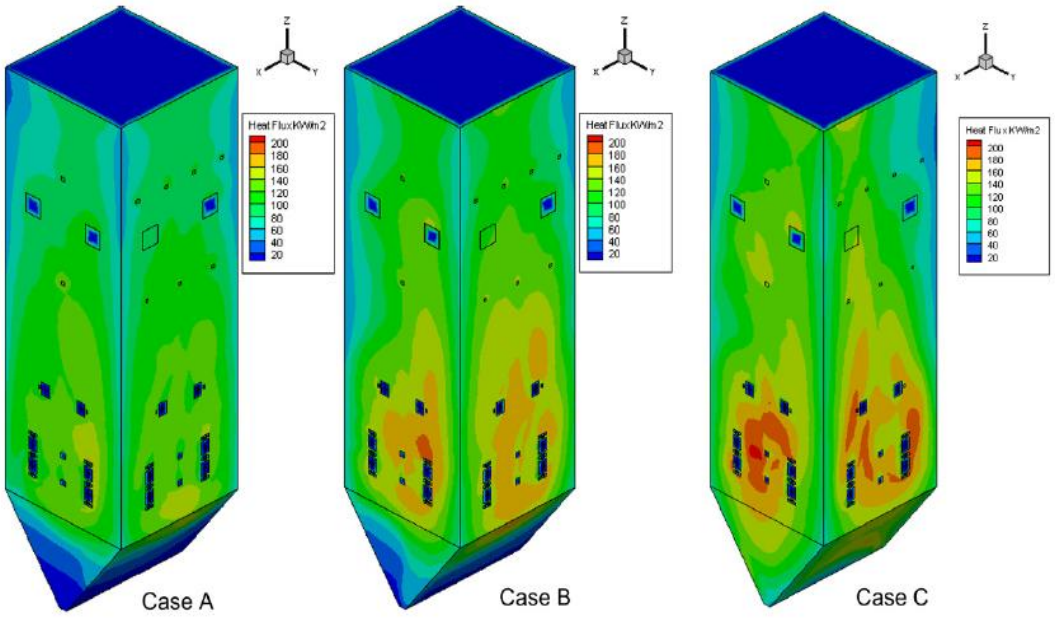

Fig. 2.5. Wall total heat flux

In all three cases, the wall temperature and the emissivity coefficient were kept constant (660K and 0.7, respectively). Therefore, Surface Incident Radiation (SIR), which is proportional to heat transferred to the steam, can act as an indicator when comparing air and oxy-fuel cases. The distribution of the total wall heat flux as well as the ratio of SIR to the total flux for all cases is shown in Fig. 2.5. In oxy-fuel conditions the total wall heat flux is increasing (case A: 326.9 MW, case B: 374.4 MW, case C: 418.5 MW). A similar trend is confirmed by the numerical work of Erfurth et al. [130] and the experiments by Tan et al. [131] for oxy-fuel conditions above 27% as in the present case (30%).

Dixon et al. [132] studied major advances in the development of bagasse combustion technologies and understanding the many processes involved in bagasse combustion and steam generation. CFD modeling has come to form an integral and critical part of this progression. The experience with CFD in the sugar industry through Sugar Research Institute has encompassed the full range of applications from fundamental code development, through the generation and commercialization of new ideas and technologies, to the resolution of practical plant problems.

The paper summarizes the numerous applications where author has achieved successful results utilizing CFD. It is demonstrated that the benefits of CFD in the commercial outcomes, for new technologies and the solution of operating plant problems, are achieved by the close interaction between the code development and validation via full scale plant simulation. This two-way interaction enhances the code fundamentals by focusing on practical issues and similarly increases the confidence in the capabilities and accuracy of the CFD predictions. Major advances have been made in the development of bagasse combustion technologies and understanding of the many processes involved in bagasse combustion and steam generation over 20 years. CFD modeling has come to form an integral and critical part of this progression. The experience with CFD in the sugar industry through SRI has encompassed the full range of applications from fundamental code development, through the generation and commercialization of new ideas and technologies, to the resolution of practical plant problems. It is required to the applicability of CFD that regular and routine validation with full scale plant data is undertaken.

The two-way interaction between development and application enhances the code fundamentals by focusing on practical issues and the need to resolve these effectively. In some cases the physical size of the problem areas that are being investigated, within a commercial plant environment, can be very small. Sugar Research Institute (SRI) now regularly applies CFD modeling to a wide variety of flow and combustion related areas as routine investigation by and design tool. It has been surprising to SRI that there remains a continuing doubt of the capabilities and value of CFD modeling to plant design and process understanding in the sugar industry by both plant operators and equipment vendors.

Ma [133] in this paper presented a CFD model that predicted the combustion of typical wood fuel in an industrial pf furnace. The key combustion processes have been modeled in detail with an Eulerian–Lagrangian approach. Models for NOx formation and the potassium species release have been developed. The potassium together with the overall volatile release is modeled using a single rate kinetic model which gives off most of the volatile at 700 – 1000 K and this matches well with the temperature regimes where potassium species are released. A potassium concentration of about 7 ppm has been predicted in the exit plane of the furnace which also falls into the typical regions of measured potassium release in the experimental investigations. Good agreement between the predicted and the measured furnace temperature and concentrations of CO_2 and NOx has been achieved. The modeling of potassium release makes it possible to calculate both the potassium concentrations in the gas flow and the remaining potassium in the biomass ash thus paving the way to the development of the advanced ash deposition models for the combustion system.

Syred [134] described the evolution of a fragmentation model for the combustion of coal and coal/biomass blends and its application to cement plant pre-calciners, cyclone gasifiers and a 500 kW furnace. It is clear that fragmentation models are necessary if accurate understanding of the paths of burning particles in coal burning plants is needed. The routines here have been initially developed for application to cement plant pre-calciners, where fine raw cement meal (dolomite and similar cementations materials) are devolatilized (to give CaO) as an initial part of the cement making process. Typical temperatures are of order 1300K with a 10 step reaction scheme using the Fluent finite rate eddy Dissipation model. This modeling combination gave good results on the modeled pre-calciner and has subsequently been extended to work on other cement plants. The inception of this work arose from studies of non slagging cyclone combustors,

where two-dimensional CFD studies showed that conventional lagrangian tracking schemes for particles in cyclone combustors retained too many particles, giving far too high burnout, retention of particles and too high temperature levels, when compared to experimental data. The more up to date model, developed by Kurniawan [135] for pre-calciners has been applied to a two stage cyclonic combustor system and has been shown to give better results than the conventional coal combustion model. However, the fragmentation model of Kurniwan [135] appears to underestimate the level of fragmentation in this device, probably due to the higher temperature level compared to pre-calciners and impaction of devolatilized, possibly already fractured/cracked particles on the walls. The final application of the model has been to a downwards firing 500 kW coal fired furnace, where better predictions of particle deposition on a deposition probe can be obtained by the use of this model.

This model has been used with the finite rate/eddy dissipation combustion model, with a 10 step reaction mechanism; this combination has worked well and usually brings the maximum predicted temperature levels closer to those measured. Each case has been tested has been run with the standard Fluent particle combustion model, and then with the fragmentation model with fragmentation switched off. Typical discrepancies are from 0.1% to 0.5%. A major problem is that very little data exists for final particle size distribution.

Werther et al. [136] in this paper discussed several issues concerning the combustion of agricultural residues. The objective was to give more information related to the effect of the physical and chemical properties of the residues on their processing as well as the combustion and emission characteristics. The paper briefly discussed:

- The process of densification of agricultural residues as a prerequisite for transportation, feeding and combustion of the residues in some furnace designs.

- The effect of the high volatile matter contents of the agricultural residues on the combustion process.
- The problems related to low melting points of the ash of some agricultural residues such as slagging, fouling, corrosion and agglomeration.
- The emission characteristics of agricultural residues.
- The design of combustors fired with agricultural residues and finally.
- The possibility of co-firing the agricultural residues with coals.

The following conclusions were drawn from the discussions:

1. The bulk densities of most agricultural residues are low. Therefore densification may be required for effective transportation, storage and firing. However, densification increases the fuel cost. It is therefore more economical to use the residues near the point of generation, in which case densification may only be considered with respect to firing, i.e. to enable easier feeding and a more efficient combustion process. The decision to densify would therefore depend on the type of residues and the local situation. Some residues such as coffee husks and coconut shells may not need densification if they are fired on site. Others such as straw must be baled or milled and fed into the furnace pneumatically. Rice husks, on the contrary, can be fed pneumatically into the furnace.
2. Agricultural residues are characterized by high contents of volatile matter. Devolatilization has been found to start at very low temperatures and the volatiles released consist mainly of combustible gases such as CO, H_2 and C*x*H*y*. Consequently volatile release and combustion are very important considerations for the design and operation of combustion systems for agricultural residues. This is particularly important in relation to the choice of the fuel feeding system and the distribution of combustion air. The combustion system can easily be upset if

constant fuel feeding is not guaranteed. Intermittent fuel feeding leads to variations in the production of volatile products and in excess air conditions, both tending to cause smoke formation as a result of incomplete combustion. To reduce the rate of incomplete combustion due to the escape of the volatiles from the combustion zone, the combustion system should be designed to allow two-stage combustion. In the first stage, mainly devolatilization and gasification would take place. The gases formed can then be completely burnt in the second zone. The combustion air should thus be distributed between the two zones depending on the volatile matter content of the material.

3. A major difficulty related to the firing of some agricultural residues is the low melting point characteristics of the ash. This property of the residues poses serious design and operation problems. These include agglomeration, fouling, slagging and corrosion. It is therefore important that the analysis of the ash characteristics should be the first step in choosing the combustion system and combustion conditions of a given agricultural residue. Here again, two stage combustion may provide a solution in the design of the combustion system. In the first stage, the process of gasification may be carried out at low temperature and a significant quantity of the ash may be removed below the grate. The configuration of the furnace should be such as to promote the removal of the ash from the flue gas. Through application of secondary air in the second combustion stage, the complete combustion of the escaping combustibles can then take place in an atmosphere with less ash. Coupled to such design considerations, the use of additives should be considered.
4. Due to the high contents of volatile matter and the low particle densities of the agricultural residues as well as the need to operate at temperatures below the

melting points of the ash, high concentrations of the unburnt pollutants as well as ash may be expected in the flue gas. However, it is possible to control these pollutants by adopting a suitable furnace design and by application of staged combustion. The contents of N and S are relatively low for agricultural residues so that low emissions of SO_2, NO*x* and N_2O may be expected. However, the combustion of some residues may lead to higher emissions of NO*x*. In such cases NO*x* emission reduction techniques which have been found useful during the combustion of wood or related biomass, may be applied to the combustion of agricultural residues.

5. Where coal power plants exist within the residue production regions, an economical way of tapping the energy from the residue would be co-firing. The combustion and emission characteristics are not negatively affected during co-combustion. However, further developments and research is still needed with respect to burner design, fuel processing and the problems of fouling, slagging and corrosion.

Sami et al. [137] in his work reviewed literature on co-firing of coal with biomass fuels. Here, the term biomass includes organic matter produced as a result of photosynthesis as well as municipal, industrial and animal waste material. Brief summaries of the basic concepts involved in the combustion of coal and biomass fuels are presented. Different classes of co-firing methods are identified. Experimental results for a large variety of fuel blends and conditions are presented. Numerical studies are also discussed. Biomass and coal blend combustion is a promising combustion technology; however, significant development work is required before large-scale implementation can be realized. Issues related to successful implementation of coal biomass blend combustion are identified.

Coal and biomass fuels are quite different in composition. Co-firing biomass fuels with coal has the capability to reduce both NO*x* and SO*x* levels from existing pulverized coal fired power plants. In addition, overall CO_2 emissions can be reduced because biomass is a CO_2 neutral fuel. The co-firing programs carried out in the United States and Europe have demonstrated that co-firing biomass with coal in large utility boilers can be beneficial to the utilities as well as to the environment. Co-firing may also reduce fuel costs, minimize waste and reduce soil and water pollution depending upon the chemical composition of the biomass used.

Co-firing technology, however, faces some technological problems. First, the issue of combustor fouling and corrosion due to the alkaline nature of the biomass ash needs attention. Ash deposits reduce the heat transfer and may also result in severe corrosion at high temperatures. Compared to deposits generated during coal combustion, deposits from biomass materials are denser and more difficult to remove. Second, the maximum particle size of a given biomass that can be fed to and burned in a given boiler through a given feeding mechanism requires additional studies. However, this issue is a combination of economics, and combustion characteristics and more work needs to be done in this area. Third, practical pulverizer performance needs to be examined. Biomass fuels may require separate pulverizers to achieve high blend ratios and good combustion performance. Since biomass fuels have lower heating value compared to coal, blend flow rate has to be increased in order to have a heat throughput same as in coal-only case.

Fundamental combustion studies must be performed, particularly for pre-mixed coal and biomass fuel blends, in order to determine combustion behavior characteristics in controlled laboratory settings. Interaction between biomass and coal particles during combustion is an area of study. The results of this basic research will aid in the design and optimization of practical coal and biomass blend facilities. Despite all the issues and

concerns, coal biomass blend combustion appears to be a promising combustion technology for electric utilities. Co-firing has moved from engineering studies to parametric tests to long-term demonstrations. Future long-term demonstrations will address many of the issues mentioned above and will help in making the co-firing technology easily available to the industry at an optimal cost.

Hupa [138] investigated that more than half of the recent large-scale FBC installations are designed to burn more than one fuel. Especially the use of various biofuels besides conventional fuels is becoming more and more common in the new FBC projects. It is a major challenge to be able to understand and predict the behavior of the FBC system when co-firing of different fuels in different proportions. This paper reviews some of the recent research on the fuels interaction in FBC. It is shown that factors such as flue gas emissions, fouling tendency or bed sintering tendency are seldom simple linear functions of the fuel mixture. Rather, non-linear relationships of some kind are much more common. The examples in the paper deal with gaseous emissions in co-firing of wood and coal, and superheater fouling in co-firing of biomass based fuels with very different ashes. Firing of several solid fuels together has always been considered to be an advantage of FBC boilers. However, some fuel mixtures show surprising behaviors and there is a lot of interesting research to be done to more quantitatively establish the influence of the fuel mixture on the key operating parameters, such as boiler efficiency, flue gas emissions, the behavior of ashes, or the corrosion. Many times the only way to learn about the firing properties of fuel mixtures is to test the fuel mixture in a pilot plant or full-scale boiler. These kinds of tests are naturally highly important, but also difficult to perform in a way, which allows for clear conclusions to be drawn. Without fundamental understanding of the behavior of fuels in mixed-firing, the pilot plant results are difficult to extrapolate to other conditions or fuel mixtures. Obviously, mixed-fuel

firing is a big opportunity and challenge for the more fundamental research. Fuel analysis techniques should be improved to give more information of the behavior of the fuels also when they are burned in mixtures. Fluidized bed combustion and emission modeling should be extended to give at least some qualitative understanding also of mixed fuel firing. Fuel ash forming matter characterization should be able to differentiate between the different ash constituents in such a way that mixed fuel effects could be predicted.

Scala et al. [95] presented a model of an atmospheric bubbling fuidized bed combustor operated with high-volatile solid fuel feedings (Fig. 2.6). It aims at the assessment of axial burning profiles along the reactor and of the associated temperature profiles, relevant to combustor performance and operability. The combustor is divided into three sections: the dense bed, the splashing region and the freeboard. Three combustible phases are considered: volatile matter, relatively large non-elutriable char particles and 3ne char particles of elutriable size. The model takes into account phenomena that assume particular importance with high-volatile solid fuels, namely fuel particle fragmentation and attrition in the bed and volatile matter segregation and post combustion above the bed. An energy balance on the splashing zone is set up, taking into account volatile matter and elutriated fines post combustion and radiative and convective heat fluxes to the bed and the freeboard.

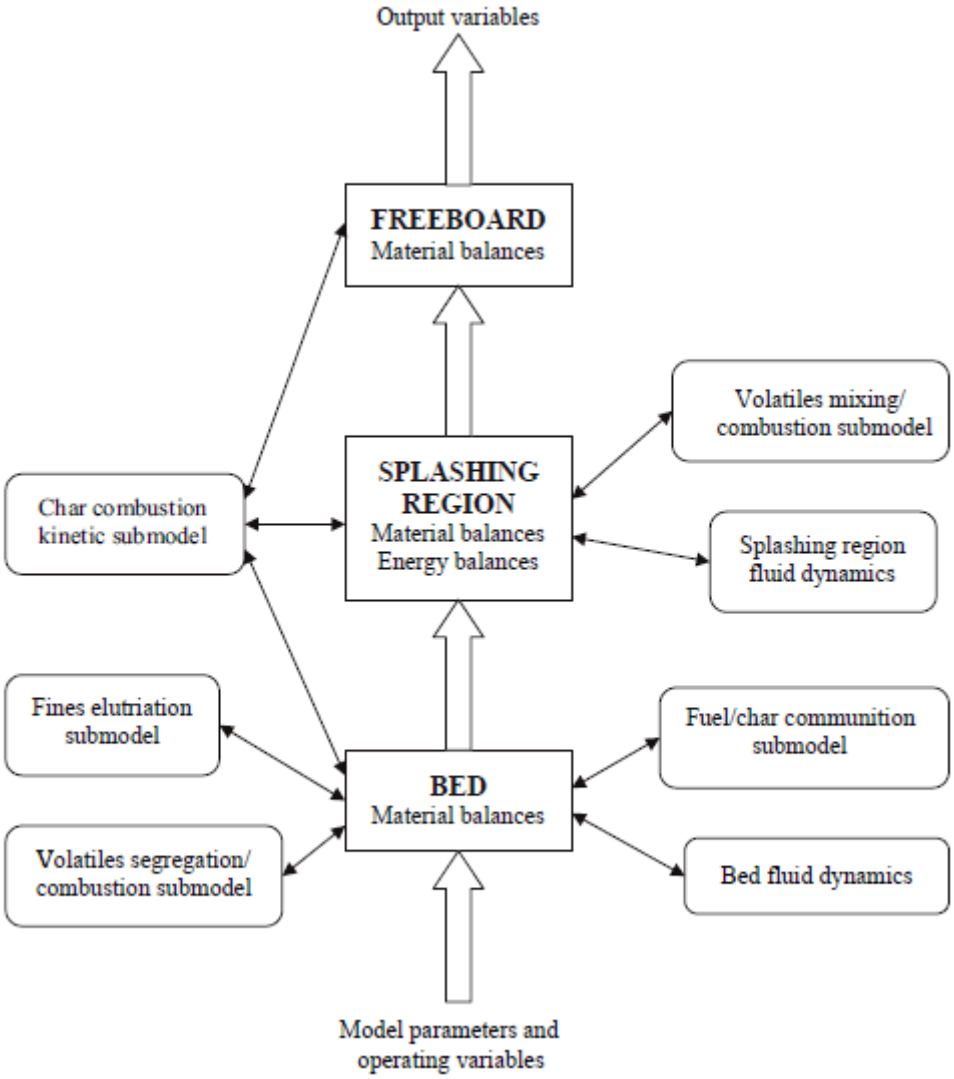

Fig. 2.6. Flow diagram of the model [95]

A specific feature of the model is that it takes into account the important processes of fuel particle fragmentation and attrition and of volatile matter segregation with respect to the bed followed by afterburning in the splashing region and/or in the freeboard. Despite the simple modeling approach, results confirm the criticality of these aspects, often disregarded in previous models, with respect to axial burning profiles along the reactor and associated performance and operability of the reactor. The model has been applied to the prediction of the performance of a combustor operated with either under-bed or over-bed feeding of a high-volatile biomass fuel. Results indicate that volatile matter segregation with respect to the bed and subsequent post combustion in the

splashing region are extensive in either case. Significant heat release occurs in this region, comparable to that relative to the bed section. However, extensive bed solid s recirculation associated to bubble bursting/solids ejection at the bed surface together with effective gas–solids heat transfer promote thermal feedback from this region to the bed. These phenomena keep the temperature in the splashing region within typically 40–50^{0}C above bed temperature.

Parameters like bed temperature, excess air, fuel feed size affect combustor performance in a predictable way. Moreover, gas superficial velocity and bed solid's particle size affect the combustor performance. Depending on the operating conditions, a significant fraction of the volatile matter may escape the splashing region unburnt. Altogether the issues of stratified combustion, of volatile matter mixing/segregation with the fluidizing gas and of fuel fragmentation/attrition emerge as key features in combustor modeling. Axial non-uniformities of burning intensity and temperature are simply and effectively addressed in the present model in the framework of an one-dimensional approach. The model represents a first step toward consideration of lateral, in addition to axial, non-uniformities, like those associated with uneven fuel spreading across the combustor, that call for a multi-dimensional description of the combustor.

Janvijitsaku and Kuprianov [139] addressed some common features and trends of the behavior of CO and NO along the height in a conical fluidized-bed combustor (FBC) firing rice husk and pre-dried sugarcane bagasse, and co-firing ‘‘as-received’’ rice husk with ‘‘as-received’’ sugarcane bagasse, for wide ranges of fuel properties and operating conditions, were summarized. Empirical models for predicting axial CO and NO concentration profiles in this fluidized-bed combustor were developed based on analysis and treatment of experimental results. Supporting correlations, including the effects of excess air, the bed temperature and fuel properties, were proposed for estimating the peak

of the CO concentration (CO_{max}) and NO concentration (NO_{max}) located in the reactor at a level of X_{COmax} and X_{NOmax} , respectively, above the air distributor. These models secured the computational error of ±25% for CO_{max} and ±20% for NO_{max}. Experimental dependencies of the relative gas concentration on the relative axial distance, CO/CO_{max} = f ($X=X_{COmax}$) and NO/NO_{max} = f ($X=X_{NOmax}$), were found to show an apparent similarity for all the fuels and firing options analyzed in this work, and could be, therefore, approximated by the fitting equations at R^2 = 0.74 - 0.90. With the proposed equations, CO and NO concentrations can be estimated for any arbitrary level (X) above the air distributor in the conical FBC, for the particular fuel properties and operating conditions.

Kaushal et al. [140] developed a one-dimensional steady state model of a riser to analyze the combustion of biomass char in circulating fluidized bed. The model is based on mass and energy balances. The model includes different sub-models that are linked together to describe the overall combustion process. The hydrodynamic sub-model highlights the physical characteristics of the bed material while the reaction sub-model deals with the chemical reactions in the different zones of the combustion chamber. The model is fuel flexible and offers the opportunity to evaluate different fuel types over wide range of composition both for solid and gases. Global reaction rates are used for the description of chemical kinetics. Model validations have been performed with measured results obtained at both 8 MW dual fluidized bed gasification plant at Guessing, Austria and with literature data on the 12 MW circulating fluidized bed boiler at Chalmers University (Sweden). The predicted trends are qualitatively compared with the published data [141,142] and it turns out that they are in fair agreement. The model predictions show that the gas composition varies significantly in the upper section above the secondary air injection. Simulation results also show that smaller size of wood or char favors the overall performance of the gasifier.

Madhiyanon et al. [143] in this study examined the combustion characteristics and performance of rice husks co-fired with coal in a short combustion-chamber fluidized-bed combustor (SFBC) with a 225 kW capacity. The experiments showed that co-firing in the FBC was feasible. Combustion efficiency (E_c > 97%) could be attained effortlessly despite tight combustor space, due to the effective positioning of the vortex ring. Nevertheless, taking hydrocarbon losses from the pertinent literature into consideration, the values of E_c were reasonably estimated to be 0.5–1.8% less than the current values. Blending ratio and k had no significant effects on E_c, for k > 1.6. The unburned carbon in the ash was a major contributor to decreasing E_c, especially with a high proportion of coal. The radial temperature profiles characterized swirl/vortex combustion of fuel particles descending along the combustor walls, whereas axial temperature profiles suggested vigorous combustion under the vortex ring. As regards emissions, 260–416 ppm NO_x (at 6% O_2) appeared somewhat high and failed to comply with Thai co-combustion standards (<280 ppm).

The comparatively great NO_x emissions arose from the high bed temperature (≈1000^{o}C); however, were comparable with bubbling FBCs. Although changes in the coal component had an immense effect on NO_x increases, occasionally the relationships were non-linear. In fact, operating conditions were crucial to NO_x development. NO_x formation can be lessened by either decreasing k, or bed temperature, a consequence of increasing k. The SO_2 emissions of 10–180 ppm (at 6% O_2) were considerably lower than Thai regulations (<236 ppm). The increases in SO_2 were contingent on, but not entirely proportionate with, the increases in the sulfur content of the fuel mix, due to increases in the coal proportion. CO increased with an increase in the coal fraction, and CO levels of 65–260 ppm (at 6% O_2) were desirable for Thailand standards (<740 ppm). Maintaining well acceptable combustion efficiency and emissions (except NO_x), the thermal

percentage of coal in the fuel mixture can reach 25% while the excess air ratio is suggested to be 1.76–2.20. Gas concentration profiles provided insights into the combustion characteristics and other essential conditions contributing to the development of gaseous species. The consumption of O_2 and production of CO further indicated that main combustion was carried within regions under the vortex ring. In addition, a reducing atmosphere – O_2 starvation and abundant CO – could decelerate NO_x evolution considerably. Ultimately, a large amount of CO was produced (>400,000 ppm) in the lower part of the combustor, while NOx was restricted to form; however, in the upper section, where O_2 conditions were favorable, a decrease in CO, and increase in NO_x and SO_2, were clearly evident.

2.3 Application of CFD in Biomass Gasification and Pyrolysis

Biomass gasification and pyrolysis are thermally degraded processes in insufficiency or absence of air/oxygen aiming at the production of solid (charcoal), liquid (tar/bio-oil) and gaseous products. The CFD models used to describe these processes have become an important analysis and design tool to achieve the flow and temperature pattern, the products concentration contour and yields. Table 2.2 summarizes some of the recent studies.

Fletcher et al. [144] developed a detailed CFD model to simulate the flow and reaction in an entrained flow biomass gasifier. The model is based on the CFX package and describes the phenomena of turbulent fluid flow, heat transfer, species transport, devolatilization, particle combustion, and gas phase chemical reactions. Biomass particulate is modeled via a Lagrangian approach as it enters the gasifier, releases its volatiles and finally undergoes gasification. Transport equations are solved for the concentration of CH_4, H_2, CO, CO_2, H_2O and O_2 and heterogeneous reactions between fixed carbon and O_2, CO_2 and H_2O are modeled. The model provides detailed information

on the gas composition and temperature at the outlet and allows different operating scenarios to be examined in an efficient manner. The initial calculations suggest that simulations to examine the effect of gasifier height and the steam flux in the upper inlets can be beneficial in process optimization. The simulation of sawdust gasification in one case gave an exit composition on a dry basis of 10% CO, 12% CO_2, 20% H_2 and 1.2% CH_4, compared with 16% CO, 14% CO_2, 10% H_2, 1% CH_4 measured in the experiments, the hydrogen generation was too high. The model with further validation against detailed experimental data, will aid with the design process of such gasifiers.

Gerun et al. [145] developed a 2D axisymmetric CFD model for the oxidation zone in a two-stage downdraft gasifier. The oxidation zone is crucial for tar cracking. The simulations fit satisfactorily to the experimental data regarding temperature pattern and tar concentration. Fig. 2.7 shows the temperature profile in the reactor. The heat of reaction is released mainly close to the injector. It induces a very hot zone in this area. The stream function is shown in Fig. 2.8a, whereas Fig. 2.8b presents the gas pathlines in the reactor. The gas path strongly depends on the initial departure point. The strong recirculation zone is located above the air injection in the centre of the reactor. It plays a major role in air–gas mixing and thus enhances the quality of the gasification. Table 2.2 lists the examples of CFD applications in biomass gasification and pyrolysis at present. The submodels used in these examples are summarized in the table.

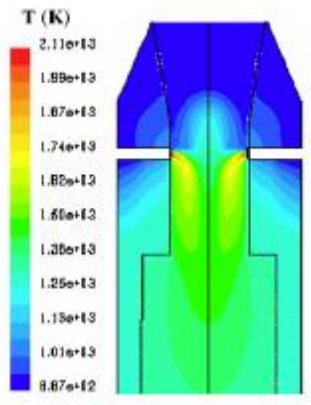

Fig. 2.7. Temperature profile in the reactor

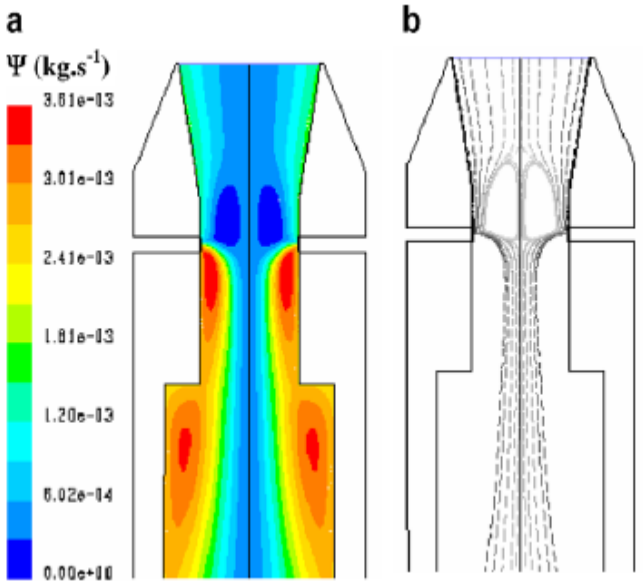

Fig. 2.8 Velocity profile in the furnace

Table 2.2. Implementation of CFD in biomass gasification and pyrolysis

Application	**Code**	**Dim**	**Aim/Outcome**	**Turb. Model**	**Extra Model**	**Agreement with Exp.**	**Authors**
Entrained flow gasifier [144]	CFX4	3D	Products mass fraction distribution; temperature contours; swirl velocity distribution	Std k - ε	Lagrangian	Acceptable	Fletcher, D. F
Two stage downdraft gasifier [145]	Fluent	2D	To investigate in detail the oxidation zone; temperature profile; velocity pattern; tar conversion mechanism study	RNG k - ε	DOM	Satisfactory	Gerun, L.
Horizontal entrained flow reactor [146]	Fluent	2D	Predictions of flow, temperature and conversion; sensitivity of the kinetic parameters of pulverized corn stalk fast pyrolysis	NA	Lagrangian	Reasonable	Xiu, S. N.
Cone calorimeter reactor [147, 148]	Code	3D	To model heat transfer and pyrolysis within dry and wet wood specimens, and the mixing and pilot ignition of the released volatiles	NA	Porous	NA	Yuen, R. K. K.
Moving	Fluent	3D	Detailed comparisons	Std	DOM	NA	Yang, Y.

packed bed [149]			between the combustion mode and gasification mode in a waste moving-grate furnace	k - ε			B.
Entrained flow gasifier [150]	CFX	2D	To model black liquor gasification, model parameters identification and sensitivity analysis	Std k - ε	Lagrangian	NA	Marklund , M.
Downdraft gasifier [151]	Code	3D	Temperature profile, pressure drop, model parametric analysis	NA	Porous	NA	Sharma, A. K.
Fluidized bed flash pyrolysis [152]	Code	3D	An integrated model proposed to predict wood fast pyrolysis for bio-oil	NA	Radiation	Good	Luo, Z. Y.

It plays a major role in air–gas mixing and thus enhances the quality of the gasification.

2.4 Application of CFD in Biomass fired and Co-Fired Combustors

The largest application of CFD models has been to power station boilers and furnaces. Many studies made in relation to coal combustion have been modified to apply to biomass combustion or co-firing. Tables 2.3 and 2.4 summarize the recent studies that apply CFD to simulate biomass combustion and co-firing boilers and furnaces. CFD modeling has established itself as a critical tool for the development of new ideas and advanced technologies. It is capable of predicting qualitative information and quantitative information to within sufficient accuracy to justify engineering design changes on commercial boiler plant.

Dixon et al. [132] summarized the CFD applications on bagasse-fired boilers in a sugar industry plant for researching the tube erosion, convection bank heat transfer, airheater corrosion, secondary air injection for furnace flame manipulation, and ignition stability and swirl burner technology. Fig. 2.9 and 2.10 show a typical CFD erosion application in a tube bank for the boiler. Gas velocity contours (a) and trajectories for several particle fractions (b) are shown for the as-constructed design (Fig. 2.9) and the

modified design (Fig. 2.10). The improvements in boiler tube erosion performance can be deduced by visual assessment alone of the predicted flow and trajectory patterns.

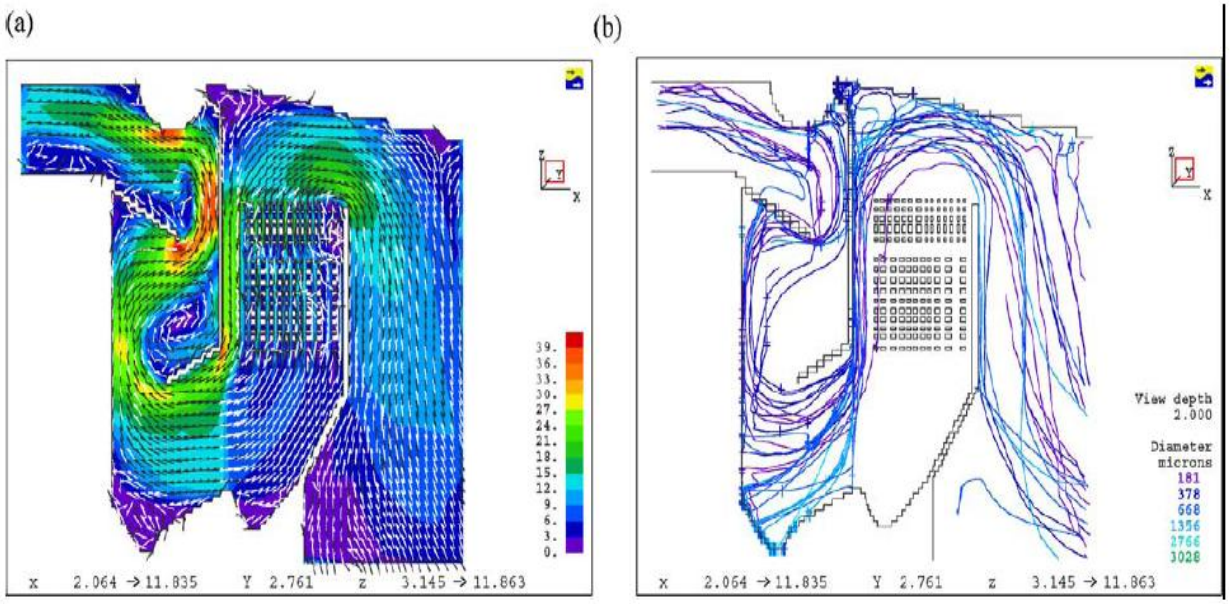

Fig. 2.9**.** Computational results of original design (a) gas velocity; (b) particle tracks

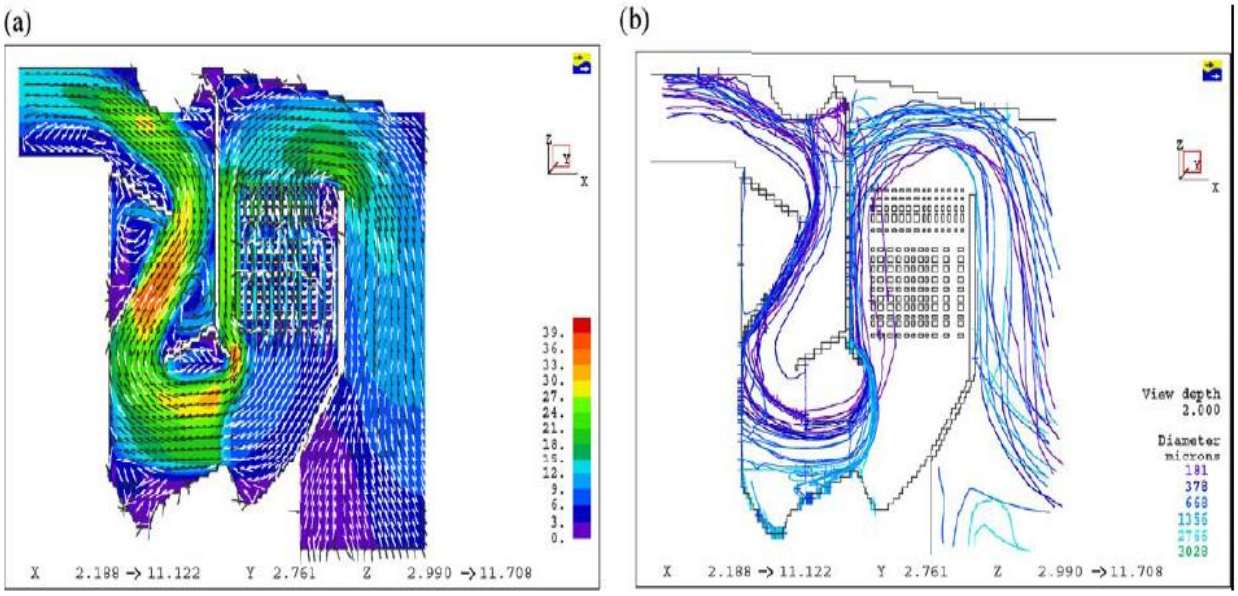

Fig. 2.10. Computational results of improved design: (a) gas velocity; (b) particle tracks

Kaer et al. [153-156] carried out CFD modeling of a 33 MW straw-fired grate boiler incorporating a standalone bed model and a commercial CFD code for gas-space computation. Figures 2.11, 2.12 and 2.13 show the predicted deposition mass flux of the first simulation, the boundary layer controlled deposition and the vapor deposition. He

concluded that poor mixing in the furnace is a key issue leading to high emission levels and relatively high amounts of unburnt carbon in the fly ash. The model was found to correctly predict operational trends same to the boiler experiment. In the future, a significant effort will be put into further improvements and validation of the modeling concept especially with respect to the deposition velocity concept and the tube bank model.

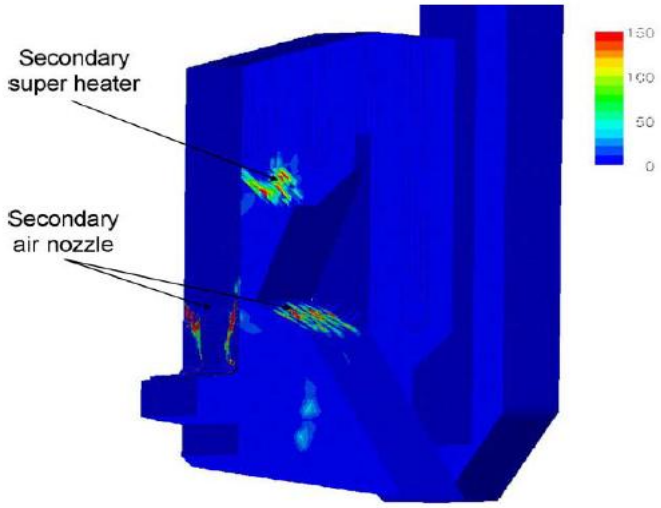

Fig. 2.11. mass flux contours

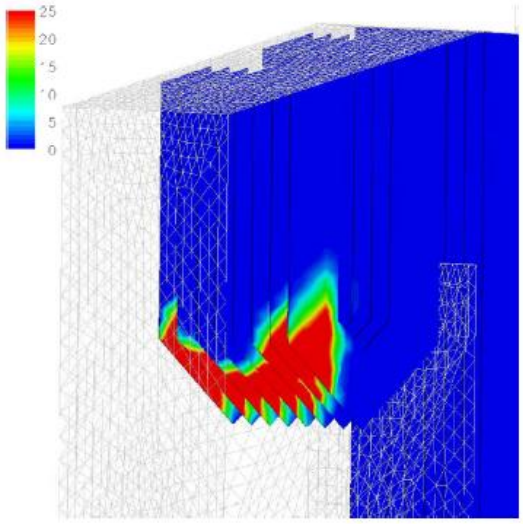

Fig. 2.12. View of SSH presenting mass flux deposition

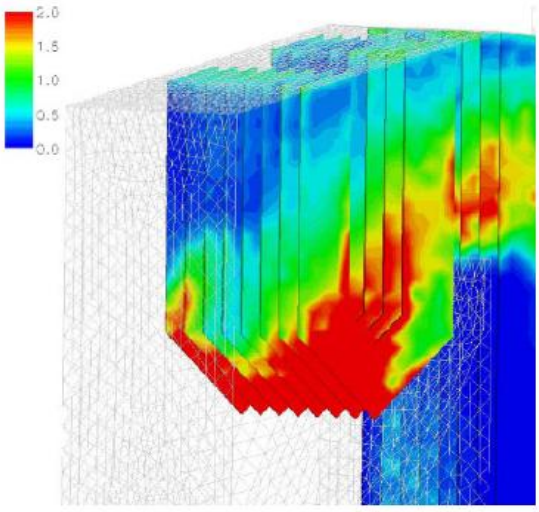

Fig. 2.13. SSH presenting vapor deposition flux

Table. 2.3 lists the recent studies of CFD applications in biomass combustion. The submodels used in these examples are summarized in the table.

Table 2.3.CFD applications in biomass combustion

Application	**Code**	**Dim**	**Aim/Outcome**	**Turb. Model**	**Extra Model**	**Agreement with Exp.**	**Authors**
Bagasse fired boilers[132]	Furnace	3D	Tube erosion; heat transfer; airheater corrosion; Swirl burner	Std k - ε	Lagrangian porous	Acceptable	Dixon, T. F.
Straw-fired grate boiler [153-156]	CFX	3D	To provide insight into the boilers; heat transfer predictions; To predict ash deposition	RNG k - ε	DTRM	Good	Kaer, S. K.
Combustion Furnace [157]	Fluent	3D	Particle tracks, temperature contours	Std k - ε	Lagrangian DOM	NA	Shanmukh aradhya, K.S
Waste rotary kiln incinerator [158]	Fluent	3D	To describe the processes occurring within the gaseous phase of the kiln and of the post combustion chamber	Std k - ε	P1	NA	Marias, F.
Bagasse fired furnaces [159]	Fluent	3D	To gain insight into the effect of moisture on the flame front.	k - ε	Lagrangian P1	NA	Shanmukh aradhya, K.S.
Tube stove [160]	CFX TASC	3D	To understand the aerothermo-chemical behavior of the stove operation in combustion and gasification modes	NA	c - phase	Excellent	Dixit, C. S. B
Waste-to energy plant [161]	Fluent FLIC		To maximize the energy recovery efficiency of waste to-energy plants	k - ω	DOM	NA	Goddar, C. D.

Dim=Dimension, Turb=Turbulence, Std=Standard, DOM = Discrete Ordinates Model (radiation), DTRM=Discrete Transfer Radiation Model, P1=P1 radiation model, Exp=experiment

The co-firing of coal and biomass has been advocated for a number of years as being advantageous on both an environmental and economic basis. The co-combustion of biomass as a minor component presents an interesting intermediate situation with a high reactivity solid. There are a number of commercially available CFD models, and the suitability of the sub-models available for biomass combustion is a key factor in selecting

an appropriate code. Table 4 summarizes the recent CFD applications in biomass co-firing. Backreedy et al. [162] carried out a CFD modeling study to examine the co-firing of pulverized coal and biomass with particular regard to the burnout of the larger diameter biomass particles. The effects of the wood particle size and shape on the burnout of the combined wood and coal char were investigated. The effect of varying the devolatilization and char combustion rate constants for the biomass component in the blend was also investigated. Fig. 2.14 shows the biomass particle tracks in the coal-biomass combustion case.

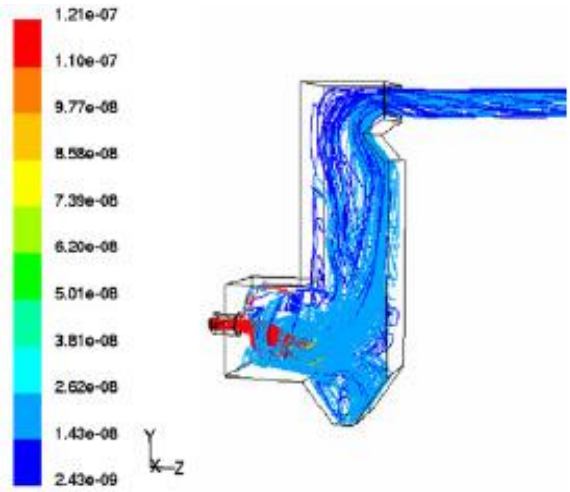

Fig. 2.14. Particle trajectories colored by their mass (kg)

Table 2.4 lists the recent studies of CFD applications in biomass co-firing. The submodels used in these examples are summarized in the table

Table 2.4. CFD implementations in co-firing with biomass

Application	**Code**	**Dim**	**Aim/Outcome**	**Turb. Model**	**Extra Model**	**Agreement with Exp.**	**Authors**
Biomass and coal co-fired [162]	CINAR	3D	A new approach based on neural networks is proposed	k - ε	Radiation, Lagrangian	NA	Abbas, T.
Co-firing [163]	Fluent 6.1	3D	To predict the behavior of the biomass in the coal flame.	RNG k - ε	P1 FG-biomass	Good	Backreedy, R. I.
Co-firing combustors [164]	Fluent UDF code		To develop a fragmentation subroutine applicable to Fluent via a UDF.	NA	Lagrangian; Fragmentation model	Reasonable	Syred, N.

Co-combustion boilers[165]	Fluent 6.1 MATLAB	3D	To optimize burner operation in conventional pulverized-coal-fired boilers	Std k - ε	DOM	NA	Tan, C. K.
Biomass utility boiler[166]	Fluent 5.6	3D	To examine the impact of the large aspect ratio of biomass particles on carbon burnout in co-firing switchgrass/coal	Std k - ε	Lagrangian DOM	NA	Gera, D.

Dim=Dimension, Turb=Turbulence, Std=Standard, DOM = Discrete Ordinates Model (radiation); P1=P1
radiation model, Exp=experiment

In the case of biomass burner studies there is considerable interest in NO_x formation and unburned carbon in ash. The literatures [133, 167-172] described the biomass combustion and NO_x formation in detail. Ma et al. [133] performed CFD application in a 1 MW industrial wood test furnace coupled with the potassium release and NO_x formation model. The potassium release during biomass combustion is still a subject of current investigation. Ma et al. assume that the biomass potassium release during devolatilization rapidly forms KOH. Fig. 2.15 shows the predicted contours of potassium concentration in the vertical symmetric plane of the furnace. Both the HCN and the NH_3 route have been considered for the NO_x formation and Fig. 2.16 shows the predicted NO concentrations through NH_3 route. The particle tracks and temperature distribution are also studied in this work. Good agreement between the predicted and the measured furnace temperature and concentrations of CO_2 and NO_x has been achieved. Table 2.5 summarizes the recent CFD applications in the NO_x emission modeling.

Mueller et al. [173] and Ravelli et al. [120] have used CFD to formulate numerical model of peat-forest residue, Refused derived fuel (RDF) respectively in bubbling fluidized bed combustors. Ravelli et al. [120] compared the devolatilization and the char burnout profiles at the entry ports level, which showed that devolatilization was starting after a short time when the fuel is injected.

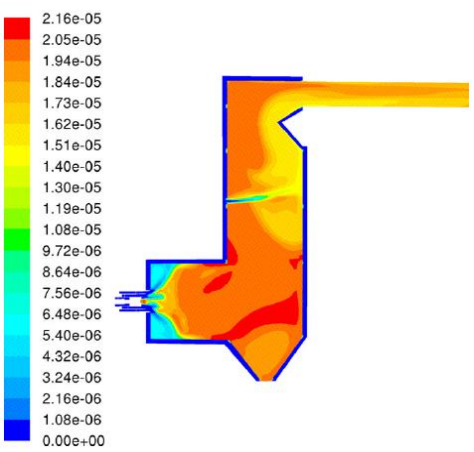

Fig. 2.15. Mass fractions of potassium

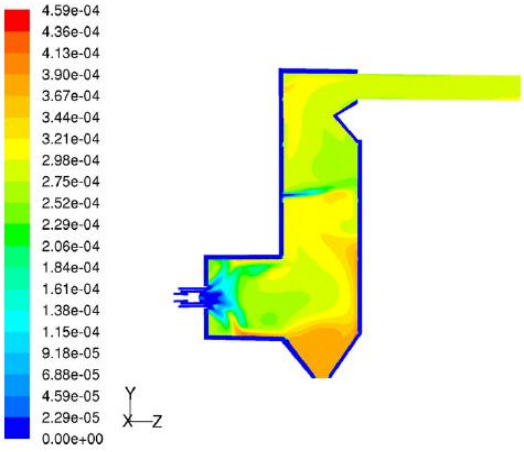

Fig. 2.16. Mass fractions of NO

Table 2.5. CFD implementation in NO_x formation of biomass applications

Application	**Code**	**Dim**	**Aim/Outcome**	**Turb. Model**	**Extra Model**	**Agreement with Exp.**	**Authors**
Test furnace [133]	Code	3D	Particle tracks, emperature contours, NO formation, potassium concentration	Std k - ε	Lagrangian; P1; radiation; NO_x Formation; potassium release ;	Good	Ma, L.
Combustion chamber [167]	Fluent 5.5	3D	Prediction of gaseous emission	SST k - ω	Lagrangian; DTRM; NO_x - model	Good	Miltner, M.
Pilot downfired combustor [168]	Fluent 5	3D	To describe the processes occurring within the gaseous phase of the kiln and of the post combustion chamber	k - ε	P1, Lagrangian; NO_x module	Reasonable	Xiu, S. N.
Fluidized beds [169]	Fluent 6.2	3D	To compare the erformance of five global ammonia chemistry mechanisms in full-scale boiler CFD modeling.	Std k - ε	DOM; Global Ammonia Chemistry Mechanisms	Well under special conditions	Saario, A.
Biomass combustion [170]	Code	ID	Comparisons of the Validity of Different Simplified NH3-Oxidation Mechanisms for Combustion of Biomass	NA	Ammonia oxidation mechanisms	NA	Norstrom, T.
Wood stove [171]	Spider	2D	To model nitric-oxide formation from fuel-bound nitrogen in biomass	Std k - ε	DTRM	NA	Weydahl, T.

			turbulent non-premixed flames.				
Bagasse fired boiler [172]	Code	3D	To apply conditional moment closure (CMC) in a bagasse-fired boiler model to obtain predictions of CO and NO in the flue gas.	Std k - ε	Lagrangian; DTRM; PDF; conditional moment closure equation	Reasonable	Rogerson, J. W.

The fragile structure of the RDF and its high intrinsic reactivity favor the fast activation of the homogeneous combustion of volatiles [Fig. 2.17(a)]. Fuel particles are expected to be broken into small fragments immediately after feeding: since a small particle is burnt faster than a big one, this would accelerate the emission of volatile from RDF. Fixed carbon combustion begins after devolatilization and takes place in different freeboard zones by varying the furnace operating conditions.

Fig. 2.17(b) shows that devolatilization takes place in the region close to the furnace exit while it is confined to the area just above the bed. Consequently, in the first case, a low percentage of the fuel can be entrained to the furnace exit before the oxidation process is completed. The two cases on low load and high load in commercial combustor have been shown in picture. The literature reveals that devolatilization depends on fragile structure, intrinsic reactivity, size, temperature and density of properties of particles. If the particles are less fragile, intrinsic reactivity is low, size is large and denser then the chances of char devolatilization occurs in bed or during flight from fuel chutes as shown in Fig. 2.17(b).

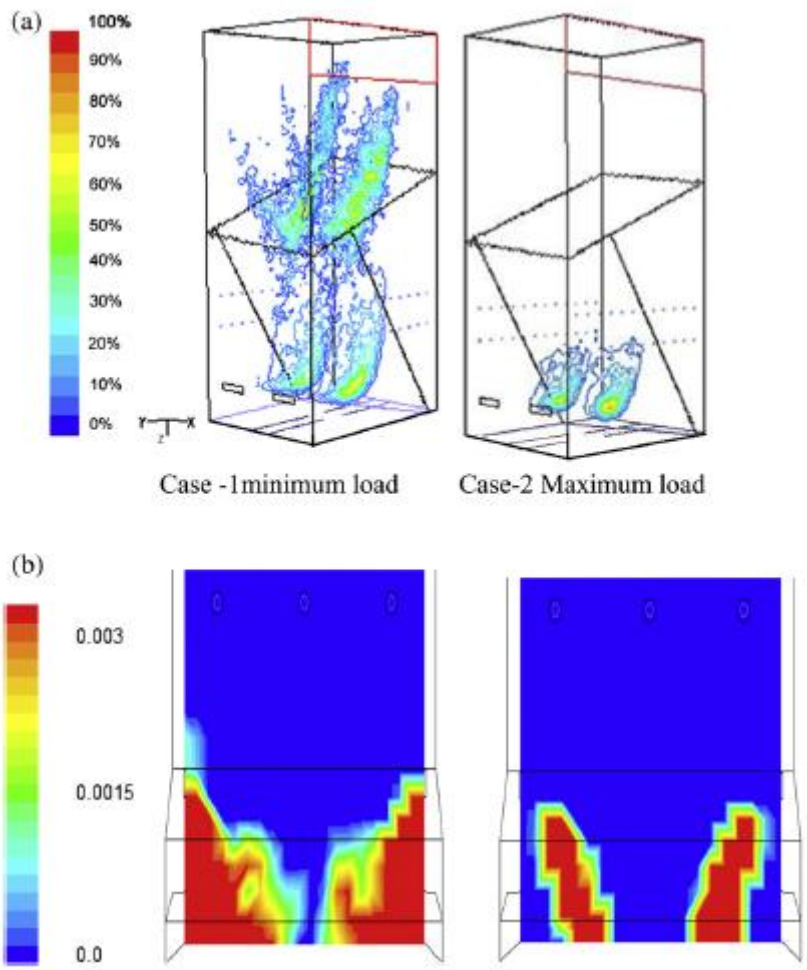

Fig. 2.17. (a) DPM devolatilization fractions [140] (b) Devolatilization of peat and forest residue [173]

The devolatilized fuel known as char burns slowly and it takes time depending upon intrinsic reactivity and size to burn completely. There is chance that some particle will not burn in bed before leaving. The light particles like rice husk will burn during trajectory. The char oxidation and char burn out profiles are difficult to study in dense bed due to computational limitations and due to surrounding of char particle by sand particle. With present computational approach it is easier to study char oxidation in freeboard of commercial as well lab scale units with discrete particle model Lagrangian approach. The char burn out is difficult to validate in real combustors and it is not validated in any of studies. In most of studies the aim is not to study the charburn out rather to validate the CFD model. The char oxidation of RDF fuel [120] in commercial combustor is shown in

Fig. 2.18. It shows that char combustion takes place in the region close to the furnace exit in case of minimum load, while in case maximum load it is confined to the area just above the bed.

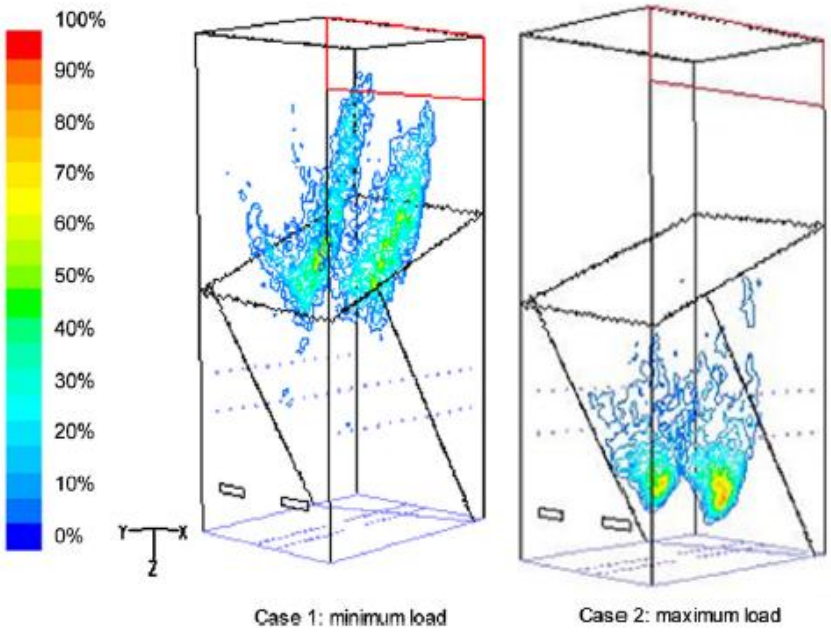

Fig. 2.18. Fractions of DPM burnout

Consequently, in the first case, a low percentage of the fuel can be entrained to the furnace exit before the oxidation process [120] is completed. In the minimum load condition, the temperature of the flue gas coming from the bed (971.2 K) is not high enough to rapidly ignite combustion thus fuel particles may be elutriated from the furnace, reducing its efficiency. On the contrary, in maximum load, the temperature of the flue gas coming from the bed (1078.5 K) causes all the fuel to be burnt. For the light weight particles like rice husk [124] the char oxidation and combustion will take place during trajectory for the case of rice husk [124] as shown in Fig. 2.19 (a) and (b).

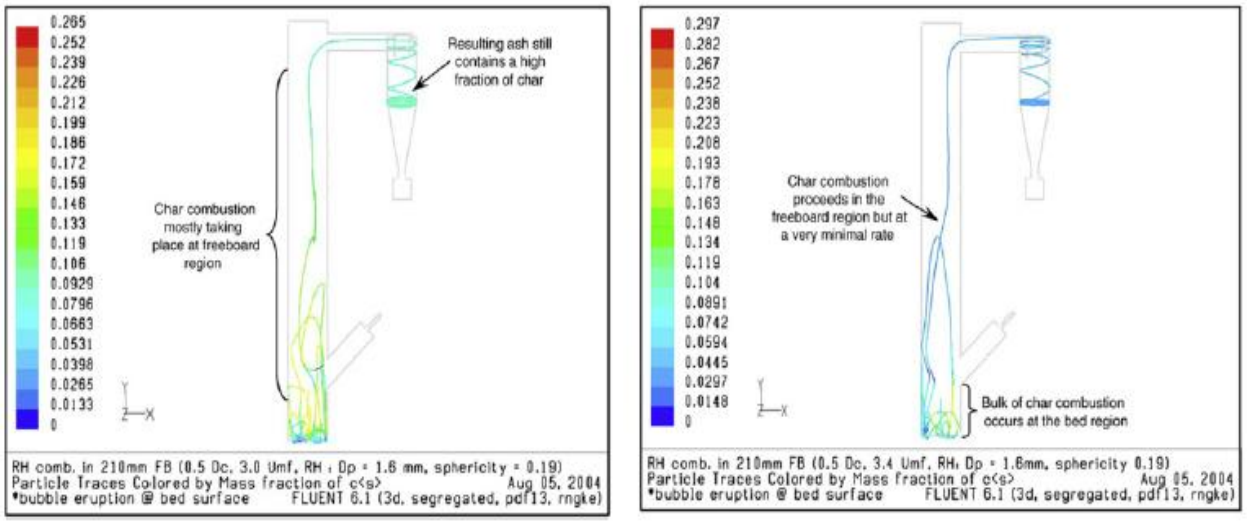

Fig. 2.19 (a) Char concentration of a rice husk particle in first case (b) Char concentration of a rice husk particle in another case

Black et al. [174] in this study used a commercial computational fluid dynamics (CFD) code to simulate the firing of coal and biomass under air and oxy-fuel conditions in an existing full-scale 500 MW coal-fired utility boiler. Results are presented for conventional air-coal combustion that corresponds well against available experimental data and an in-house empirical model. Maintaining the same thermal input and exit oxygen concentration, CFD was used as a predictive tool with standard physical submodels, to examine the effects of firing under air–biomass, oxy-coal and oxy-biomass conditions. The oxy-fuel conditions were investigated at oxygen concentrations of 25% and 30% by volume for a wet flue gas recycle.

The effects of firing biomass in both air and oxy-fuel conditions are predicted to have a lower total heat transfer to the tube walls, with a lower furnace exit temperature in the boiler than the coal-fired cases. This may be attributed to the effects of large biomass particles, which have a lower total surface area and therefore causes a reduction in the radiative heat transfer to the tube walls as well as an increase in carbon in ash (CIA) predictions. For oxy-coal firing, the study suggested that the optimum oxygen concentration for heat transfer to be closely matched with air–coal, lies between 25% and

30%, but for oxy-biomass firing a value greater than 30% may be needed. This study highlights the possible impact of changing the fuel and combustion atmosphere on the heat transfer characteristics of an existing power plant boiler, underlining that minor redesign may be necessary when converting to biomass firing under air and oxy-fuel conditions.

The CFD predictions of heat transfer to the tube bank walls and the gas temperatures leaving the tube bank sections were found in good agreement with the in-house model. Heat transfer to the water walls is dominated by radiation, and the rate of radiative heat transfer is closely related to the correct resolution of the temperature field, since thermal radiation is proportional to the fourth power of temperature. A cross section of the temperature distribution through the third column of burners and the furnace exit temperature is shown in Fig. 2.20(a). The four separate rows of flames can be clearly seen, where the release and combustion of volatiles takes place. The burnout of the char particles is then completed in the region above the volatile flames in the combined stream of hot gases rising towards the superheaters. Comparison with available data shows that the heat transfer to the water walls and the temperatures at each section are matched closely, but the predicted distribution of heat transfer differs more between the superheaters, FRH and SSH sections. This can be possibly attributed to the differences in modeling approaches between the CFD code and in-house model. Without further experimental data, such as flow field or chemical species measurements, it is difficult to fully validate the CFD predictions. However, the total heat transfer to all the heat exchanger sections considered is predicted with 2% accuracy between the CFD and in-house models. The CFD results are therefore deemed to give a good representation of the heat transfer in the boiler and are used for comparison in subsequent sections.

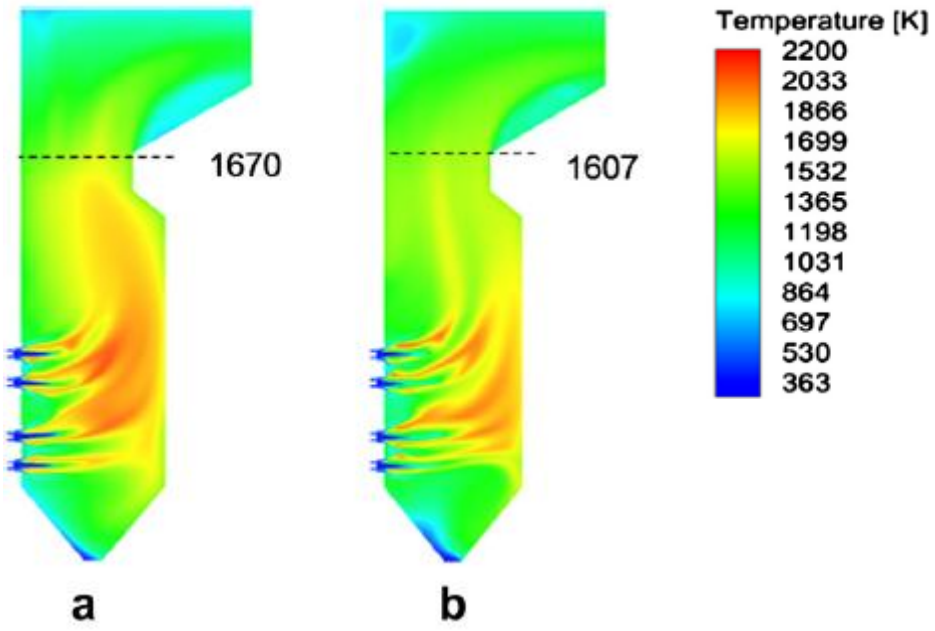

Fig. 2.20. Temperature contours (a) air–coal, (b) air–biomass

Comparing Fig. 2.20(a) and (b), a different temperature distribution and lower furnace exit temperature for air-biomass can be seen. High temperature regions near the burner exit corresponds to the intense volatiles flames that are shown in both cases. However when comparing the burnout region above the flames the temperature of the burnout zone is visibly reduced for the biomass case. This may be attributed to differences in particle size, as coal particles are much finer and char combustion takes place mainly in the furnace, however, the combustion of large biomass particles will be slower and therefore the temperature in the burnout zone, and before the exit of the furnace, is reduced. Predictions of the carbon in ash (CIA) evaluated after the FRH section showed higher values for the biomass than for coal, with values of 11% and 0.64%, respectively. An increase in CIA is expected when firing biomass, due to presence of larger particles as well as the ash content being generally much lower for biomass, which results in the remaining carbon taking up a larger percentage of the fly ash.

Zhang et al. [175] considered light weight biomass as a potential fuel to be used in industrial and power-producing furnaces and boilers. This paper presents a

comprehensive numerical study of co-firing chunk coal and a kind of light weight biomass, oat hulls (Avena sativa), in a stoker boiler. In this comprehensive model, a one dimensional steady state coal bed model already verified through experimental measurements was employed to describe the combustion process on the bed and an oat hulls devolatilization sub model derived from experiments was added to predict the devolatilization process of oat hulls. Through the study of oat hulls co-firing with coal combustion it was found that light biomass, similar to pulverized coal, burns in suspension (following the air flow). The particle trajectory shows that the devolatilization of oat hulls occurs shortly after injection into the boiler. The flow pattern indicates the importance of air system tuning in optimizing the design. For larger oat hull particles, they tend to reach the back wall of the furnace which can result in slagging problems. Also, the peak temperature inside the furnace inversely varies with the co-firing percentage of oat hulls. This numerical study supports the thermal and economic potential of using unprocessed light weight biomass on the existing combustion facility.

The cases examined range from 5% to 30% of the heating value coming from the oat hulls. The results showed that the flame temperature inside the furnace decreased with oat hull co-firing. Besides the high temperature zone above the coal bed, another slim high temperature zone in the upper part of the boiler (shown in Fig. 2.21) was detected. This zone shows the combustion of fixed carbon of the oat hull particles. Due to a small portion of fixed carbon in the oat hulls, the peak temperature in this new zone is lower than that above the coal bed; therefore, the highest temperature zone was still near the coal bed.

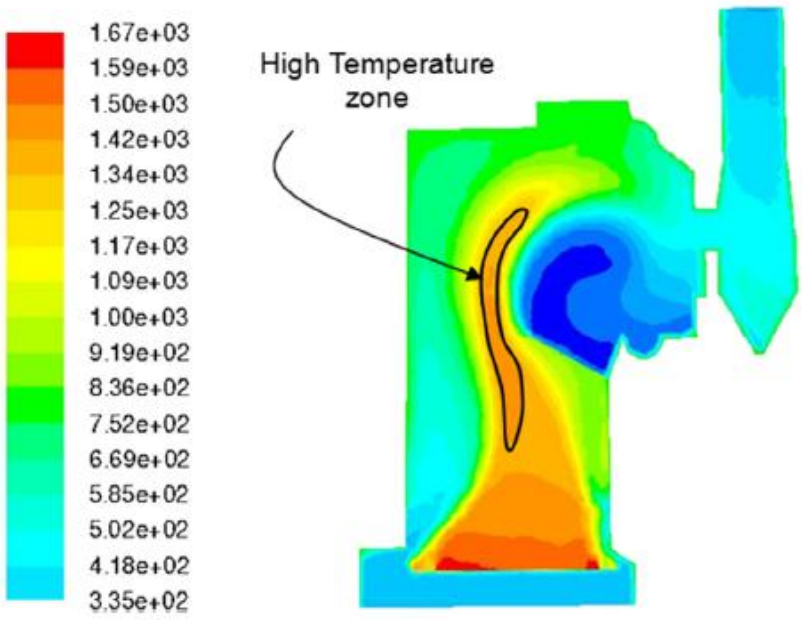

Fig. 2.21.Temperature contours of co-combustion of oat hulls

Because of the oat hull's high oxygen content, the mass concentration of oxygen inside the furnace increased with the co-firing percentage. Fig. 2.22 (a-d) shows the mass fractions of oxygen at co-firings of 5%, 10%, 20% and 30%. These figures all show a continuous increase in average oxygen mass concentration above the coal bed. In the case of co-firing smaller percentage of oat hulls (i.e. 5%), the oxygen depletion zone is still evidently above the bed. As the mass fraction of oat hulls increases, a new oxygen depletion zone resulting from the solid carbon combustion of the oat hull particles begins to appear in the upper part of the boiler. This depletion zone is still an improvement because it is smaller than the low oxygen zone in the lower part of the boiler.

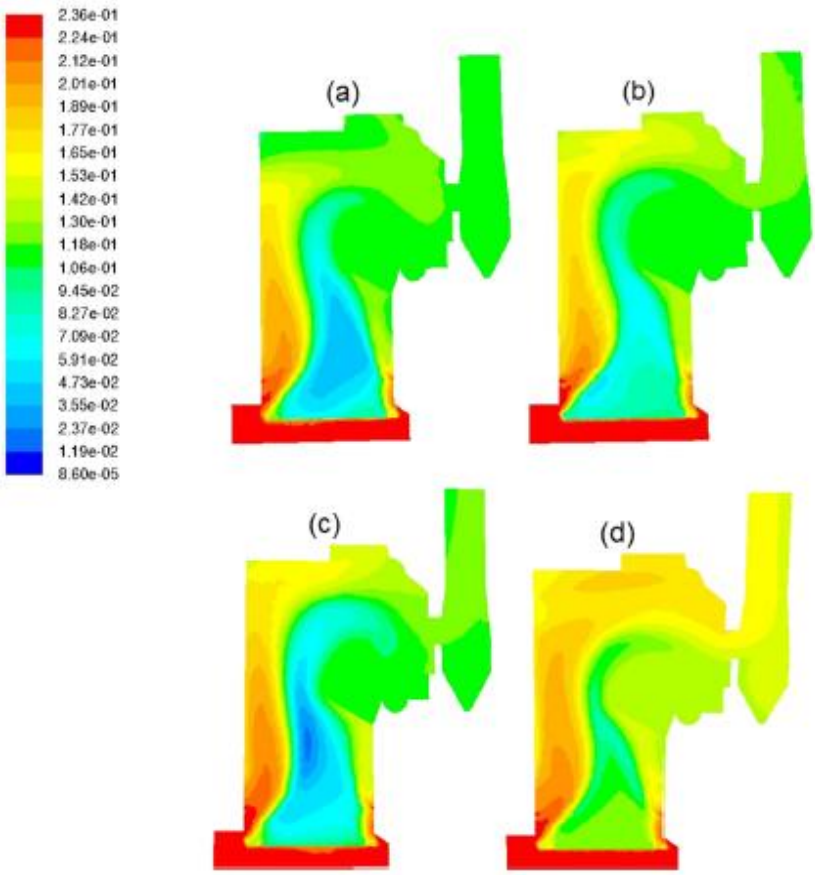

Fig. 2.22. Mass concentration of oxygen for various oat hulls % age (a) 5 (b) 10 (c) 20 and (d) 30

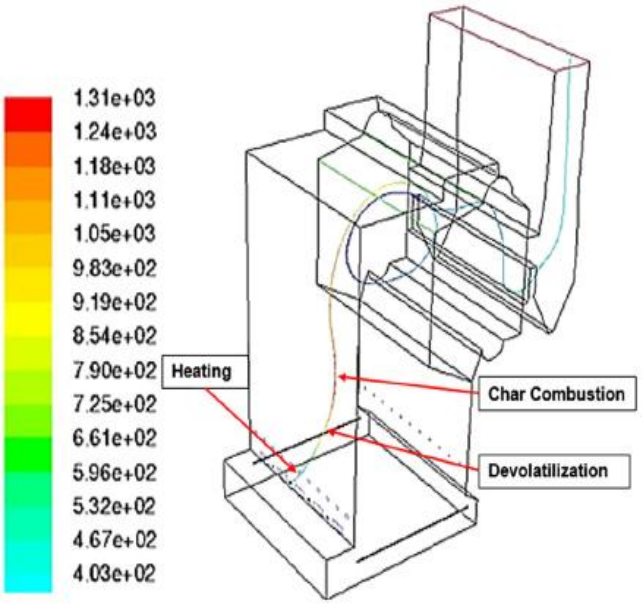

Fig. 2.23. Particle track coloured by temperature

Due to its light weight, oat hull particles tend to travel along the fluid paths inside the furnace. Since particles devolatilization is tied to both particles and surrounding gas

temperature, particle location and travel inside the furnace is also of interest. Fig. 2.23 shows the oat hull's temperature, corresponding to the three reaction stages during the combustion process: heating, devolatilization and combustion. The devolatilization occurs close to the front wall, indicating a fast reaction rate. The char combustion that happens in the upper part of the boiler, matches what was seen in the temperature contour.

Singh et al. [176] in this paper summarized the CFD modeling tool to study combustion and gasification of fuels in fluidized bed devices. There is evidence that CFD can be used as a powerful tool to predict characteristics of fuels during combustion and gasification processes in fluidized bed units. CFD has played an active part in analysis of the distribution of products, heat flux, flow, temperature, ash deposits, CO, SOx and NOx emissions during combustion and gasification of fuels in fluidized bed. These parameters could affect the performance and design. No evidence of Eularian-Eularian TFM CFD model influencing the design of industrial fluidized bed units when combustion and gasification issues involved.

The CFD model results are satisfactory and have made good agreements with the experimental data in many cases. However, the simulations still have many approximate models as well as some assumptions. To ensure CFD simulations are more than just theoretical exercises like two-dimensional units, experimental validation is necessary to facilitate the model accuracy.

CFD modeling of commercial fluidized bed considering combustion and gasification aspects using Euleriane-Eulerian TFM approach still required to explore. Due to variation in size of biomass particles the Eulerian-Eulerian approach with biomass considering combustion/gasification issues in dense fluidized beds is not possible until wide approximations are chosen. No studies have been reported on CFD simulation

investigating both the bed and freeboard simultaneously and applied either technique to both dense bed and riser/freeboard of commercial units.

The understanding of Eulerian technique to fluidized beds with thermo-chemical reactions is still in a development stage. Several mechanism models are available but none of them is suitable for industrial scale boilers when then thermo-chemical conversion of fuels is considered. At present stage application of DPM Lagrangian technique with gas phase to freeboard with thermo-chemical reactions is seems to satisfy fully which can affect and enhance the performance to industrial scale fluidized bed boilers. There are many aspects of fluidized beds where the application of CFD modeling still needs to be explored. The aspects like fuel combustion/gasification behavior during feeding, mixing of fuel in the dense bed, ash sintering, fuel characteristics, char reactivity and inventory, fragmentation of fuel in dense bed with CFD still needs to be explored.

Although there are still some obstacles such as inability in accurate simulation of large 3-dimensional problems on an affordable computer in particular, in large-scale sophisticated plants, the trend of widespread application of CFD in the fluidization industry will continue in the 21st century. With the progressing of the computing power and the development of chemical and physical models, the CFD application in the combustion and gasification of fuels in fluidized bed units will more widely spread in the future.

2.5 Gaps from Literature

Literature review starting from basic fluidization models up to CFD analysis of biomass alone and co-firing based FBC studies is done. It is revealed that CFD modeling is useful tool for investigating and optimizing combustion process in a fluidized bed technology of boiler, even in case of co-fired combustors fuelled by biomass and coal. However few difficulties are faced and limitations are found in performing the numerical simulation of highly complex industrial fluidized bed boilers by using limited computational domain.

But With the advancement in the hardware technology and the improvement in models of and physical interest and reactive chemistry, the CFD implementation in incineration and gasification of fills in fluidized bed systems will all the more broadly spread later on. Following observations are noticed during literature study:

- The studies for co-firing or biomass derived FBC units were found mostly for small scale pilot plants or experimental set ups. Studies on real plant FBC furnace were found missing which encouraged this study.
- All the studies were done using single biomass fuel; CFD studies using different biomass forms were found missing in literature.
- All co-firing studies have been done for the same direction of fuel feeding systems. No reference were found for both underbed and overbed fuel feeding systems.
- CFD studies to be done on such a large domain furnace were found limited scope in literature especially in Indian scenario.

CHAPTER 3

PLANTS DETAILS AND DATA COLLECTION

Captive Power Plant, Ambuja Cement limited, Punjab has the distinction of being the first successful project in HOLCIM group in India. CPP is the internal unit of Ambuja Cement limited (ACL) which a pioneer cement production company of India. The plant capacity is 30 MW. It is necessary to mention here that Ambuja not being government organization has taken upon itself the corporate social responsibility to use sustainable fuel for power generation so as to indulge the social benefits of nearby regions in the form of employment of local people or farmers by engaging them in collection and selling of the agro residues to the industry, which otherwise goes waste and produce adverse effects on environment if burnt in open.

CPP, Ropar initiated in using biomass fuels due to few following reasons:

- It supports sustainable development by reducing the CO_2 emissions.
- Economic benefits: Biomass fuel is cheaper as compared to fossil fuels.
- Environmental benefits: It promotes preservation of natural recourses and reduction in Green house gases.
- Social benefits:

✓ It leads to value creating opportunities.

✓ It is a step forward creating effective waste management, thus avoiding land filling/open burning.

✓ It creates employment opportunities.

✓ It helps saving public funds, otherwise needed to build waste incinerators.

Technical specifications of CPP are given below:

- HP boilers - TBW make
  - 2 X 45 TPH, 79kg/cm^2, 495^{0}C (underbed cum overbed)
  - 1 X 80 TPH 79kg/cm^2, 495^{0}C. (underbed cum overbed)
  - Single drum , AFBC boilers
  - Fuel : 70% Coal and 30% biomass
- Steam turbine generators – BHEL make
  - 2 X 15 MW Extraction cum condensing turbine
  - 490^{0}C
  - Generator : 6.6 kV , 15 MW with BL exciter
  - Gear box : 7700/1500 Triveni Lufkin make
- Coal handling plant - Macmet
  - Capacity 100 TPH , size - 6 mm
  - Primary crusher : 125 TPH toothed double roll
  - Secondary crusher: 150 TPH fixed blade impactor
- Biomass handling plant
  - Capacity 25 TPH
- Ash handling plant – UCCI Ltd.
  - Dense phase conveying system.
  - Fly ash, coarse ash and bed ash silos.

  (Modified with MBL dome & blow valves)

Different parameters of plant are given in Table 3.1. Up to 2005 the plant worked on 100% usage of rice husk, for which they received successful CER verification.

Table 3.1: Plant parameters

Capacity	30MW
Type of bed	AFBC
Bed cross-sectional area	$41m^2$
Steam temperature	495^0C
Feed Water Temperature	172^0C
Distribution plate	Nozzle type
Bed material	Crushed refractory
Fuel used	70% coal with 30% Biomass
Fly-ash collector	ESP
Fuel feed rate	11TPH
Fuel density	$100 – 105\ kg/m^3$

Rice husk is a processed fuel from industry and user friendly being clean and available in ready to use size (length = 6mm and width = 0.5 to 1mm approximately) where as other biomass fuels are available in random sizes and require further processing to bring it to required size of 6mm (used at CPP). Due to this reason the number of buyers of rice husk has surpassed the number of suppliers in the region and it became difficult to run the plant on rice husk alone throughout the year due to lesser availability. Initially when the technological developments were not capable enough to adopt the rice husk as a regular fuel it was treated as a waste by the farmers and rice producing firms and supplied to the newly emerged technology based plants at a very reasonable cost. With the passage of time as the demand for biomass fuel increased, for rice husk in specific, its cost surpassed the cost of conventional fuel as well other biomass fuels. The rice husk costs Rs 1.30/- approximately for 4.2 MJ of energy generation. On the other hand the cost of other biomass fuels is around 85 paisa for equal amount of energy generation. Hence they started using different biomass fuels at CPP. As Ambuja is primarily a cement producing organization, the bed ash disposal remains no issue for CPP, Ambuja. Bed ash and

unburnt obtained from flue gases is collected in the ash silos with the help of pneumatic conveyers from where it is supplied to the clinker silos (in cement production unit) to mix with it which is used in the formation of cement. Biomass handling Plant capacity of the unit is 25TPH. They are having ash handling plant, with dense phase conveying system.

CPP is using different fly ash, coarse ash and bed ash silo's modified with MBL dome and blow valves. The plant is using fluidized bed combustor of 45TPH which runs over both biomass and coal. Fuel is fed to the conveyor belt through rollers and from the conveyor belt it is fed to the combustor for combustion. Due to less availability of any particular biomass they are always used in mixture. The process layout of the plant is shown in Fig. 3.1.

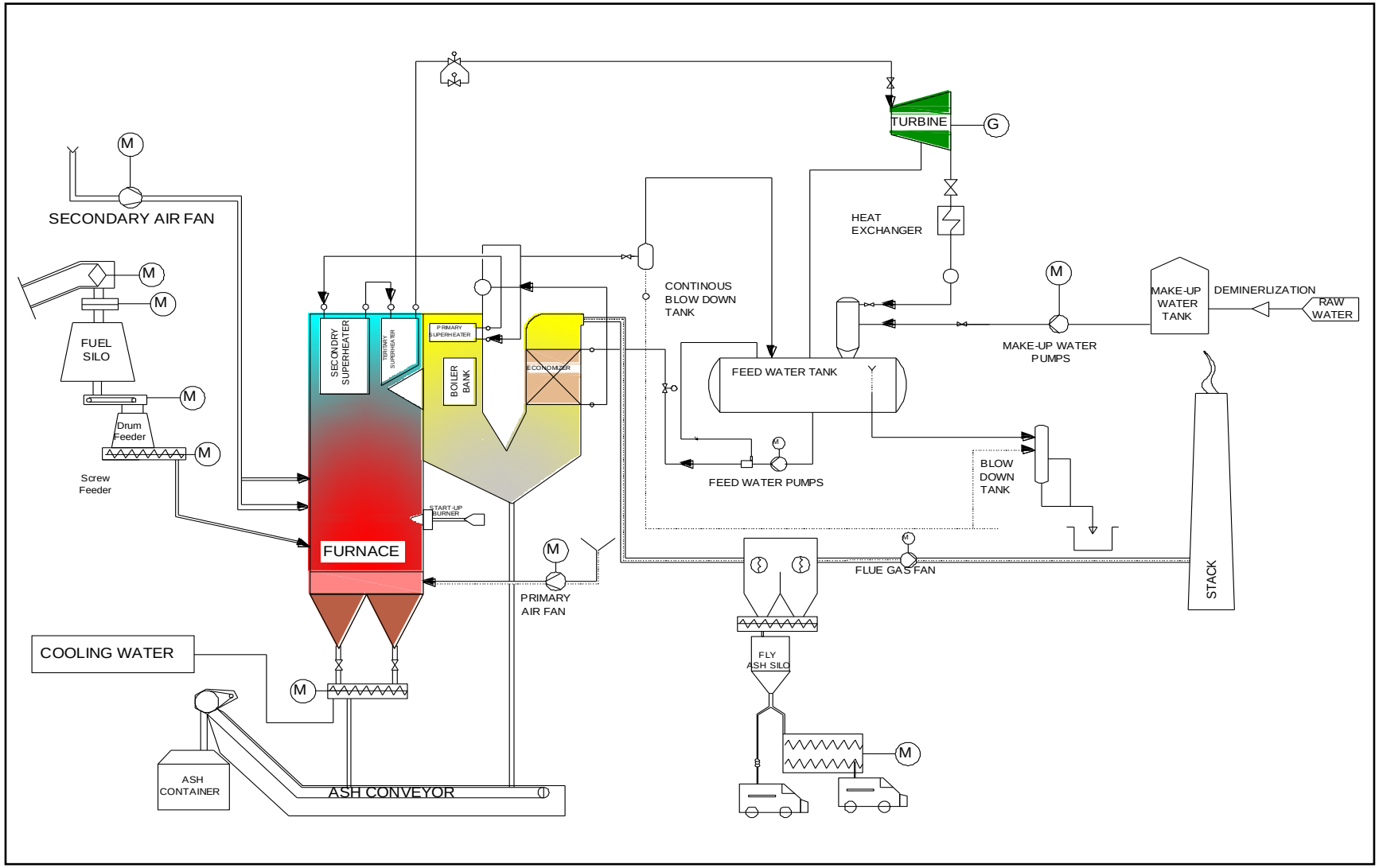

Fig. 3.1: Process layout of CPP

3.1 Different Fuel Usage at CPP

Biomass fuels primarily have Woody and Non woody forms. Woody biomass include chips and buckles and Non woody forms are divided in to two further categories viz. biomass from field agro residues like paddy straw, sugarcane trash and stalks. The other is from industrial agro residues like rice husk, saw dust and wood chips. A few of biomass fuels used at CPP are shown in Fig. 3.2. Different biomass fuels are fed to the boiler with fuel feeders.

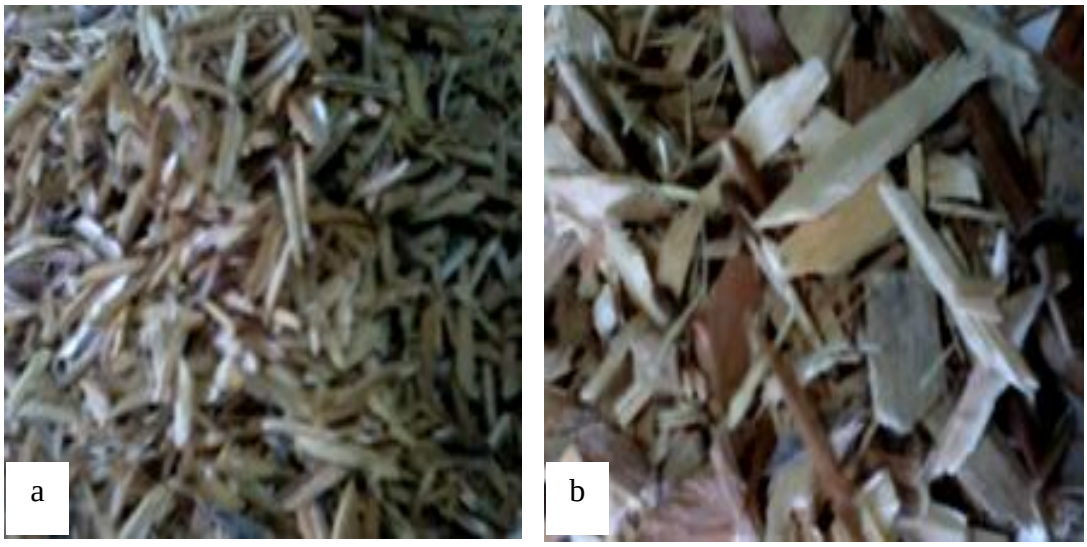

Fig 3.2: (a) Rice husk (b) Wood chips

CPP, Ropar initiated in using different biomass fuels to promote preservation of natural recourses and reduction in usage of fossil fuels. The ultimate analysis and proximate analysis of various biomass fuels used has been done and given in Table 3.2 and Table 3.3 respectively.

Table 3.2: Ultimate analysis of various biomass fuels

Species	Coal	Rice husk	Saw dust	Wood chips
Carbon	36.22	35	31	35
Hydrogen	2.64	3	3.7	5
Nitrogen	1.09	1.25	0.4	0.65
Sulphur	0.55	0.18	0.17	0.05
Moisture	4.39	12	25	20
Ash	47.86	15	5	5
Oxygen	7.25	34.45	35	34
GCV(kcal/kg)	3500	3500	3400	3600

Table 3.3: Proximate analysis of biomass fuels

Contents	Coal	Wood chips	Saw dust	Rice husk
Moisture	4.39	9.93	8.75	5.22
Ash	47.86	13.43	39.89	14.54
Volatile	17.97	65.48	41.63	66.4
Fixed carbon	29.78	11.16	9.73	13.84

3.2 Biomass an Environment Friendly Fuel

All biomass fuels are environment friendly due to following reasons:

- All biomass fuels are CO_2 neutral and therefore do not contribute to the GHG emissions.
- One ton of biomass fuel replaces around one ton of F grade coal & therefore saves equal amount of CO_2 emissions.
- In absence of co-firing agro waste residues in boilers, these would be either burnt in open fields or left to decay. This leads to generation of methane, a very harmful GH gas.

3.3 Technology Evolved in CPP

Following technological developments have been done for successful implementation of biomass fuel at the plant:

- For biomass being voluminous in size sufficient storage space is required. Keeping that in mind covered shed for storage during rainy season is constructed as shown in Fig. 3.3

Fig. 3.3: Storage space and covered shed

- A heavy duty shredding machine is procured to shred wooden logs to chips to maintain the required size for supplying inside the furnace (Fig.3.4)

Fig. 3.4: Shredding machine

Fig. 3.5: Conveying system

- Fuel conveying system was modified to cater to the needs of variety of biomass fuels as shown in Fig. 3.5.

Fig. 3.6: Grabber

Fig. 3.7: Crusher

- Locally developed grabber fitted on tractor which lifts the lantana bushes & feeds to shredding machine Fig. 3.6.
- Instrumentation control loops were tuned to take care of variations in the fuel feed material.
- Locally developed dung flakes crusher is installed which crushes the flakes & feeds "on line" to the next conveyor Fig.3.7.

3.4 Challenges in Usage of Biomass Fuels

Although due to the above said benefits of using bio fuels in to the field of energy generation, yet few challenges are also found in using biomass fuels which are listed below:

- Ash evacuation problem from ash hoppers of the boiler takes place due to high alkali content and sticky properties of ash.
- After burning of saw dust, fouling and hard soot deposits in super heater area are found due to high alkaline and low fusion temperature of as shown in Fig.3.8. Also fouling effects were found in APH tubes (Fig. 3.9) which require frequent cleaning with water jets and air jets (Fig. 3.10)

Primary superheater zone Radiant and convection superheaters

Fig. 3.8: Soot deposits on pressure parts

- It is observed that dome valve seat undergoes frequent damages and cutting due to high silica present in biomass fuels.

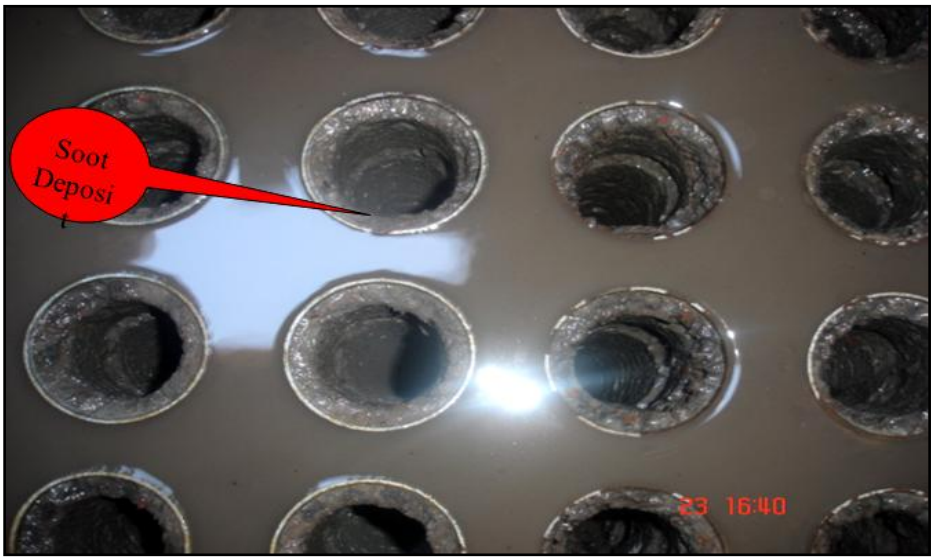

Fig. 3.9: Soot deposits inside APH tubes

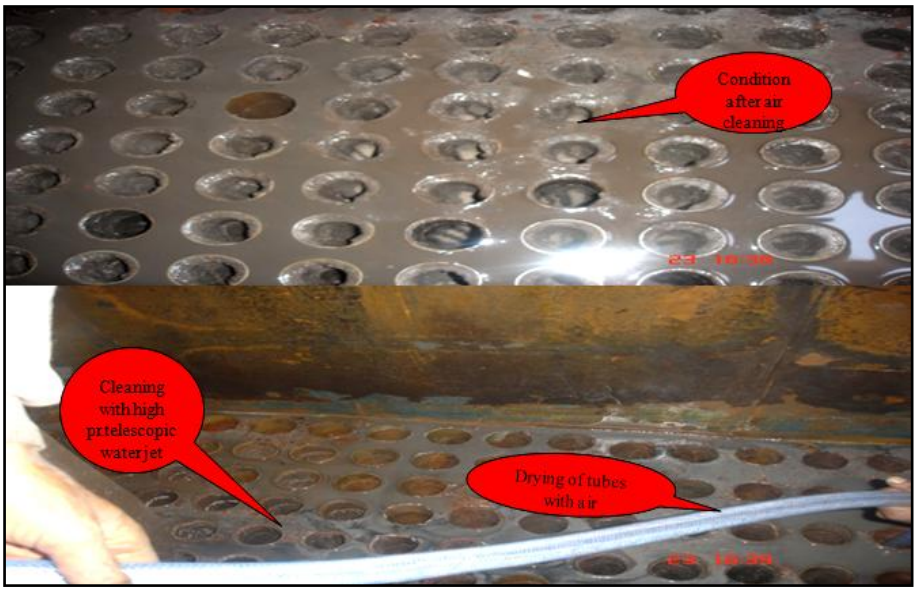

Fig. 3.10: Cleaning of APH tubes with air and water jets

3.5 Brief Overview of CPP Boiler

The boiler package supplied by Thermax Babcock &Wilcox, Pune, India and has been designed for 45 TPH steam output designed for firing with 70% coal and 30% biomass. This boiler is single drum design, natural circulation, water tube and balanced draft

having under bed cum over bed fuel feeding system, top supported pressure parts and bed plate design and wind box bottom supported.

Fuel combustion takes place in an Atmospheric Fluidized Bed Combustor (AFBC) fixed at the boiler bottom. Fuel is stored in bunker. Drag chain feeders are connected at the bottom of surge hoppers (below the bunker). The fuel is fed by these feeders to under bed fuel feed pipes and transported to the furnace bottom for firing inside the bed. For coal firing under bed firings used and for Biomass over bed firing is used.

As a complete unit the boiler plant is equipped with the following circuits.

- Feed water and steam system
- Pressure parts circuit.
- Boiler steam circuit.
- Boiler blow down circuit.
- Sample coolers.
- Chemical dosing system.
- Combustor/Furnace.
- Combustion air/Over fire air system.
- Fuel handing, storage and fuel feeding system.
- Start up oil firing system.
- Flue gas circuit.
- Refractory and insulation.
- Electrical and instrumentation.
- Electrostatic precipitator.
- Chimney

3.6 General Description

The main parameters of the boiler are

Maximum continuous Rating	45 TPH
Steam pressure	67 kg/cm^2
Steam Temperature	495 ± 5^0C
Fuel Fired	70% coal + 30% Biomass

The boiler has been designed to confirm to Indian Boiler Regulations (IBR). The boiler is divided into a combustion zone i.e. furnace and non-combustion zone i.e. economizer, air heater etc. The furnace sides; front and rear are of membrane panel construction which provides a gas tight sealing. For all the four water wall bottom headers, water is fed through supply pipes from down comers. The sidewall, front wall and rear wall panel tubes and top headers are connected to the steam drum through risers. The front wall paned tubes form the roof of the furnace.

Feed water is pumped from detractor to economizer through feed water pump. The feed water form economizer outlet is then led to the steam drum; steam is generated in the furnace wall tubes .The resulting water, steam mixture from the riser tubes of membrane panel returns to the steam drum where the steam is separated from water. The saturated steam is led through the supply pipes to the PSH Intel header. From the PSH inlet header steam passes through the coils to PSH outlet header, then steam is led to attemperator and then to the SSH inlet headers and passed through coils to the SSH outlet header, finally from the SSH outlet header, steam is passed to the main steam line to turbine.

Combustion of the fuel takes place in the boiler bed where the fuel is spread with the help of the coal feed nozzles fixed in the bedplate. Combustion air is sucked from the plant environment by the motor driven forced draft (FD) fan and conditioned air is passed through specially designed air nozzles which are welded in distributor plate or bed plate. Primary air fan air is used for transportation of fuel. Balanced draft condition inside the furnace suitable for combustion is being maintained by induced draft (ID) fan.

Four openings are provided in the rear wall of the boiler. Flue gases generated, pass through the super heater coils and led to economizer then to air pre-heater, ESP and finally into the stack by ID fan.

The starting, stopping and safe shut down of boiler are done by manual intervention systematically and sequentially through DCS control system from control room. Details of equipments, their brief operational maintenance features are elaborated in the subsequent sub sections.

Over bed Fuel (biomass) feeding system comprises the following.

- Biomass silo
- Twin drum feeder or extractor
- Screw feeder or conveyor

3.7 Component Description

3.7.1 Biomass silo

From the fuel processing plant the biomass fuel enters the biomass silo of different capacities through bell conveyers. The existing two number biomass storage silo is reused by CPP as shown in Fig. 3.11

Fig. 3.11: Biomass silo

3.7.2 Slice gate for biomass silo

A manually operated isolating sliding gate is provided at the bottom of biomass silo, before fuel enters twin drum feeder. By isolating this gate, maintenance job can be taken up in the respective twin drum feeder.

3.7.3 Twin drum feeder or extractor

Twin drum feeder is placed just below the biomass silo. It extracts the biomass and then biomass fuel enters in the screw feeder. These twin drum feeders are motor driven supplied by Thermax Limited (TL) and the speed is controlled by automated drives and through reduction gearboxes as shown in Fig. 3.12. Fuel control can be achieved by varying the speed of the twin drum feeder. Twin drum assembly with coupling, gear box and motor coupling with covered cap is supplied by TL.

Fig. 3.12: Twin drum feeder and screw feeder

3.7.4 Screw feeder

There are two screw feeders provided below the twin drum feeder as shown in Fig. 3.12. These screw feeders are motor driven and the speed is controlled by automated drives and through reduction gearboxes. Fuel can be achieved by varying the speed of the feeder.

3.7.5 Slide gate at screw feeder outlet

A manually operated isolating sliding gate is provided at the bottom of screw feeder. Before starting the screw feeder the sliding gate should be in open position and feedback should come to the DCS. This interlock is used as a screw feeder start permissive. Pneumatically operated limit switch is used for slide gate open/close feedback. Side gate at screw feeder outlet with open/close limit switch is pneumatic operated.

3.7.6 Expansion bellow outlet of screw feeder

Expansion bellows are mounted at the outlet of screw feeder to take care of boiler expansion during combustion as shown in Fig. 3.13. TL supplies these expansion bellows.

Fig. 3.13: Expansion bellows

3.7.7 Pneumatic spreader

Pneumatic spreader is mounted on the furnace wall as shown in Fig. 3.14. Panel opening tubes are provided to mount the pneumatic spreaders. Mounting box is provided to mount the spreaders. Trajectory plates are provided to throw the fuel inside the furnace. Again trajectory plates can be adjusted for fuel spreading inside the furnace. Hot air tapping is taken from APH duct near wind box to provide spreading air to pneumatic spreaders.

Fig. 3.14: Pneumatic spreader

3.8 Bed Filling

Bed material size and chemical property must be maintained strictly as per the specification for smooth start up and efficient operation, it also necessary to confirm that the material must be dry without moisture. Following procedure is adopted for bed filling:

- Shift the bed material to the feeding platform.
- Start the ID fan as per fan start up procedure.
- Adjust the furnace pressure.
- Start FD fan as per fan start up procedure.
- Open the entire compartment wind box damper.
- Isolation dampers to burner, over fire air and primary air lines shall be kept closed.
- Open FD fan suction damper or increase the fan speed and maintain the wind box pressure.
- Maintain furnace pressure.
- Note down the wind box pressure of individual compartments.

- Bed material may be filled manually through opening provided on the sidewall panels for view port cum bed material filling opening.
- Bed material filling should be done in batches. It should not be done in one stretch as it will cause accumulation of material at the drop point and restrict the fluidization of bed material at this location.
- Bed material shall be filled up to 275 to 300 mm heights above the bubble cap top, which is to be verified physically.
- Prior to confirm the bed height, it is recommended to fluidize the compartments thoroughly to spread the material uniformly. It may require fluidizing the compartments one by one with higher air duct pressure so as to distribute the bed materials evenly across combustor.
- On confirming if the bed material is uniformly distributed, it is a must to study the minimum fluidization wind box pressure. Record the minimum fluidization wind box pressure and airflow for the start up compartment, as the same is a guiding parameter during coal firing.

3.9 Boiler Start Up and Pressurizing

Following procedure is adopted for boiler startup and pressurizing:

ID fan is first started according to start up procedure.

- FD out let pressure is maintained up to 600-650mm water column by operating fan suction damper or by varying the fan speed.
- Then the compartment damper is opened one by one and the fluidization is obtained by increasing the FD discharger pressure.
- Minimum and maximum air pressures required to fluidize the bed should be taken care of and then the bed level is physically checked. It should be 250-300mm above the bubble cap.

- Then the bed is fluidized and it is ensured that no heaping of bed matrix is remained in the compartment.
- Once this activity is completed, then all the fans are stopped.
- For startup bed, charcoal is be uniformly sized to 15-25mm. Tamarind wood charcoals, free from moisture and dust is however preferred.
- The dry charcoal is uniformly fed into the bed and ensured that charcoal is spread 1 ft away from water wall panel and from adjacent compartment.
- Considering the start up bed area and the bed material quantity, charcoal requirement is calculated as per start up. This quantity may vary with the type of charcoal and start up which needs to be established during boiler commissioning & further start ups.
- The minimum quantity of charcoal to be filled in the startup compartment is 15% of the total weight of the bed material above the bubble cap in startup compartment.
- Now the boiler is ready for light up manual mode till steady steam flow is ensured. At this stage, it is helpful if the furnace draft control is taken to auto mode.

3.10 Biomass Firing

Biomass is fired through over bed firing. Prior to biomass firing it is mandatory to check the twin drum feeder, Screw feeder and pneumatic spreader. Then 30% Biomass is to be fired with 70% coal firing.

3.10.1 70% coal firing + 30% biomass firing

For 70% coal firing, above procedure is referred. Biomass is introduced through over bed firing by starting pneumatic spreader, screw feeder and twin drum feeder. First the over

bed firing is stabilized by starting single feeder, then the second feeder is started for increasing boiler load with 30% biomass firing.

CHAPTER 4

CFD ANALYSIS

Computational fluid dynamics is a technique which is emerged from the combination of fluid dynamics and numerical methods along with a hi-tech support of powerful computer systems to run large simulations in minimum timeframe. CFD may be defined as the set of different techniques by which computer become capable of providing a number of numerical simulations of mass flow and heat exchange [177]. CFD technique is used for analyzing the systems which involve mass flow, heat exchange and other processes such as combustion involving number of chemical reactions and gasification by means of digital computer systems. Computational fluid dynamics is also considered as a useful technique for industries involved in power generation. It can evaluate complete fluid flow separations, temperatures profiles and mass distributions of species with their particle trajectories and many more along with pollutant concentrations with high accuracy. In the other words it is a high quality technique which can very effectively be used for presuming heat exchange and mass transfer, mass flow, combustion, chemistry involved and other similar processes.

CFD model works on the basis of few basic assumptions that make it capable of calculating local changes in temperature and pressure, velocity profiles, gas composition, fuel particle tracks and others for a given domain. The Navier–Stokes equations in a CFD code are generally solved by implying a discretization technique, in which a given problem of calculus is transformed into a given number of algebraic correlations and then these equations can be solved by digital computer by using a suitable solution technique. A discretization technique is applied with a solution methodology to obtain the numerical solution of heat exchange and mass flow problems. Among various discretization

methods studied so far, the most commonly used methods are the Finite difference method (FDM), the Finite volume method (FVM) and the Finite element method (FEM).

In the beginning of Computational fluid dynamics (CFD), finite difference method was the most popular technique because it was mathematically simple, accurate and efficient. However, they are best suitable for uniform grids only which contain regular computational domains. With the passage of time the CFD codes with new advancements and new features as its application to industrial problems, also provided the methods which may even solve complex geometries. By using finite difference method to complex geometries, they are converted into simple domains by converting them into algebraic equations and then solving these equations. But due to these transformations the governing equations become complicated and may cause a loss of computational accuracy and efficiency. In view of that the finite volume methods can be adopted directly on the entire domain without any conversion. Finite volume methods are actually a generalized form of the finite difference technique. These methods use governing equations in integral form instead of differential form of equations. It gives more flexibility in formulating complex domains. The Fluent, a well-known CFD code, which is used to simulate various flow field problems, is based on the finite volume discretization scheme [120]. Hence, a CFD solution changes the continuous flow domain in to a domain of discrete elements by constituting a grid. In case of the continuous flow situation, every variable of flow is applied at each location in the fluid flow system. For example, the pressure in case of continuous flow situation shown in the Fig. 4.1(a) below may be given as:

$$\rho = \rho(x), \quad \text{where } x \text{ lies between 0 and 1} \qquad (4.1)$$

In case of scattered domain, every variable of fluid flow is applied at the grid positions only as shown in Fig. 4.1(b), the pressure is applied at the grid locations only.

$\rho_{i=} \rho(x_i)$, i varies from 1 to N (4.2)

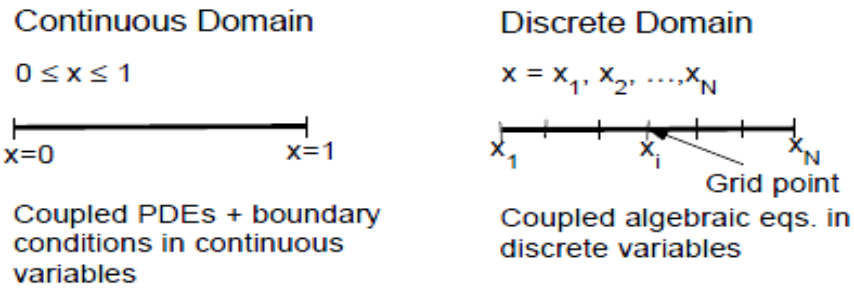

Fig. 4.1 (a) Domain in continuous form (b) Domain in discrete form

In CFD technique, the various variables of flow can only be computed at grid locations. After interpolating the values at all locations of grid the values at different positions may be computed. The boundary conditions and the leading partial deferential correlations are applied in the form of the regular variables like $\rho$and$\vec{V}$etc. These may be approximated in case of scattered elements in the form of the scattered variables such as $\rho_{i,}$ $\vec{V}_i$ etc. The system of discrete elements is actually a group of number of algebraic correlations in the scattered domain. These discrete systems involve more number of computations repeatedly in the form of a set of matrix which are solved in a sophisticated computer. This approach may be applied to any flow domain of interest.

4.1Finite-Difference Method Discretization

For the simple understanding of the details, we can apply the basic ideas of CFD after implementing them in the one dimensional correlation as follows:

$$\frac{du}{dx} + u^m = 0; \qquad 0 \leq x \leq 1;\ u(0) = 1 \tag{4.3}$$

Let us assume, m = 1 and the correlation to be linear. Then we assume, m = 2 case and the correlation be nonlinear. The grid may be derived in to different discrete coordinates for the above mentioned equation m = 1 as shown in Fig. 4.2:

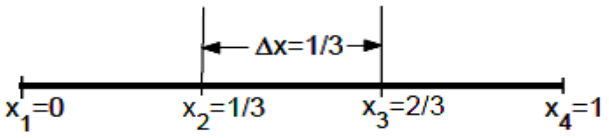

Fig. 4.2: Equally spaced grid

The grid is divided in to four equally spaced points. The distance between these points is Δx. The guiding correlation is applicable at all the points and written as

$$\left(\frac{du}{dx}\right)_i + u_i = 0 \tag{4.4}$$

here i is having some value at position x_i. u_{i-1} can be expanded by Taylor's equation to obtain the equation for $(du/dx)_i$ in form of u at different positions of the grid:

$$u_{i-1} = u_i - \Delta x \left(\frac{du}{dx}\right)_i + O(\Delta x^2) \tag{4.5}$$

After rearrangement we get

$$\left(\frac{du}{dx}\right)_i = \frac{u_i - u_{i-1}}{\Delta x} + O(\Delta x) \tag{4.6}$$

Some errors would found in $(du/dx)_i$ by the reason of few ignored parameters in the Taylor's equation. This error is known as truncation error. Because the truncation error in the above equation is $O(\Delta x)$, this equation may be considered accurate for first-order.

Putting equation (4.6) in eq. (4.5) and neglecting high power equations in the Taylor's equation, we obtain the correlation of scattered elements as given below:

$$\frac{u_i - u_{i-1}}{\Delta x} + u_i = 0 \tag{4.7}$$

The solution explained above for obtaining the one dimensional equation of scattered elements by the expansion of using Taylor's equation, is called the finite deference technique. But most of the CFD packages apply the FVM or FEM because they are more

suitable for analyzing fluid flow and heat transfer in larger and complicated domains. For instance, the Fluent package applies the FVM whereas ANSYS applies the FEM. In the upcoming section the methodology of finite-volume technique is explained but still the finite-deference approach is adopted to understand the general ideas that are almost same for the deferent techniques of discretization in which the finite-deference technique is the most easily understandable.

4.2 Finite-Volume Method Discretization

In a grid of domain a number of quadrilaterals are found. In the finite-volume technique, this shape is called a "face or cell" and the grid position is referred as a "node". In two dimensional problems, triangular cells could also be generated. In 3-D domains, cells are usually of hexahedral shapes, tetrahedral shapes, or in the form of prisms. In the finite-volume technique, the conservation equations are implemented to the volume of domain in integral form. The continuity equation for uniform time independent state is given by:

$$\int_s \vec{V} \cdot \hat{n} dS = 0 \tag{4.8}$$

The integration is done for the surface *S*, where $\hat{n}$ is the normal to the surface. This correlation indicates that the fluid volume that flow into the domain volume would remain zero. Choose a four sided face as given in Fig. 4.3.

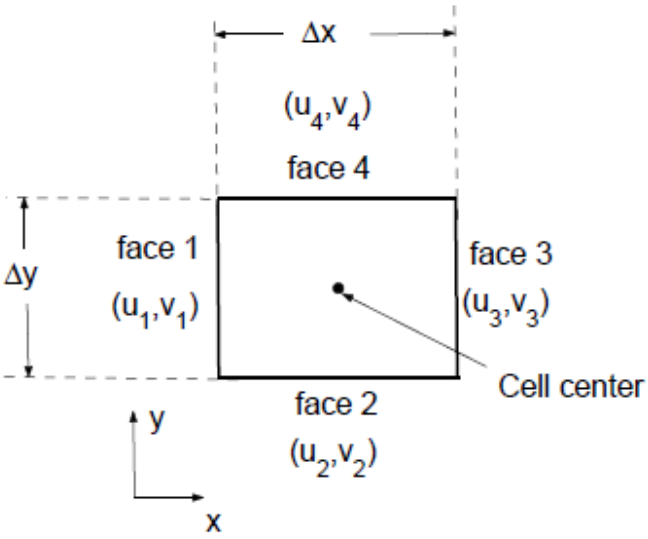

Fig. 4.3: Rectangular cell

The velocity at cell *i* is selected as $\vec{V}_{i} = u_i\hat{\imath} + v_i\hat{\jmath}$. Thenapplying the correlation for mass (4.8) to the domain volume we get.

$$-u_1\,\Delta y - v_2\,\Delta x + u_3\,\Delta y + v_4\,\Delta x = 0 \tag{4.9}$$

The given equation is the scattered type of the equation of continuity for the cell. It is similar if we add the mass flow rate and control volume equal to zero. Doing this it can be ensured that the total fluid flow into the face would be null and thus the mass is utilized for the face. The quantities at the center of the cells are utilized. The cell values can be calculated by number of iterations of the values of the center of cell at the nearby cells.

On the similar manner correlations for scattered elements for the momentum and energy conservations can be achieved for the cell. These concepts may be easily applied to any shape of the cell in two dimensional or three dimensional domains or any conservation equation.

4.3 Discrete System and Boundary Conditions

The correlation achieved for a discrete system previously by using the FDM was

$$\frac{u_{i-u_{i-1}}}{\Delta x} + u_{\mathrm{i}} = 0 \tag{4.10}$$

After rearrangement, it becomes

$$-u_{\mathrm{i\text{-}1}} + (1 + \Delta x)u_{\mathrm{i}} = 0 \tag{4.11}$$

If this correlation is applied to the one dimensional grid as considered previously at the locations *i* = 2, 3, 4 then it is used as

$$-u_1 + (1 + \Delta x)u_2 = 0 \text{where } i \text{ is equal to } 2 \tag{4.12}$$

$$-u_2 + (1 + \Delta x)u_3 = 0 \text{where } i \text{ is equal to } 3 \tag{4.13}$$

$$-u_3 + (1 + \Delta x)u_4 = 0 \text{where } i \text{ is equal to } 4 \tag{4.14}$$

The correlation for scattered domain is not used at the boundary value (i=1) because u_{i-1} is not fixed. In place of it the valley which is generally applied is

$u_1 = 1$ (4.15)

Correlations (4.12) - (4.15) constitute a matrix of algebraic equations by using four variables such as, u_1, u_2, u_3 and u_4. This matrix is written as:

$$\begin{bmatrix} 1 & 0 & 0 & 0 \\ -1 & 1+\Delta x & 0 & 0 \\ 0 & -1 & 1+\Delta x & 0 \\ 0 & 0 & -1 & 1+\Delta x \end{bmatrix} \begin{bmatrix} u_1 \\ u_2 \\ u_3 \\ u_4 \end{bmatrix} = \begin{bmatrix} 1 \\ 0 \\ 0 \\ 0 \end{bmatrix}$$

In finite – volume method the discrete equations can be applied to the grid points at the interior of the domain. Near the boundaries of the cells or grid points, the correlations for discrete elements and boundary inputs may be used in combined form. Finally a set of algebraic equations is obtained, whose values are equivalent to the values of independent scattered unknowns. However the procedure remains similar for the above mentioned correlation of the model, but the implementation become more difficult.

In the Fluent also similar to the other CFD packages, a number of features are provided for applying different boundary inputs for example pressure at entrance, exit pressure and velocity inlet etc. It is important to mention here that to select and apply the suitable boundary inlet is most important feature to achieve a perfect solution of your project. To implement suitable boundary input it is also very necessary to go through the different options available in any of the CFD code.

4.4 Nonlinearity

For a fluid the momentum conservation equation is a nonlinear equation because the convection term used in it $(\vec{V} \cdot \nabla)\vec{V}$.The other Phenomena such as different chemical reactions and turbulence inside the domain cause more nonlinearities. Usually it becomes very difficult and challenging job to obtain the practical solution of the complex flows

due to high non linearity present in the governing equations. The effect of the nonlinearity can be understood from simple one dimensional example if we put m = 2:

$$\frac{du}{dx} + u^2 = 0; \quad 0 \leq x \leq 1; \quad u(0) = 1 \tag{4.16}$$

The solution of this correlation, which is similar to that is given in (4.7) is mentioned as when m = 1

$$\frac{u_{i} - u_{i-1}}{\Delta x} + u_i^2 = 0 \tag{4.17}$$

This is an algebraic correlation in nonlinear form. In this equation the term u^2_i is the cause of nonlinearity. The nonlinearity can be nullified if the equations be linearised by selecting an arbitrary *imaginary value* for the solution and then run the solution up to number of iterations until unless the imaginary value agrees with the solution to a satisfactory level of tolerance. Let the imaginary value for u_i is u_{gi}. Then

$$\Delta u_i = u_i - u_i - u_{gi} \tag{4.18}$$

After rearrangement and doing squaring of this correlation we get

$$u_i^2 = u_{gi}^2 + 2 u_{gi} \Delta u_i + (\Delta u)^2 \tag{4.19}$$

Here $\Delta u_i \ll u_{gi}$, and neglecting Δu^2_i term it gives

$$u_i^2 \cong u^2_{gi} + 2 u_{gi} \Delta u_i = 2 u_{gi} + 2 u_{gi} (u_i - u_{gi}) \tag{4.20}$$

Now,

$$u_i^2 \cong 2 u_{gi} u_i - u^2_{gi} \tag{4.21}$$

After linearization the approximate value (eq. 4.17) becomes

$$\frac{u_{i} - u_{i-1}}{x} + 2 u_{gi} u_i - u^2_{gi} = 0 \tag{4.22}$$

As $u_g \rightarrow u$ the error of linearization becomes zero

We need to put the guess values u_g at the grid points in order to calculate the finite-deference approximation. One can start from the first iteration with an initial guess value. The value of u achieved in the earlier interpolation may be applied as the imaginary value for the upcoming iterations.

$u^{(1)}_{g}$ = Initial guess, Iteration 1

$u^{(2)}_{g} = u^{(1)}$, Iteration 2

$u^{(l)}_{g} = u^{(l-1)}$, Iteration l:

The level of iteration is signified by the superscript. Iterations are continued until the solution is converged. This process is applicable to all CFD codes in which all the conservation equations are linearised by removing the nonlinear terms. However few working details may vary from code to code. It is important to recall that the linearization is achieved by using a imaginary value and then number if iterations are performed continuously until the solution converges.

4.5 Turbulence Modeling

The flows are generally identified and classified in two types, one is laminar flow and the other is turbulent flow. Laminar flows are that flows in which velocity fields vary smoothly in flow domain with respect to time and in which any laminate does not create cross currents around each other. These flows take place when the viscosity of fluid remains very large so as to dominate any fluctuations taking place during flow which take place due to imperfect boundaries or other reasons. Such flows take place at lower range of the Reynolds number. Reverse to it, the turbulent flows are distinguished from laminar flow by large and random perturbations in the velocity and pressure of fluid in the flow domain with respect to time. These perturbations and fluctuations occur due to

irregularities which rise rapidly. These fluctuations are stopped only when nonlinear interactions in the flow become the reason behind breaking down them into small whirls which are dispersed in the form heat energy. These flows take place at the higher values of Reynolds numbers.

The turbulence profile over a time domain for the variable of flow *u* at a given location in domain is given in Fig. 4.4. The averages are differentiated in to three types:

1. Average based on time
2. Average based on volume and
3. Ensemble average

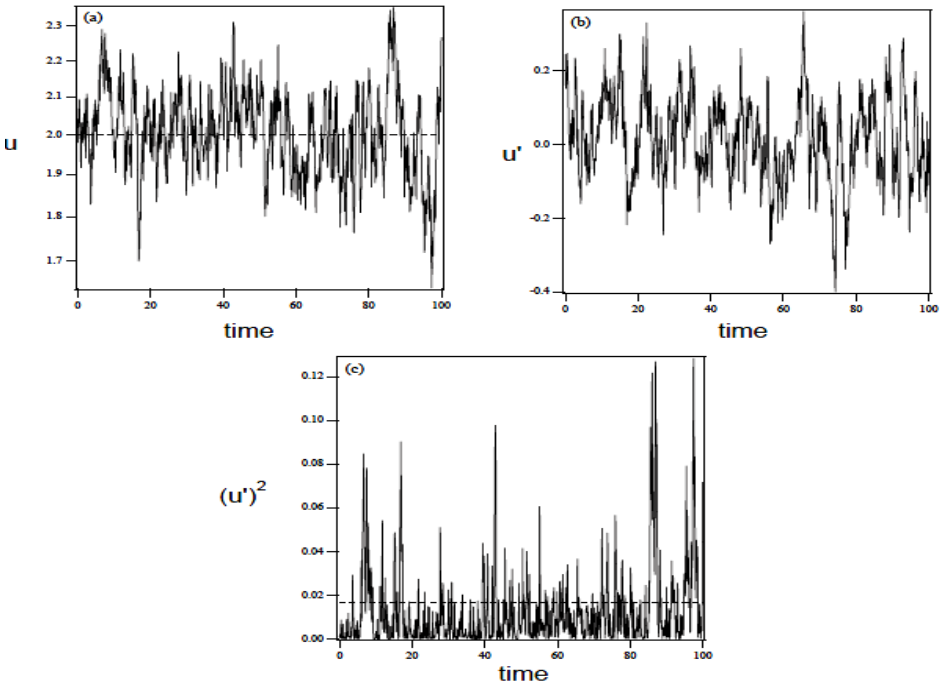

Fig. 4.4: Time history profile of a location in a turbulent flow (a) Velocity profile (b) shows fluctuation in the velocity component (c) shows the square value of the varying velocity. Dotted lines in (a) & (c)show the mean values of time.

Mathematically the mean of the values is known as the ensemble mean, in which the problem is repeated again and again and then the average value of the required parameter is calculated at the same location with respect to time in every trial. But in real

problems, this is not usually performed. In place of it a mean volume or mean of time or amalgamation of both is done by assuming that they are equal to the total mean. For example, one may consider the mean of time for a stable flow as

$$\bar{u}(y) \equiv \lim_{\mathcal{T}\to\infty} \frac{1}{2\mathcal{T}} \int_{-\mathcal{T}}^{\mathcal{T}} u(y,t)dt \tag{4.23}$$

The variation in the velocity from the average value is generally diven as

$$\acute{u} \equiv u - \bar{u} \tag{4.24}$$

As by the definition the average value of fluctuation is zero i.e $\overline{\acute{u}}$ = 0, a better measure of the variation, is to evaluate the mean of the square of a changing variable. Figures 4.4 (b) and 4.4(c) show fluctuation for velocity u^0 and the square of that velocity, u'^2 over a time domain. It is important to mention here that the average of velocity u'^2 is always greater than zero.

The equations which govern a turbulent flow are almost similar as in case of laminar flow; no doubt, the calculation of turbulent flow becomes very complicated in any flow region. The correlations of turbulent streams may be solved by two different approaches. One is Direct numerical simulations (DNS) and the other one to solve the Reynolds Averaged Navies Stokes (RANS) equations. In DNS the sophisticated computers solve the Navier Stokes equations in integral form and remove all of the fluctuations whether spatial or temporal. In actual practice the solution procedure for turbulent flow is same as for laminar flow, except all the variations in velocity and pressure must be resolved smoothly. The implementation of DNS is supposed to be limited to simple geometries for e.g., flow through channels, boundary layers and air flow over jets. Also these simulations are extremely expensive to run. The other approach solving Reynolds Averaged Navies Stokes (RANS) equations is found in more number of the CFD codes like Ansys or Fluent. RANS equations are easier to implement as they command the average velocity and pressure and these parameters vary slowly in flow

domain with respect to time.

To demonstrate a flow problem, one can select a complete turned turbulent flow in a passage of length 2*H*. As discussed previously that by using RANS one can only solve the average velocity $\bar{u}$ (*y*). If one finds the average of the Navies Stokes correlations and then solves the problem then the equation obtained is given below:

$$\frac{d\overline{\grave{u}\acute{v}}}{dy} + \frac{1}{p}\frac{d\bar{p}}{dx} = v\frac{d^2\overline{u(y)}}{dy^2} \tag{4.25}$$

With boundary conditions as

$$y = 0 \ \frac{d\bar{u}}{dy} = 0, \tag{4.26}$$

$$y = 0 \ H\bar{u} = 0, \tag{4.27}$$

The quantity $\overline{\acute{u}\acute{v}}$ is known as the Reynolds stress. This quantity is a higher-order term and should be calculated by the known values of $\bar{u}(y)$ and their derivatives. The reliability of the computations is primarily dependent on the modeling quality of this quantity.

Reynolds stress may be calculated with the help of two parameters of turbulence, the dissipation rate of turbulent energy $\mathcal{E}$ and kinetic energy of turbulence *k* as given below:

$$\mathcal{K} \equiv \frac{1}{2}\left(\bar{\grave{u}} + \overline{\grave{w}^2}\right) \tag{4.28}$$

$$\mathcal{E} \equiv v\left|\left(\frac{a\grave{u}}{ax}\right)^2 + \left(\frac{a\grave{u}}{ay}\right)^2 + \left(\frac{a\grave{u}}{ay}\right)^2 + \left(\frac{a\grave{v}}{ax}\right)^2 + \left(\frac{a\grave{v}}{ay}\right)^2 + \left(\frac{a\grave{v}}{az}\right)^2 + \left(\frac{a\grave{w}}{ax}\right)^2 + \left(\frac{a\grave{w}}{ay}\right)^2 + \left(\frac{a\grave{w}}{az}\right)^2 \tag{4.29}$$

where ($\grave{u}\grave{v}\grave{w}$) is vector quantity of varying velocity . The kinetic energy is considered null for the laminar flow and in case of turbulent flow its value is taken up to five percentage of the kinetic energy of the average flow. These models constitute a number of turbulence sub-models and generally known as *k*–ε models. Importantly these models are used in most of the CFD packages including Fluent.

4.6 Classification of Meshes

With the developments in CFD codes in terms of advanced algorithms, more computational space has become available to CFD based researches which resulted in better solver techniques. Amongst all these advancements one of the best results is the development in the mesh techniques and extension of the mesh elements and their connectivity with each other. The classification of the mesh elements is usually done on the basis of their connectivity or on the type of elements available.

4.6.1 Classification on the basis of connectivity

On the basis of connectivity the mesh elements are classified as of two types: structured or unstructured.

(a) Structured Meshes

A structured mesh is a type of mesh which is regularly connected to the elements and can be shown by 2D or 3D set of elements. In this mesh the type of elements is restricted as quadrilateral in two-dimensional geometry and hexahedral in case of a three-dimensional geometry. Due to the regularity in the connectivity of the elements the space is conserved because the geometrical relationships amongst all the elements are dependent upon their storage arrangement.

(b) Unstructured Meshes

Unlike structured mesh the unstructured mesh elements are connected to each other in a irregular manner. The unstructured mesh cannot be stored as 2-dimensional or 3-dimensional array in computer programme. In this type of mesh any type of element may be used by the solver. The space accumulation in case of unstructured mesh is also more as comparable to structured mesh.

4.6.2 Hybrid meshes

A hybrid mesh consists of both structured mesh and unstructured mesh at different portions. The knowledge of hybrid mesh deals with how the mesh is actually used. The term “hybrid” should not be confused with the term “mixed”. The term "mixed" is used when the mesh is made of both unstructured mesh elements and structured mesh elements especially when they are used in an unstructured form.

4.6.3 Classification based upon element type

Other classification of the meshes is done upon the basis of size and shape of the elements used. Based upon the form of analysis and solution needs of the specific problem, meshes may be two-dimensional (2-dimensional) or three-dimensional (3-dimensional). The elements used in 2-dimensional meshes are triangles or rectangles, and common elements used in 3-dimensional meshes are tetrahedral or hexahedral. As discussed earlier, based upon the choices of connectivity the types of element used may be restricted, so there may sometime be overlap between classification based upon connectivity and based upon element type.

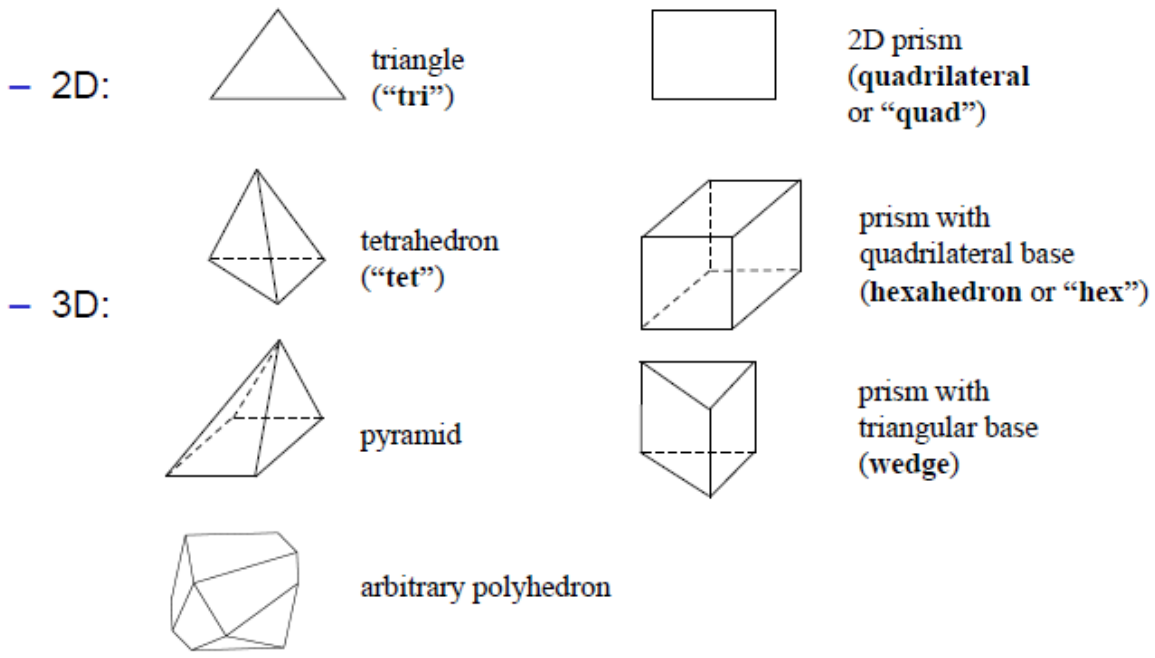

Fig. 4.5: Different shapes of 2-dimensional and 3-dimensional mesh elements

In a 2-dimensional mesh, all mesh elements are placed in a mentioned plane. In many cases, 2-dimensional mesh elements are placed in the XY plane. However, they may be placed to different coordinates or specific plane also. The types of 2- dimensional mesh elements which are mostly used are quadrilaterals which are also known as quads and triangles which are also known as tris, as shown in Fig. 4.5. 3-dimensional mesh nodes cannot be placed in a single plane. Mostly used 3-dimensional mesh elements are hexahedral which are also known as hexes or hex elements and tetrahedral or tets, square pyramids or simply pyramids and extruded triangles or wedges or triangular prisms, as shown in Fig. 4.5. It is important to mention here that all the above mentioned elements are connected to each other by the faces which belong to the above mentioned 2-dimensional elements. Some of the presently used CFD codes also use polyhedral elements, which can be connected by any number and types of cells.

As all the 3-dimensional elements are connected by 2-dimensional elements in the domain, it is quite obvious that 3-dimensional meshes are bounded by 2-dimensional elements at the boundaries. Mostly used software packages and their solvers use connected elements altogether in a surface mesh. By doing this it becomes easier to apply the boundary conditions and rendering the mesh so as to obtain the better visualizing results. The algorithms used for meshing usually start the meshing from connecting surfaces of the domain before applying the meshes to the interior of the domain. These algorithms are also called as interior algorithms. For these algorithms, the formation of a high quality surface mesh is always a task of prime concern. Researchers have performed a broad work in the field of optimized and high quality surface mesh formation. Since the meshes are usually generated geometrically by the amalgamation of 2-dimensional and 3-dimensional mesh elements, they are also sometimes called as 2.5-dimensional meshes.

4.7 Type of Mesh

Hexahedral mesh is the most preferable to attain precisely high accuracy. The mesh should possess sufficiently high density so that it should conform all the features of flow and mass distribution, but on the same side this density should not be that much high that it conform other unwanted features of the flow and thus forcing the CPU to put unnecessary burden on it and taking more time to run the simulations. For example in case of a wall in the problem domain, the mesh near to the wall is of fine quality with more number of elements so as to compute the boundary layer flow. For this, preferably quadrilateral, hexahedral and prism elements are used instead of triangles, tetrahedrons and pyramids. Quadrilateral and hexahedral elements may be easily expanded where a completely developed and 1D flow is available.

4.8 Skewness

The skewness inside a mesh is an indirect measure of the type of the mesh in terms of its quality and its application to the problem. In case of increased skewness one would obtain comparatively less accuracy for the domain which is interpolated. There are generally three modes of finding the skewness in a mesh:

Skewness calculation on the basis of equilateral volume:

This is a default method which is applied to triangles and tetrahedral only. Where

$$\text{Skewness} = \frac{\text{Optimum size of cell} - \text{size of cell}}{\text{Optimum size of cell}}$$

Skewness based upon the deviation from equilateral angle:

This method is applicable to all the cells or faces and shapes but most of the times used for prisms and pyramids

$$\text{Skewness} = \max\left[\frac{\theta_{max} - 90}{90}, \frac{90 - \theta_{min}}{90}\right]$$

Equiangular skew

Other commonly used indication of quality of mesh is equiangular skew:

$$\text{Equiangular Skew} = \max\left[\frac{\theta_{max} - \theta_e}{180 - \theta_e}, \frac{\theta_e - \theta_{min}}{\theta_e}\right]$$

here:

θ_{max} is the largest angle of the element,

θ_{min} is the smallest angle of the element,

θ_e is having a value of 60 degrees for a triangle and 90 degrees for a square.

A skewness of zero is undoubtedly considered as the most suitable value which could be obtained and a skewness of value 1 is always undesirable. For hexahedral and quadrilateral elements, skewness must not be more than 0.85 to achieve good results. In case of triangular elements, skewness must not be more than 0.85 and for quadrilateral elements skewness must be less than 0.9.

4.9 Smoothness

Another important factor is smoothness. The size of the mesh should be carefully changed in order to achieve error free solution. If the size is suddenly changed then there is utter possibility of developing errors in the nearby cells.

4.10 Aspect Ratio

Aspect ratio may be defined as the ratio of largest side to the smallest side in a face as shown in Fig. 4.6. In ideal conditions it is equal to one to obtain the perfect solution. For three dimensional flows, it should be nearly one. In addition to that, the changes in the size of the face should be minimum e.g. the sizes of adjacent cells should not have a variation more than 20%. With a large aspect ratio the interpolation errors of large magnitude may take place.

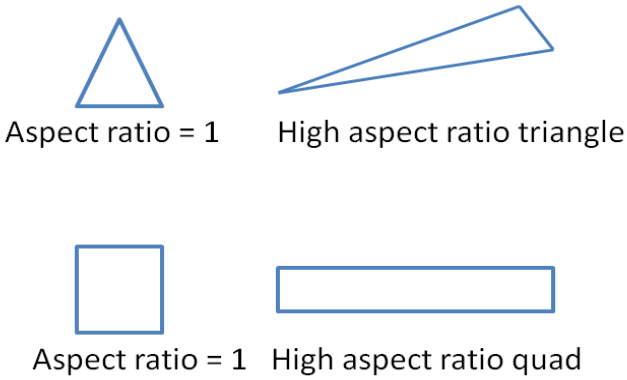

Fig. 4.6: Aspect ratio

The quality of mesh is an important parameter in deciding the precision and perfection of the simulation. The quality of mesh depends upon a few parameters like distribution around node points, smoothness and skewness. The distribution of the nodes inside the mesh and density are the primary attributes of the mesh which plays a significant role in resolving all the issues related to flow such as layers of fluid, separated flow regimes, shock waves, mixing zones and boundary layers.

Sometimes important features of the flow are changed due to inferior resolutions in the important regimes of fluid flow. For instance, the effect of different pressure gradients to find out the separation inside flow domain depends highly on the resolution of the boundary layer along the flow separation. Generally, the flow paths should not be represented by the cells less than five. Most of the time large number of cells is required to completely resolve the path. In the regions like mixing zones or flow layers with shear forces the mesh should be of fine size elements so that the variation in the flow variables could be controlled. Consecutive changes in the volumes of the cells placed between adjacent elements may develop more errors. Truncation error exists due to presence of a difference between partial derivatives available in the guiding correlations and assumptions presumed for their solution. The structure of the face based upon its aspect ratio and skewness also has a deep impact in deciding the accuracy of the numerical solution.

As discussed earlier, skewness exists due to the difference between the shape of the face and the shape of an equivalent face of similar volume. Faces with more skewness are having less accuracy and are responsible for less stable solution. For instance, meshes with quadrilateral cells have vertex angles nearly 90^0, while the optimal meshes with triangular cells have angles nearly 60^0 and thus having all the inclinations below 90^0. Aspect ratio gives the value of the magnitude of the expansion of the face. In case of anisotropic flows if the number of cells is less and aspect ratio is more, then inaccurate results would be produced. Generally aspect ratio is not exceeded from 5:1 in the critical parts of the flow regime. However the effect of smoothness, resolution and cell shape on the stability and precision of the simulation procedure is primarily based on region of flow field being solved. For a case, the cells with less value of skewness are acceptable in the flow regimes with less mixing rates but such cells are highly unacceptable in the regions with higher flow gradients. Because the regimes with strong flow gradients are not identified at the initial stages of solution so, a fine quality mesh should be generated over the entire flow domain.

The complete formulation of the geometry under study is usually performed in GAMBIT using various combinations of vertices, edges and faces. However sometimes another user friendly modeling packages are also used by the researchers which has a file import interface with the solver. The geometry is then meshed either by dividing each edge or face into given number of mesh points or specifying the interval between the mesh points. Both uniform and non-uniform meshing can be done as per the requirement. The boundary zones are specified for e.g inlet port, fuel inlet zones, outlet ports and walls etc. The grid is then checked to verify the skewness and the aspect ratio criterion so as to satisfy the required criterion. After that the complete geometry is sent to the analysis module through export command. In the solver different models of flow turbulence,

energy and heat transfer, combustion or particle track may be applied according to the problem of domain.

4.11 Modeling Approach in CFD

CFD is a technique which is emerged from the amalgamation of fluid dynamics and numerical methods along with a hi-tech support of powerful computer systems to run large simulations in minimum timeframe. CFD may be defined as the set of different methodologies by which computer become capable of providing a number of numerical simulations of the flow of fluid and heat exchange. CFD technique is used for analyzing the systems which involve fluid motion, heat exchange and other processes like combustion involving number of chemical reactions and gasification by means of digital computer systems. Computational fluid dynamics is also considered as an important technique for power sector. It can evaluate complex flow separations, temperatures mass distributions of species, their particle trajectories and many more along with pollutant concentrations with high accuracy. In the other words it is a high quality technique which can very effectively be used for calculating heat and mass exchange, fluid flow, combustion and chemistry involved along with other similar processes.

CFD model works on the basis of few basic assumptions that make it capable of calculating instant deviations of temperature profiles and pressure, gas species, velocity, fuel particle tracks and others in a given domain. The Navier–Stokes equations in a CFD code are mostly solved by implying a discretization technique, in which a given problem of calculus is transformed into an array of algebraic correlations and then these correlations can be solved by digital computer by using a suitable solution technique. A discretization technique is applied with a solution methodology to obtain the numerical solution of heat exchange and problems of motion of fluid. Among various discretization

methods studied so far, the most commonly applied techniques are the Finite difference method (FDM), the Finite volume method (FVM) and the Finite element method (FEM).

With the advancements in algorithms to be used in CFD by the virtue of its enhanced computational capabilities, computational fluid dynamics is proved to be a very successful new tool in analyzing hydrodynamics and combustion. While it has become a standard mechanism for single-phase fluid flows, it is also emerging as a useful tool for multiphase complex systems, such as fluidized beds. More focus and research is required for the more suitable implementation of CFD in the field of fluidized bed combustors' modeling and simulation especially on large scale. Two types of approaches are used to implement CFD analysis to solid - gas fluidized bed combustors. First is Lagrangian modeling approach which is based on the molecular dynamics using discrete particle solution and the second is Eulerian–Eulerian modeling approach (also known as mutifluid) which uses continuous modeling mechanism in which both gas phase and solid phase are supposed to be a continuous phase based on continuum mechanics. Gera et al. [178] has provided a detailed comparison between these two approaches.

Eulerian approach works on the theory of balancing equations of mass, momentum, and energy for both the phases i.e gas and particle on macroscopic level. In Eulerian modeling approach the gas and the particle phase are treated as a continuous media and accordingly it is assumed that every element of the whole computational domain is occupied by both the phases. The gas phase is known as continuous or primary phase and the particle phase is known as dispersed or the granular phase. These phases are interpreted by the volume fractions and are connected through the drag force as given in the momentum equation and explained by Wen and Yu's [105] equation for a dilute system, Ergun [179] suggested another relation for a dense system, and Gidaspow et al. [180,181] used the correlation which is a combination of both the equations for

fluctuating systems. The field variables such as the solid velocities and gas velocities, volume fraction of solids and granular temperature of solids are calculated by averaging their values. The kinetic theory of granular flow (KTGF), which is based on empirical correlations, is applied to formulate mathematical relations to find the particle-particle interaction and to solve the conservation equations.

Eulerian–Eulerian modeling approach has been adopted as most commonly used approach for numerical simulation of fluidized bed systems. In this scheme the solid phases and gas phase are presumed as continuum phases. In this approach, the number of particles present in the system is modeled using continuous medium mechanism. The fuel particles are generally assumed to be identical with each other with same density and diameter. The basic approach in formulating the multifluid model is to assume both the phases as interpenetrating continuum, and thus to constitute balances of continuity, momentum and energy equations for each phase in integral form, with suitable boundary conditions for phase interactions.

Lagrangian approach or discrete particle solution is achieved by using Newton's law of motion for the solid phase. By applying this approach the path trajectories of the particles and the motion of selected particles can be traced. The interrelations between the particles are solved either by a particle dynamics of potential force [182] or by collision mechanism of particles [183]. In this method, the gas phase is computed separately by calculating a number of Navier-Stokes correlations based on mean values over a average time domain, on the other hand a big number of fuel components, air pockets or droplets are tracked to solve the solid phase over the selected flow field. In the Lagrangian scheme used for two-phase flow, the Newtonian equations of flow are solved for every fuel particle. While solving these equations the effects of particle interactions and gas forces acting on the particles are also included. As discussed earlier particle interactions are

solved by the collision mechanism [178,183] or particle dynamics approach [182, 184]. The discrete phase solution, DPM, is a particle tracking model, which is used to calculate the particle velocity and the corresponding particle track due to multi body interactions or collisions [185]. Particle track models are used for multiphase flows where an Eulerian model or continuum approach is not suitable. Undoubtedly by using DPM based models different properties of the particles which get affected during flow may be studied, but at the same time they require more computational space and time. Due to this limitation of more computational space, the Eulerian–Lagrangian models are usually applied to a selective number of particles. Therefore, continuum models are preferably used for simulations as they apply macroscopic hydrodynamics. Fig. 4.7 shows the multi level modeling scheme based upon the information gathered from different simulations.

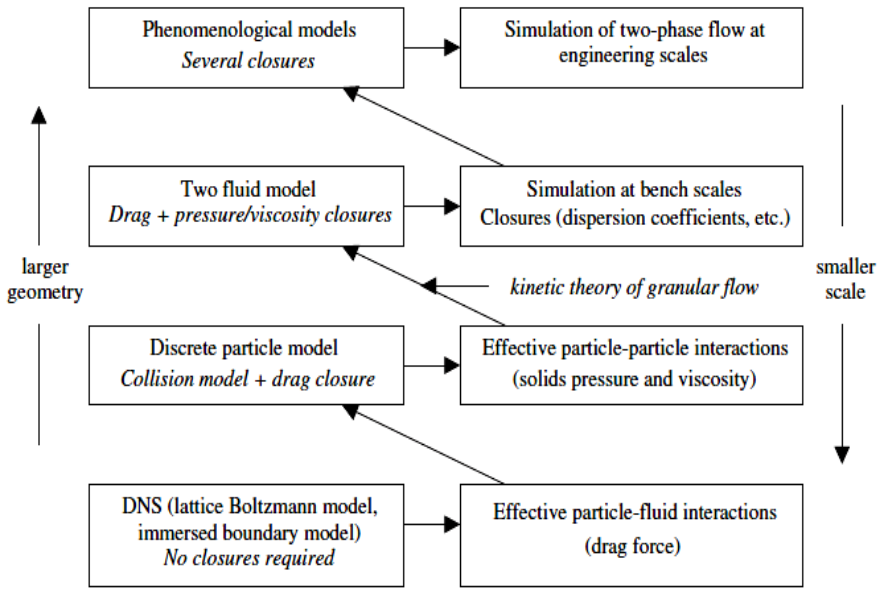

Fig. 4.7: Multi-level modeling scheme [186]

In case of the Lagrangian approach, the mass, momentum, and energy of the discrete phase is exchanged with the gas phase through the conservation equations. These equations are also responsible for the changes in volume fractions of different phases present in the domain. For each and every single fuel particle which travels in the flow field throughout the domain, their trajectories, heat exchange and mass transfer

calculations are achieved by a performing a force balance of the local parameters of the continuum phase. In this way, the external forces which act on the fuel particle like gravitational force, buoyant force, aerodynamic force and the forces produced due to collisions amongst particles and drag forces produced between the particles and the side walls of the combustor can be calculated at the same time along with the motion of the particles by using local entities of solid fuel and gas.

A Lagrangian equivalent may be used to derive a momentum equation based on Eulerian approach by averaging the phases of the particles. Depending on the outcomes and objectives of research and the type of methodology used, each approach has few advantages and limitations. By the use of above definitions of two approaches we may discuss the merits and shortcomings of each formulation.

4.12 Mathematical Description of CFD Models

The governing equations which are used while performing CFD analysis in Fluent consist of mathematical models of chemical reactions and gas phase. The CFD model applied in the present study used principle of mixture fraction approach or two fluid model (TFM). In TFM both the gas phase and particle phase are considered a continuum phase. The solution of the conservation equations for the mass, momentum and inter phase heat exchange through energy balance equations as follows:

Mass balance equations:

Gas phase:

$$\frac{\partial}{\partial t}(\varepsilon_g \rho_g) + \nabla \cdot (\varepsilon_g \rho_g v_g) = 0 \tag{4.30}$$

Solid phase:

$$\frac{\partial}{\partial t}(\varepsilon_s \rho_s) + \nabla \cdot (\varepsilon_s \rho_s v_s) = 0 \tag{4.31}$$

Momentum balance equations

Gas phase:

$$\frac{\partial}{\partial t}(\varepsilon_g \rho_g v_g) \nabla \cdot (\varepsilon_g \rho_g v_g) = \nabla \cdot \tau_g - \varepsilon_g \nabla p + \varepsilon_g p_g g - \beta(v_g - v_s) \tag{4.32}$$

Solid phase

$$\frac{\partial}{\partial t}(\varepsilon_s \rho_s v_s) + \nabla \cdot (\varepsilon_s \rho_s v_s v_s) = \nabla \cdot \tau_s - \nabla P_s^* - \varepsilon_s \rho_s g - \beta(v_s - v_g) \tag{4.33}$$

Energy balance equations:

Gas phase:

$$\frac{\partial}{\partial t}(\varepsilon_g \rho_g h_g) + \nabla \cdot (\varepsilon_g \rho_g h_g v_g) = -\nabla \cdot \varepsilon_g \cdot q_g + \alpha(T_g - T_s) + \tau g \cdot \nabla \cdot v_g + \varepsilon_g \left[\frac{\partial}{\partial t} p + v_g \nabla p \right] \tag{4.34}$$

Solid phase:

$$\frac{\partial}{\partial t}(\varepsilon_s \rho_s h_s) + \nabla \cdot (\varepsilon_s \rho_s h_s v_s) = -\nabla \cdot \varepsilon_s \cdot q_s + \alpha(T_g - T_s) \tau_s \cdot \nabla \cdot v_s + \varepsilon_s \left[\frac{\partial}{\partial t} p + v_s \nabla p \right] \tag{4.35}$$

$$hi = \int_{Tref}^{T} c_{p.i} dT_i \quad and \quad qi = -k_i \nabla T_i \tag{4.36}$$

The mass flow rate of coal as obtained from the plant is 2.083kg/s, flow rate of biomass is 0.7kg/s, velocity of air taken as 0.5m/s.

4.12.1 Devolatilization models

The process of devolatilization starts when the temperature of fuel attains a particular range. Various models of devolatilization for biomass have been formulated in the recent times e.g the constant rate mode (the default model), the single kinetic rate model and Kobayaski model. These models have been reviewed by a number of researchers [187-191]. Fundamental approaches used are one-step mechanism and multi-step mechanism.

In the present study constant rate model has been applied. This model explains that volatiles are released at a constant rate:

$$- \frac{1}{f_{v,0}(1-f_{v,0})m_{p,0}} \frac{dm_p}{dt} = A_c \quad (4.37)$$

Where

m_p = particle mass (kg)

$f_{v,0}$ = fraction of volatiles initially present in the particle

$m_{p,0}$ = initial particle mass (kg)

A_c = rate constant (s^{-1})

The rate constant A_c is defined as part of modeling inputs with default values derived from Fluent solver. In present study the devolatilization model constant taken for coal and biomass are $15s^{-1}$ and $10s^{-1}$ respectively and mass flow rates of both the fuels are already mentioned in above equations.

4.12.2 Homogenous reactions

After the devolatilization of solid fuel and degeneration of gas species, they react with each other with the help of oxidizer supplied at primary or secondary air ports. The heat gets generated by these homogeneous reactions which is responsible for the combustion of char and release of volatiles. The homogenous reactions which occur inside the combustor are given as:

$CH_4 + O_2 \rightarrow CO + H_2 + H_2O + heat$ (4.38)

$CO+H_2O \leftrightarrow CO_2+ H_2$ (4.39)

$O_2 + 2H_2 \leftrightarrow 2H_2O$ (4.40)

The combustible fraction of coal is taken as 31.14% and mass flow rate of primary air is taken as 5kg/s.

4.12.3 Heterogeneous reactions

Char is the residue which is remained after the devolatilization of solid fuel. Reactions taking place between char and the gas species are known as heterogeneous reactions which are complex in nature and involve the mass balance of diffusion rate of the oxidizing components of the oxidizer from the body of the solid fuel particles with the chemical interaction of these components with the char on the surface. The rate of diffusion of char particles is found by the rate of diffusion of oxygen from the body of the solid fuel and the rate of reactions taking place at the surface. It depends on the composition of the constituent fuels, their size, porosity and the particle temperature. The general heterogeneous reactions taking place inside the combustor are given as:

$$C_{char} + ½\ O_2 \rightarrow CO + heat \quad (4.41)$$

$$C_{char} + CO_2 \rightarrow 2CO \quad (4.42)$$

$$C_{char} + H_2O \rightarrow CO + H_2 \quad (4.43)$$

The detailed literature on the homogeneous reactions and heterogeneous reactions can be studied from [193,194]. The fuel particle size is taken as 0.005m and temperature is taken as 380K as obtained from plant. Burout stoichiometric ratio is 2.67.

4.13 Additional Physical Submodels

Navier-Stokes equations describing basic flow equations like mass, momentum and energy are not found sufficient to model gasification and combustion of fuel in fluidized bed boilers. Additional physical models are also needed to represent all physical processes. These models include heat exchange in combustor, mass transfer, diffusion and turbulence models etc. In the present report commonly used models are discussed, however Bakul et al. [195] have provided more description of advanced models of physical processes taking place inside FBC systems.

4.13.1 Turbulence modeling

Due to fluctuation in velocity fields inside combustors turbulence takes place. Due to these fluctuations the quantities of transportation like mass concentration of species, momentum and energy distribution are also fluctuated. These fluctuations are generally having higher frequencies but of small scale. Due to the reason they require more computational space to get simulated and usually are expensive and difficult to apply in practical industrial problems. So these governing equations are ensemble-averaged and time-averaged over the domain. In this way they are modified to suppress the high frequencies and remove small scales which results in a new manipulated set of correlations which require less computational space and thus be solved on affordable costs. However, these simplified equations have other unknown variables, which are also required to determine by the turbulence models. The choice of turbulence model to be applied actually depends upon various parameters such as the knowledge of physical process taking place inside the problem domain, the computational space available, accuracy and the time required to complete the numerical simulation.

Turbulent flows are based on the fluctuations present in velocity fields which take place by the reason of irregular geometrical shapes or large rates of fluid motion. Turbulence has an effect over the heat transfer and mass flow rates and imparts a major contribution in the phenomena like combustion and gasification of fluidized bed combustors [196]. In case of laminar flows, The Navier-Stokes equations can be computed easily, but in case of highly agitating flow the direct numerical simulation (DNS) approach is proved to be quite lengthy and costly in terms of computational space to obtain the complete solution of the transport equations. The DNS approach is only suitable to simple turbulent flows in which Reynolds numbers remains up to a medium range. In case of flows in which Reynolds number reaches a higher range due to more

turbulence through complex geometries, Navier-Stokes equations are very difficult to solve in usually available less computational space. Keeping that in mind, it is necessary to predict the scales of turbulence earlier before applying a turbulence model in large scale commercial applications. Generally two techniques are used to compute the Navier-Stokes correlations. One is Reynolds averaging and other is filtering. Both techniques provide some other parameters in the basic correlations and they are necessarily be computed in case of turbulence.

(a) Reynolds-Averaged Navier-Stokes models

The Reynolds-averaged Navier-Stokes (RANS) equations are used to solve the transport equations by averaging all the flow quantities over a time domain in which all the quantities of turbulence can be analyzed. The RANS technique is applied by dividing all the features of the primary correlations present at some instant into the mean values and varying parameters, as given by:

$$\phi = \bar{\phi} + \phi' \tag{4.44}$$

The mean of the variables used for a flow domain is utilized to consider the effects of fluctuations in density produced due to agitation in flow. This technique uses mean of Reynolds stress terms over a time domain in conservation equations which are computed for turbulence modeling. The Reynolds-averaged technique is applied most of the times for practical engineering applications.

Mostly used RANS models apply the concept of eddy viscosity (EDC) based on the Boussinesq hypothesis to compute the Reynolds stress terms. The hypothesis worked on the basis that when the turbulence is increased then the effective fluid viscosity is also increased. On account of this viscosity and thus mean velocity gradients the Reynolds number is also increased which is proportional to the mean velocity. The commonly used models in which Boussinesq hypothesis is used are *k*-ω, Standard k-ε, RNG *k*-ε,

Realizable *k*-ε and its variants and few others [191]. The Reynolds-averaged Navier - Stokes equations are solved by Reynolds stress model (RSM) by computing transport correlations directly for the Reynolds stresses along with another correlation for the rate of dispersion. The explanation of RSM and other earlier mentioned models may be obtained from Bakul et al. [195]. In most of the studies standard *k*-ε has been used for gasification and incineration of fuels in FBC boilers. In present study *k*-ε turbulence model has been used. The model may be applied either by setting the values of *k* and ε or by setting turbulence intensity and hydraulic diameter. In present work the turbulence intensity is taken as 5% and the hydraulic diameter for coal and biomass is taken as 0.15m and 0.5m respectively.

(b) LES based models

LES stands for Large eddy simulation in which transport equations are solved by allowing direct analysis of highly turbulent flows. In LES, sorting of whirls is done with the help of mesh size. The whirls which are of small size as comparison to the mesh element are filtered. LES gives better results in case of large whirls in comparison to DNS where whirls are modeled which are of small size as comparison to size of the filter. This happens because the smaller eddies are having length scales which are found by the viscosity of the fluid, thus they are isotropic in nature at large values of Reynolds number while the large turbulent eddies depends on mean velocity gradients and geometries of flow regimes and they are highly anisotropic in nature. LES provides a more accurate technique in which errors are reduced which are produced in RANS and offers an alternative method for simulation of turbulence However, the implementation of LES to industrial furnaces fuelled by biomass is still in the developing stage due to its computational requirements [191].

4.13.2 Mixture fraction model

Non premixed combustion model (NPM) is generally used to simulate combustion in which two fluid mixture fraction approach based on probability density function (PDF) is applied. In this technique the transport equations are solved for one or two mixture fractions of fuels as conserved scalars. In this technique, the transport equations are not individually solved for fuel streams, but the concentrations of individual stream of interest are retrieved from the given mixture fraction. Hence, the chemical equations which are usually not known are not individually solved but they are solved using some assumption based reaction mechanism like non-equilibrium chemistry and equilibrium assumptions. Physical quantities of fuel species and data required for equilibrium are obtained from the database of solver and the influence of turbulence and chemical reactions is retrieved from PDF or a probability density function. The PDF analysis technique is considered computationally efficient method because in this technique the transport equations of species of interest are not required to solve on large scale without any reason.

The mixture fraction variance is used to describe the turbulence and chemical reactions. Formulation of above mentioned opted conserved scalar entity, *f*, in the given flow field also computes other important scalar entities like temperature and density without solving their individual transport equations. In addition to describing the chemical reaction mechanism, the values of mixture fraction at all the locations in the flow domain may be utilized to calculate the local values of other gaseous entities. If another fuel is also used in the combustion, then the local values would be calculated from the mixture fraction (f_{fuel}) of fuel, the secondary partial fraction $p_{sec,}$ and enthalpy H^*.

$$\overline{\varphi_i} = \overline{\varphi_i}\left(f_{fuel,} p_{sec,} H^*\right) \tag{4.45}$$

$$\overline{\varphi_i} = \int_0^1 \int_0^1 p_1(f_{\text{fuel}})\, p_2(p_{\text{sec}})\, \varphi_i(f_{\text{fuel}}, p_{\text{sec,}} H^*)\, \mathrm{d}f_{\text{fuel}}\, \mathrm{d}p_{\text{sec}} \tag{4.46}$$

The elemental composition in the form of ultimate analysis is given as input to this model. Here Φ_i represents the instantaneous species concentration and H^* is enthalpy which is also generated in PDF table.

4.13.3 Surface combustion

After the volatile component of the particle is completely evolved, a surface reaction begins which consumes the combustible fraction of the particle. Fluent provides a choice of four heterogeneous surface reaction rate models for combusting particles:

- The diffusion-limited rate model
- The kinetics/diffusion-limited rate model
- The intrinsic model
- The multiple surface reactions model

In the present study the kinetics/diffusion-limited rate model has been used. This model assumes that the surface reaction rate is determined either by kinetics or by a diffusion rate. Models of Baum & Street [197] and Field [198] are used in Fluent to find:

Diffusion rate coefficient:

$$D_0 = C_1 \frac{[(T_p + T_\infty)/2]^{0.75}}{d_p} \tag{4.47}$$

And kinetic rate

$$R = A_i \, e^{-(E/RT_p)} \tag{4.48}$$

They are generate a char combustion rate of

$$\frac{dm_p}{dt} = -A_p \frac{D_0 R}{D_0 + R} \tag{4.49}$$

Where A_p is the surface area of the particle, A_i is kinetic-limited rate pre-exponential factor, whose value is 0.01 in the present study. E is activation energy, whose value is 7.9×10^5 j/kg.mol. C_1 is diffusion rate constant whose value for coal and biomass is 1×10^{-8} and 5×10^{-10} respectively.

CHAPTER 5

RESULTS & DISCUSSIONS

5.1 Experimental Observations at CPP Ambuja

As discussed earlier CFD modeling of a large capacity fluidized bed boiler has been done in the present study. Captive Power Plant (CPP) of Ambuja Cement Limited, Ropar, Punjab, India is opted for study. CPP, Ambuja generates 30 MW of power running on three units. Two units are having capacity of 45 TPH and one having capacity of 80 TPH. The investigations have been done on 45 TPH boilers. All the boilers are designed for biomass combustion. However, in case of less availability of biomass fuel they may run on coal. Here, a comparison of 100% rice husk usage (using data of 2005) has been done with co-firing and coal usage in terms of power generation and emissions. Test runs are not done for rice husk because it is not presently in use. During study, it was observed that the secondary air consumption in case of biomass combustion was more as compared to conventional fuel, because biomass contains high moisture content and burns in the gas phase in freeboard region. The bed temperature in case of biomass fuel remains less as compared to conventional fuel; however flame is generated near the regions of inlet ports of biomass due to its instantaneous combustion and travel along the height. Bed temperatures at different eight sections of both the boilers running on coal and biomass in share were obtained and shown in Fig.5.1.

A clear increase in the bed temperatures of coal fired boiler is observed as compared to co-firing boilers. Keeping that in mind the bed height in case of biomass fuel is kept less, as if the bed height in case of biomass is kept more the overall temperature of furnace falls down and combustion quality deteriorates in that case.

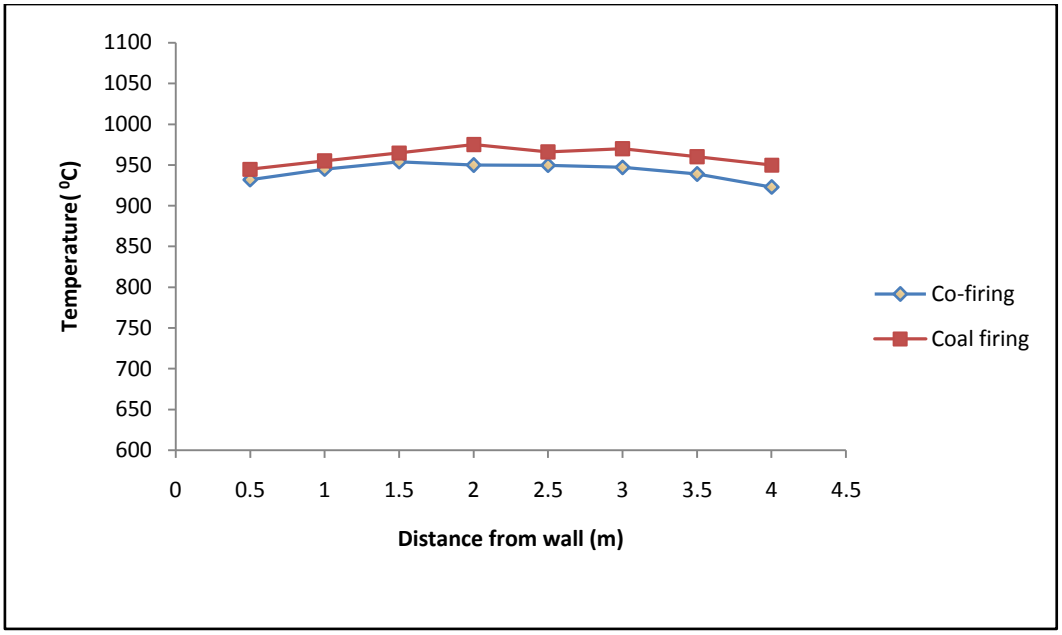

Fig. 5.1: Temperature profiles of the bed

In case of coal, at least 500^0C temperature is required to maintain over the bed for initiating the ignition. To maintain a certain high value of temperature limit in case of coal, the bed height is kept more so that to accommodate more material over the bed and to control its temperature. The variation of steam temperatures presented is slightly high in case of coal firing as shown in Fig.5.2.

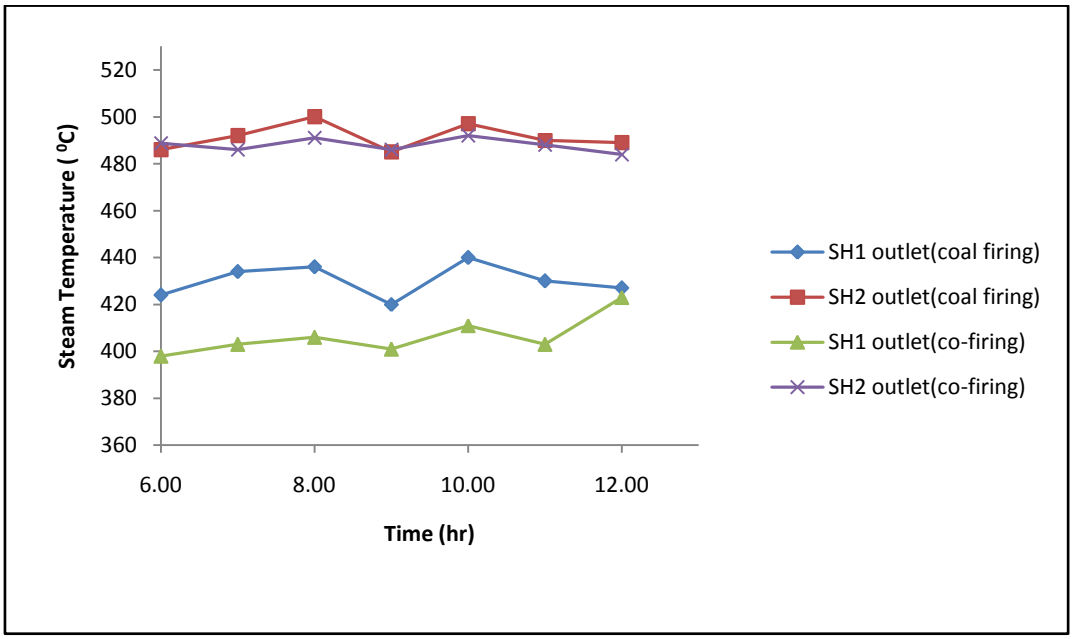

Fig.5.2: Records of steam temperatures

The analysis of observed data during the study period and the standard working in the stipulated time period shows that biomass co-firing does not affect the plant operation directly, that is why the variation of the observed data was found within the permissible limit during the whole day and was not changed by the co-firing runs. As a concluding remark, it is said that biomass co-firing does not have a major effect on the working condition of any particular combustor. However a slight variation in the mean values of flue gas entrainment during the investigation is observed which are given in Table 5.1.

Table 5.1: Flue gas emissions reported from the plant

	Coal	**Co-firing**	**Test method**
O_2 (% vol)	8.9	9.8	IS: 13270
SO_2(mg/Nm^3)	76	70	APHA -Air
NO_2 (mg/Nm^3)	28	23	APHA -Air
CO (% vol)	0.4	0.4	IS: 13270
CO_2 (% vol)	9.5	8.9	IS: 13270
Ash content (% by wt.)	40	30	IS: 1350 (Part 1)

The enhanced value of O_2 in the flue gas in case of rice husk and co-firing is a mark of the enhanced value of secondary air going in to the combustor. NO_x values tend to increase in case of coal firing as temperature remains on higher side in case of coal firing. These higher temperatures explain the reason behind the increased values of NO_x emissions. CO emissions were found almost same in both the cases. CO_2 entrainments can also be approximated on the basis of carbon content obtained from the ultimate analysis of the fuel and the excess air used for combustion inside the boiler. One ton of biomass fuel replaces around 0.85 tons of coal & therefore saves equal amount of CO_2 emissions (Indian Network for Climate Change Assessment 2010) [199]. SO_2 formation does not depend upon the combustion conditions inside the furnace but depends upon the sulphur content of the fuel. In case of biomass sulphur content remains negligible around

0.18 (% by wt.) and f-grade coal is used at CPP which is also having very less sulphur content which is 0.35 (% by wt.).

5.2 Simulation Results

5.2.1 Bed temperatures of co – firing and coal firing

5.2.1.1 Monitoring data and different boundary conditions

Fuel particles for both biomass and coal were traced by using a framework of Lagrangian technique using Discrete Particle Modeling (DPM) approach. In DPM, both the particle phases, in the form of discrete particles, and a continuous phase, in the form of the gas flow field, are considered by the interphase transfer of mass, momentum and energy exchange. These parameters are derived from the basic combustion process models of heating, devolatilization and char burnout. Different input values and boundary conditions for DPM are given in Table 5.2.

Table 5.2: Input data and boundary conditions

Diameter of coal particle (m)	0.005	Diameter of biomass particle (m)	0.002	Mass flow rate secondary air (kg s^{-1})	1
Flow rate of coal (kg s^{-1})	2.083	Flow rate of biomass (kg s^{-1})	0.7	Mass flow rate of primary air (kg s^{-1})	5
Coal inlet temperature (K)	380	Biomass inlet temperature (K)	380	Turbulence intensity (%)	5
Hydraulic diameter at coal inlet (m)	0.15	Hydraulic diameter at biomass inlet (m)	0.5	Heat transfer coefficient at in-bed SH ($Wm^{-2}K^{-1}$)	200
Devolatilization model constant for coal (s^{-1})	15	Devolatilization model constant for biomass (s^{-1})	10	Burnout stoichiometric ratio	2.67
Combustible fraction of coal (%)	31.14	Combustible fraction of biomass (%)	12.58	Kinetics limited rate activation energy(j/kg.mol)	$7.9x10^{5}$
Mass diffusion-limited rate constant (coal)	$1x10^{-8}$	Mass diffusion-limited rate constant (biomass)	$5x10^{-10}$	Kinetics limited rate pre-exponential factor	0.01

The standard k–ε model is has been applied for modeling turbulence, with the volumetric reaction rates being controlled through an eddy dissipation approach in which the rate of reaction is determined by the turbulence and by the mixing rate of both reactants and final produces. Non premixed combustion model (NPM) is generally used to simulate combustion in which two fluid mixture fraction approach based on probability density function (PDF) is applied. In this technique the transport equations are solved for one or two mixture fractions of fuels as conserved scalars. In this technique, the transport equations are not individually solved for fuel streams, but the concentrations of individual stream of interest are retrieved from the given mixture fraction. Hence, the chemical reaction equations which are usually not known are not individually solved but they are solved using some assumption based reaction mechanism like non-equilibrium chemistry and equilibrium assumptions. Physical quantities of fuel species and data required for equilibrium are obtained from the database of solver and the influence of agitation and chemical reactions is retrieved from PDF or a probability density function. The input values used in NPM are given in Table 5.3.

Table 5.3: Input values of NPM

Species	Fractions in coal	Fractions in biomass
Carbon	0.4877	0.3153
Hydrogen	0.4236	0.4356
Oxygen	0.0732	0.2424
Nitrogen	0.0125	0.0061

Fig. 5.3 is showing temperature contours of boiler working on co-firing, in which biomass is supplied from biomass ports at a height of 2m from the bed. Fig. 5.4 is

showing temperature profile of another boiler running on coal. As discussed earlier the bed temperature in case of coal firing remains more in comparison to co-firing because biomass burns in the freeboard zone. However in case of co-firing the temperatures along the biomass ports are showing a higher range due to instantaneous burning of biomass in suspension in the form of flame. The CPP boiler bed is divided in to four equally spaced regions simply based on the uniform location of temperature sensors and coal feed ports. Fig. 5.1 is showing eight temperature values of these regions having two values each. The bed temperatures in case of co-firing were up to 1223K and in case of coal firing the bed temperatures were found up to 1260K.

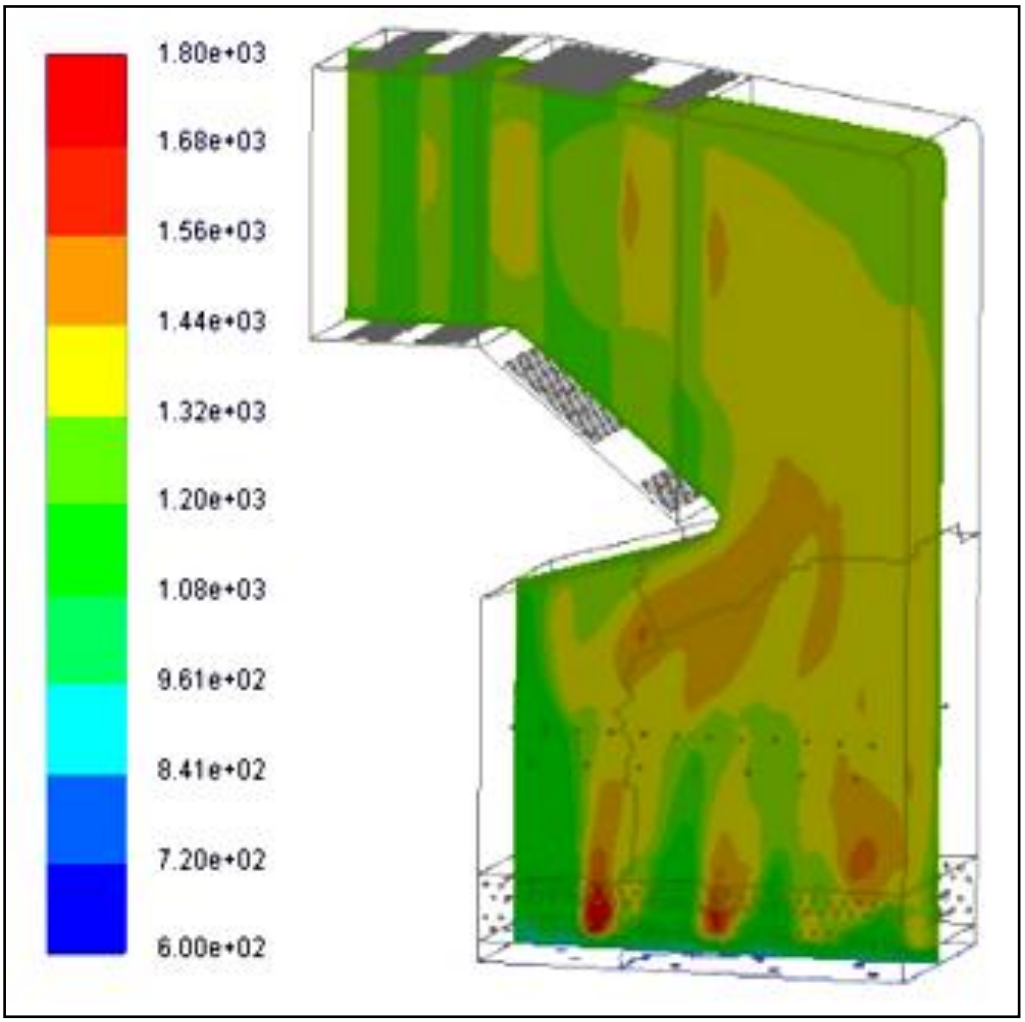

Fig.5.3: Temperature contours of co - firing (K)

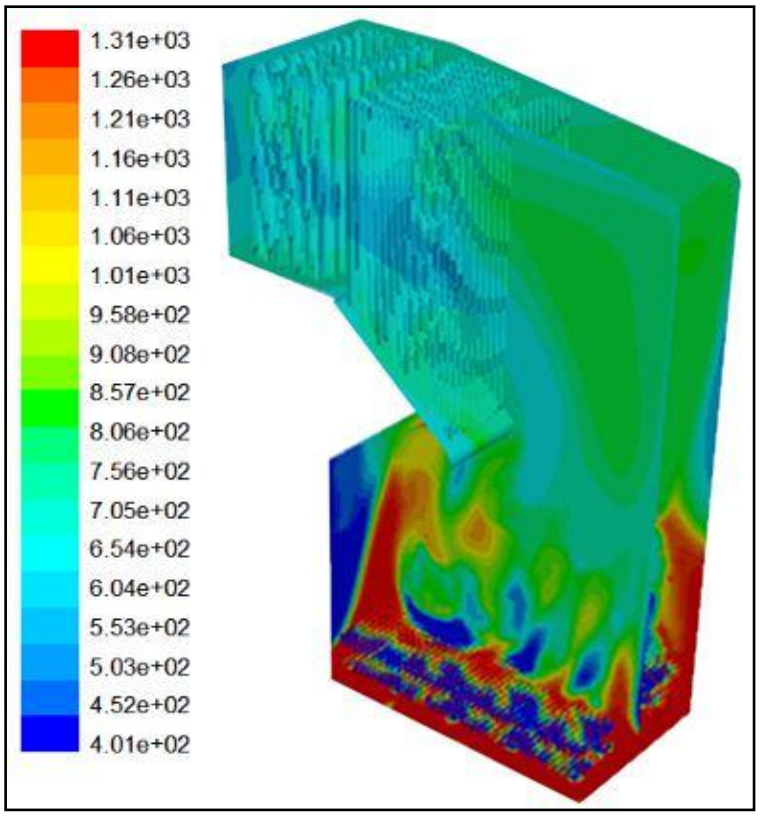

Fig.5.4: Temperature contours of coal firing (K)

The simulation results show the higher range of bed temperatures in case of coal firing as comparable to co-firing. However few lower range sections are also appearing due to presence of primary air. The simulation results are showing actual process trends, with an agreement to real process.

5.2.2 Temperature contours and mass species

The simulation results of mass fraction and temperature contours of CPP boiler are shown from Fig. 5.5 to Fig. 5.11. Mass fractions of CO_2 are shown in Fig. 5.5**.** Maximum value of the CO_2 fraction was obtained at the regions where the flame generation takes place due to instantaneous combustion of biomass fuel, near the feed ports (at a height above 2m), in the suspension at the highest range of temperature as shown in Fig.5.6. CO_2 concentration was found minimum over the bed due to presence of primary air. During

field study CO_2 concentration at the exit of the furnace was obtained to be 0.133 (Table 5.4).

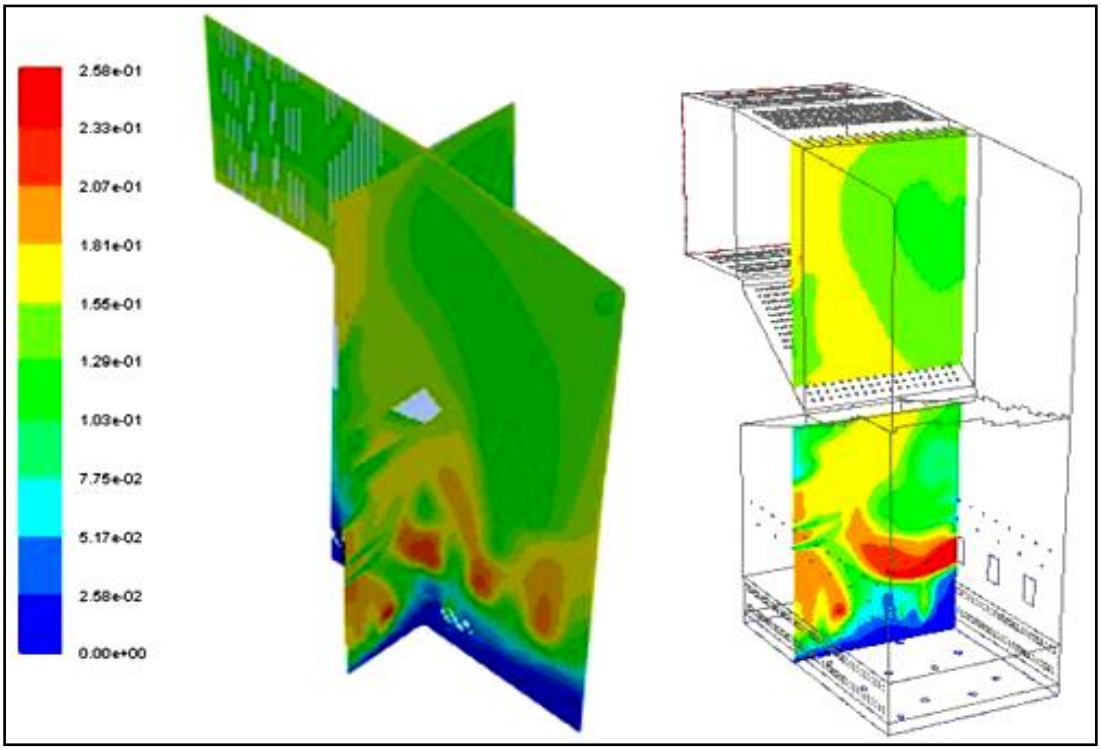

Fig.5.5: Mass fractions of CO_2 (70% coal+30% biomass)

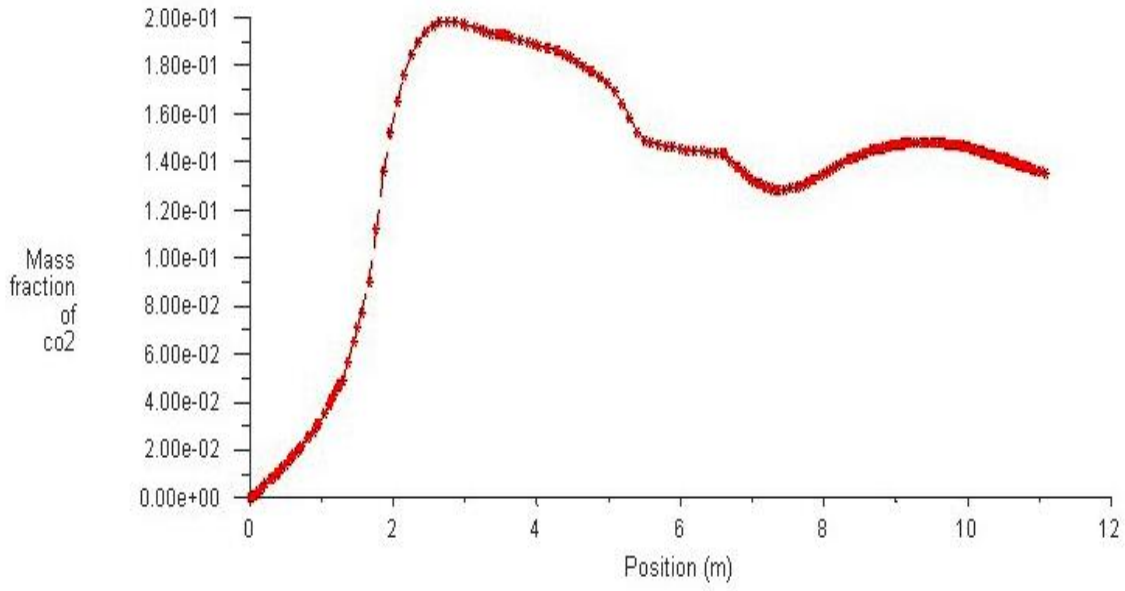

Fig. 5.6: Mass fraction of CO_2 along the height

From simulation results it was found to be 0.14. The % age change in results was found to be 5. Mass fractions of O_2 are shown in Fig.5.7. O_2 concentration was found maximum in

the vicinity of the bed (below 1.5m, Fig. 5.8) due to supply of primary air from sixteen feed ports. The O_2 concentration at the furnace exit was 0.105 and from model results it was obtained as 0.112. The % age change in the actual value and model results was found to be 6.25.

Table 5.4: Comparison between model results and experimental data

Variables	**Simulation results**	**Monitoring data**	**%age change**
Flue gas temperature at the furnace outlet (K)	1140	1123	+1.9
Bed temperature (K)	1200	1223	-2.4
Chemical species at the furnace outlet (mass fraction)			
CO_2	0.14	0.133	+5
O_2	0.112	0.105	+6.25

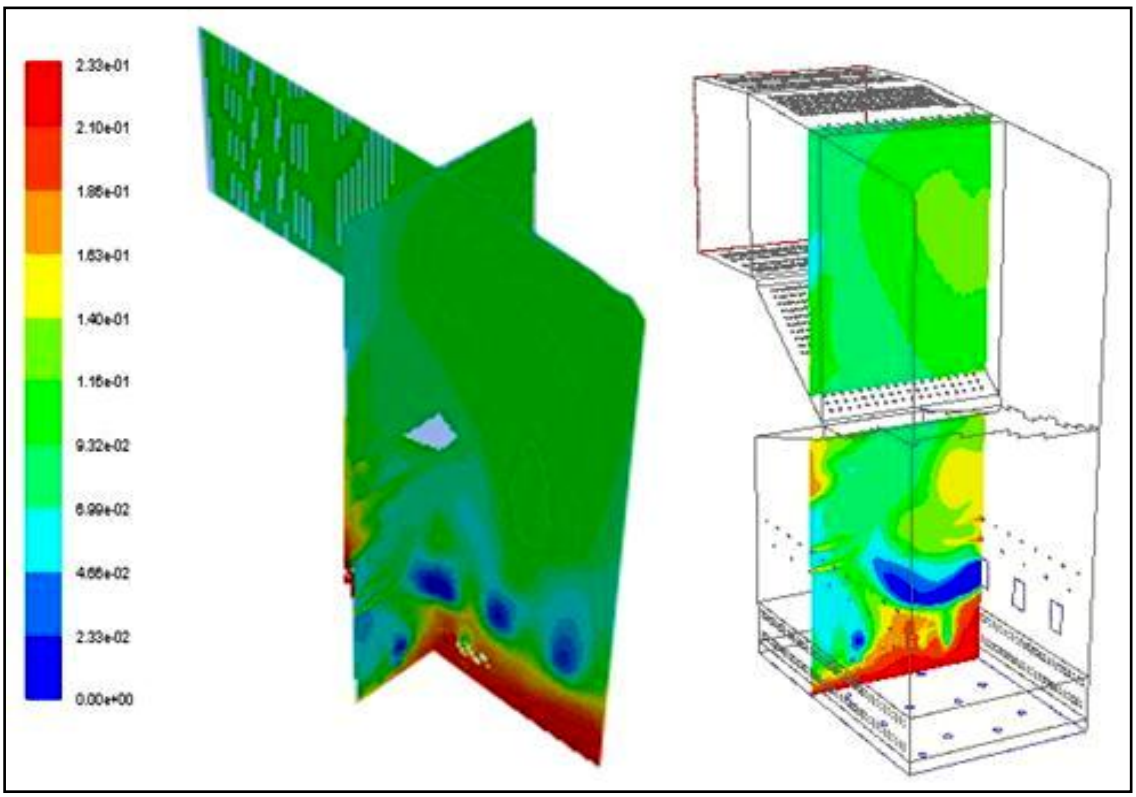

Fig. 5.7: Mass fractions of O_2 (70% coal+30% biomass)

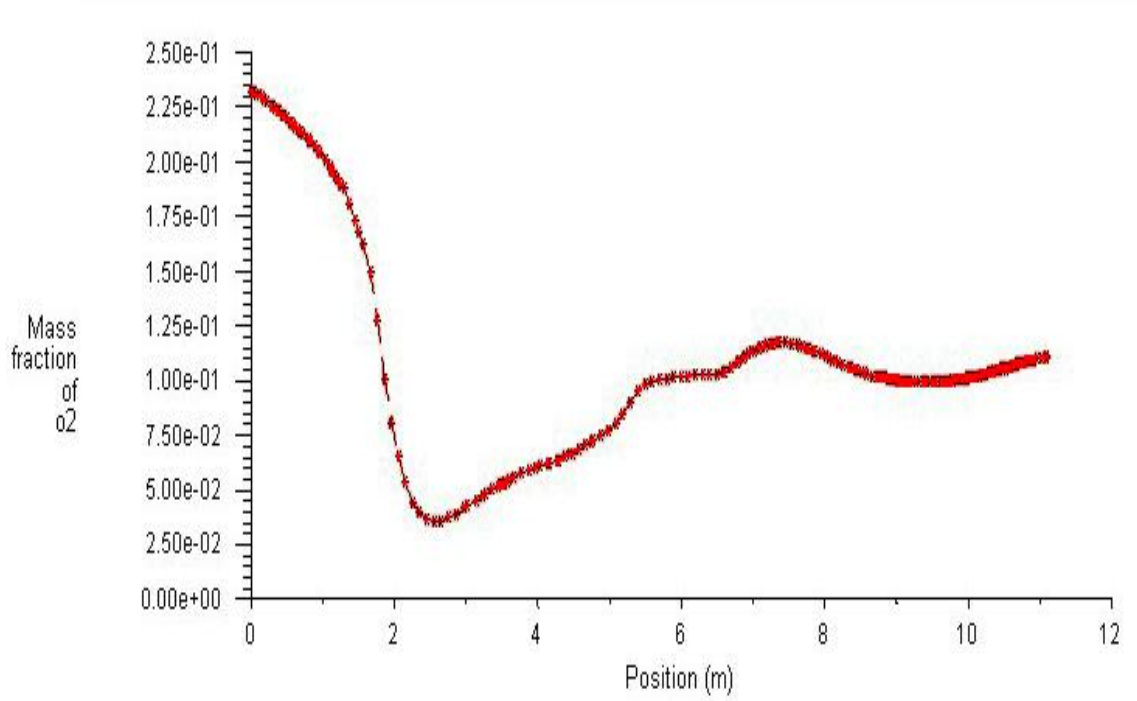

Fig.5.8: Mass fractions of O_2 along the height

Temperature contours of CPP boiler are shown in Fig. 5.9. The way of initiation of ignition certainly decides the temperature profiles inside the furnace domain. As discussed earlier the hottest area of the combustor can be located where the greatest portion of the char gets changed in to CO_2 [120]. Consequently, maximum temperatures were found, at the regions, where CO_2 generation was maximized. It is also to understand that the O_2 generation decreases greatly where a larger amount of fuel is burnt (Fig. 5.7). In the vicinity of the bed the temperature contours were obtained up to 1200K. The actual bed temperatures vary up to 1223K. The % age change in both the results was found 2.4. The temperature of the flue gas at the boiler exit was 1123K. The temperature obtained from model results is 1140K. The change in the experimental value and model results was found to be 1.9%. Temperature contours for two more different ratios of 50% coal with 50% biomass and 80% coal with 20% biomass were also obtained and shown in Fig. 5.10 and Fig. 5.11 respectively. It was observed during higher biomass fraction (Fig. 5.10) the

flame generation became predominant as compared with less fraction of biomass (Fig. 5.9 with 30% biomass and Fig. 5.11 with 20% biomass) due to instantaneous combustion of biomass.

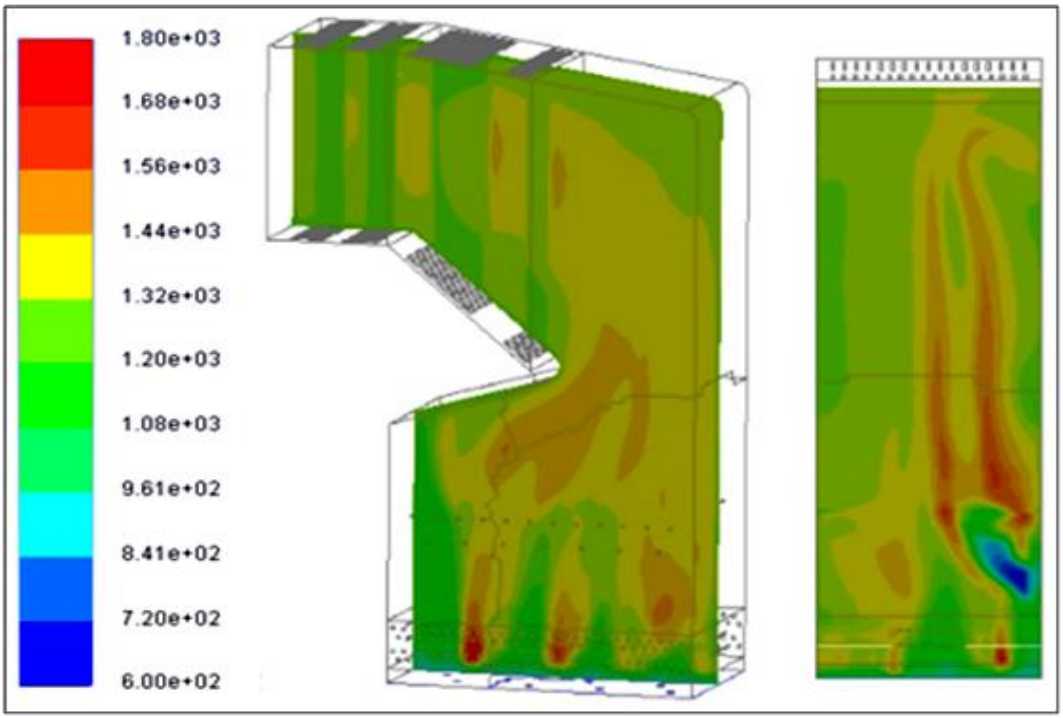

Fig. 5.9: Temperature contours of CPP boiler (K) [70% coal+30% biomass]

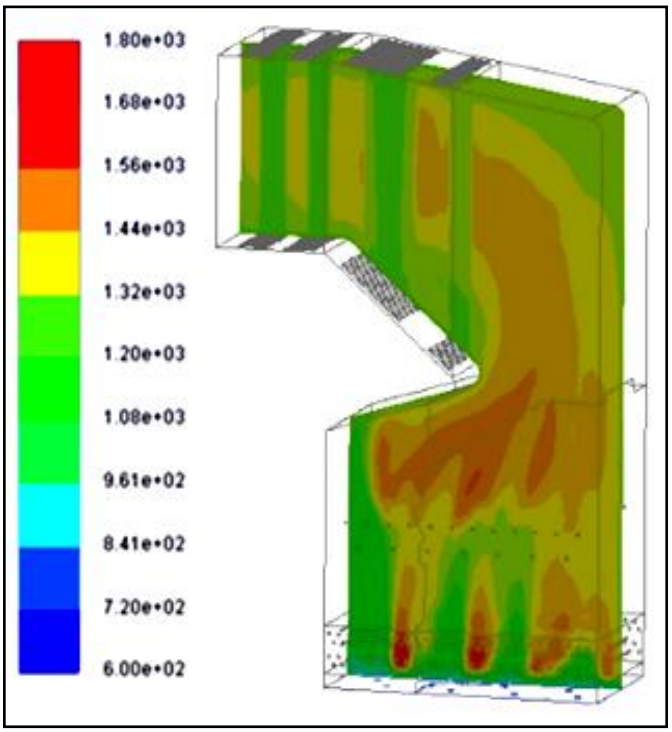

Fig. 5.10: Temperature contours of CPP boiler (K) [50% coal+50% biomass]

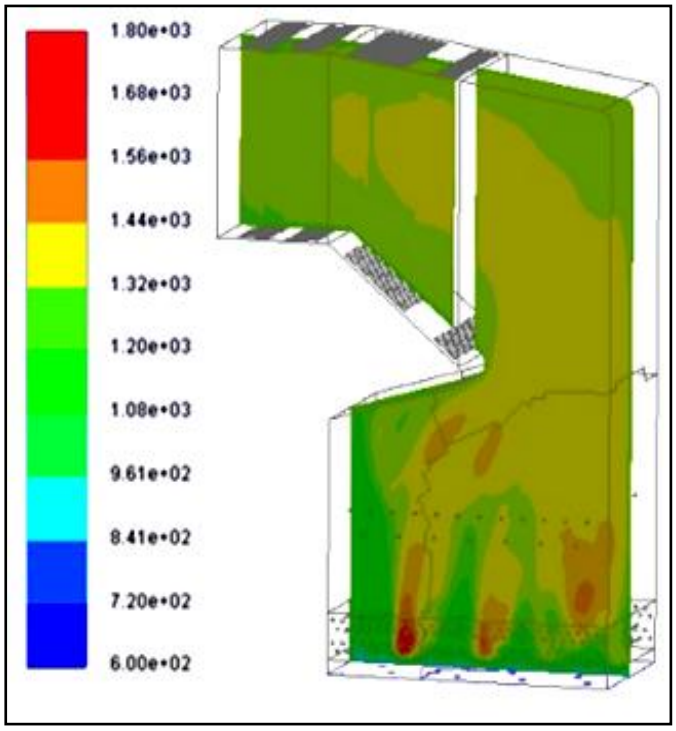

Fig. 5.11: Temperature contours of CPP boiler (K) [80% coal+20% biomass]

Mass fractions of CO_2 at ratio of 50% coal and 50% biomass are shown in Fig. 5.12. As discussed earlier when biomass fraction is increased, the flame generation becomes predominant and for the reason CO_2 fraction increased near the input ports as comparable to initial ratio of coal and biomass (70% coal+30% biomass) as shown in Fig. 5.5. Mass fractions of O_2 at ratio of 50% coal and 50% biomass are shown in Fig. 5.13.

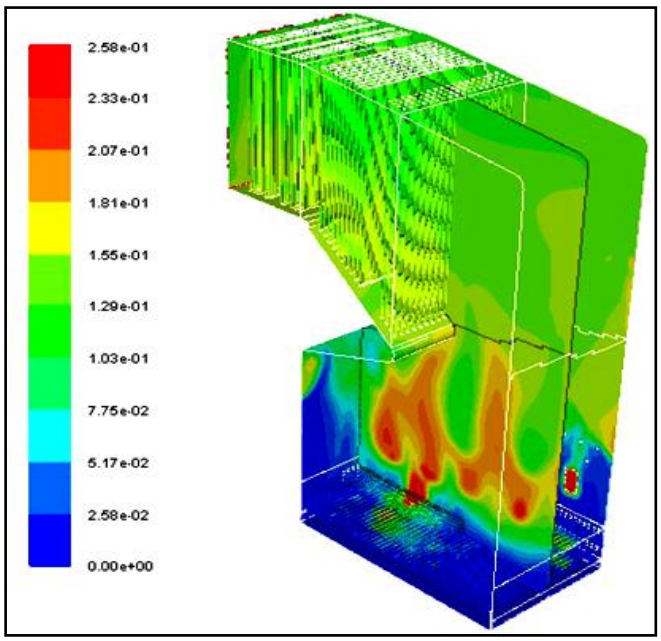

Fig. 5.12: Mass fractions of CO_2 (50% coal+50% biomass)

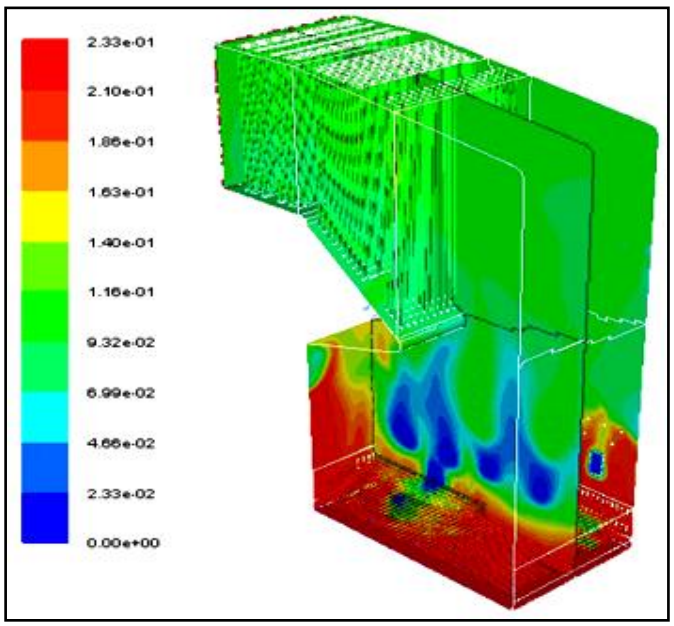

Fig. 5.13: Mass fractions of O_2 (50% coal+50% biomass)

As discussed earlier that the O_2 generation decreased greatly near the input ports where a larger amount of fuel was burnt as comparable to initial ratio of fuel (70% coal+30% biomass) or where CO_2 concentration was maximum. The mass fractions of CO_2 and O_2 at ratio of 80% coal and 20% biomass are shown in Fig. 5.14 and Fig. 5.15 respectively. No significant change was found in these results of mass fractions of CO_2 and O_2 as comparable to initial ratio of fuel (70% coal+30% biomass). However the value of CO_2 and O_2 remained same at the exit as 0.14 and 0.112 respectively in all the cases.

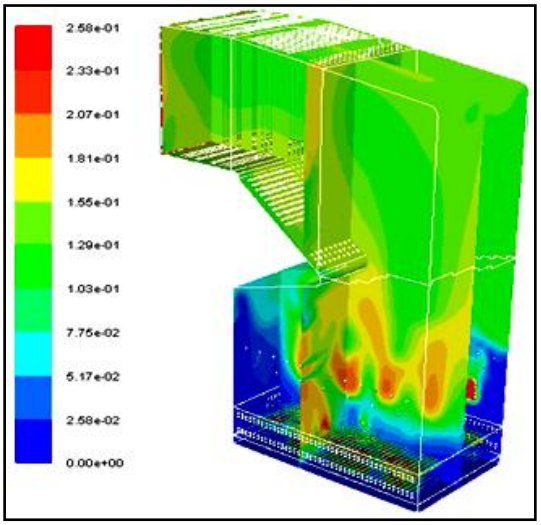

Fig. 5.14: Mass fractions of CO_2 (80% coal+20% biomass)

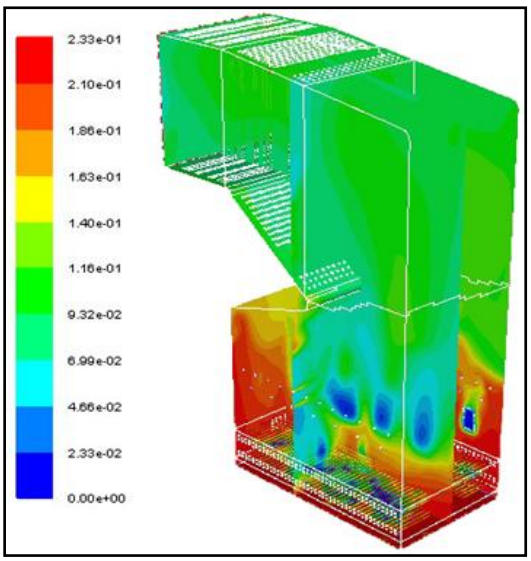

Fig. 5.15: Mass fractions of O_2 (80% coal+20% biomass)

5.2.3 Trajectories of biomass and coal

The coal is delivered to the furnace by an underfeed supply from 16 ports uniformly distributed over the bed. It is supplied at a fuel flow rate of 2.083 kg s^{-1} with a mean mixture fraction of 0.373. The component in radial direction of the flow is selected as 0.866 and the axial component as 0.5. The biomass fuel is delivered by an overfeed supply from four feed ports at a height of 1.8 m as shown in Fig. A 3.1. The supply comes from a biomass handling plant with a vibrating screen of 25 TPH capacity. The biomass fuel is supplied at a feed rate of 0.7 kg s^{-1} at a secondary mean fraction of 0.2 with the help of belt weighers to monitor the flow.

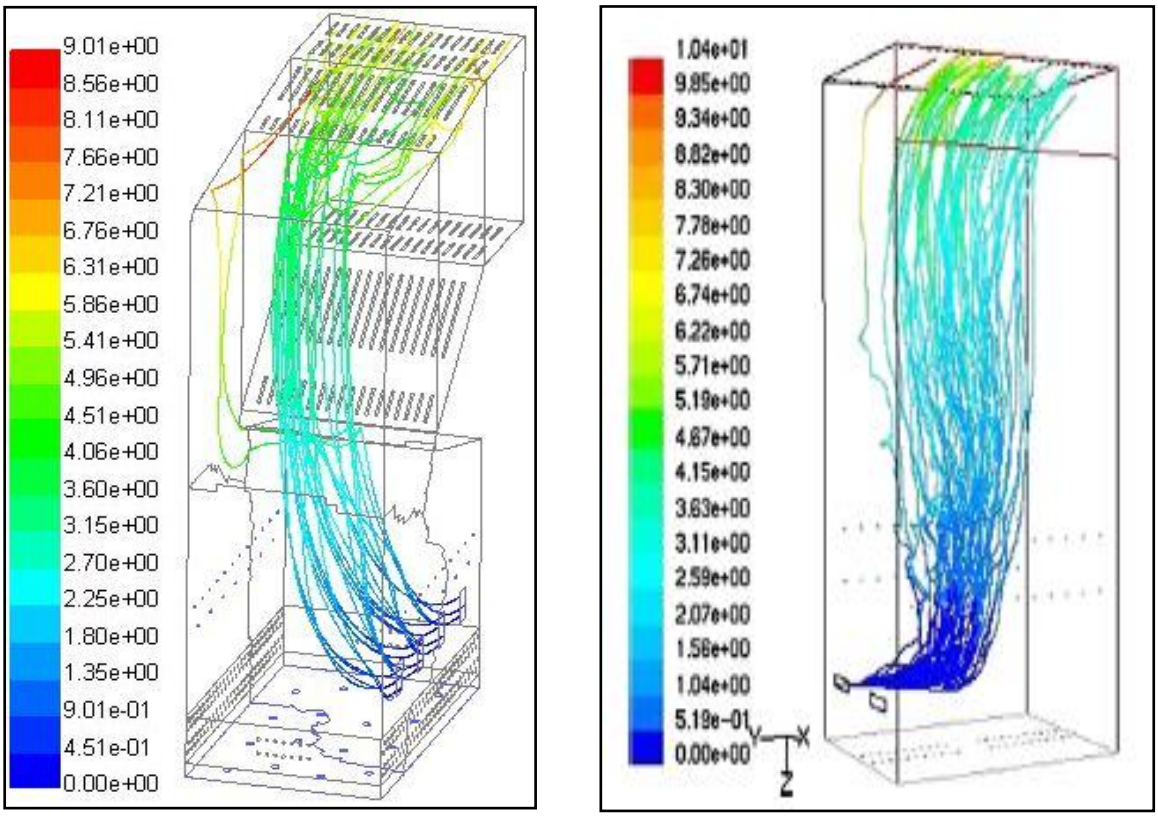

(a) (b)

Fig. 5.16: Particle traces shown by residence time(s) for (a) biomass (b) RDF [140]

The grid is partitioned into different planes and orientations depending on boundary conditions, internal components and visualisation of contours at different times.

The planes taken into account for DPM of burnout and devolatilization are at x = 1.2, 2.5, 4 and 5.4 m for biomass and at z = 2, 2.05, 2.1, 2.45 and 2.55 m for coal. Because of the large computational space required, it is necessary to use parallel processing. Particle traces showing the residence times for biomass and coal are shown in Figs. 5.16 (a) and 5.17, respectively and the trends were found similar to Ravelli et al. [120] shown in Fig. 5.16 (b) for RDF.

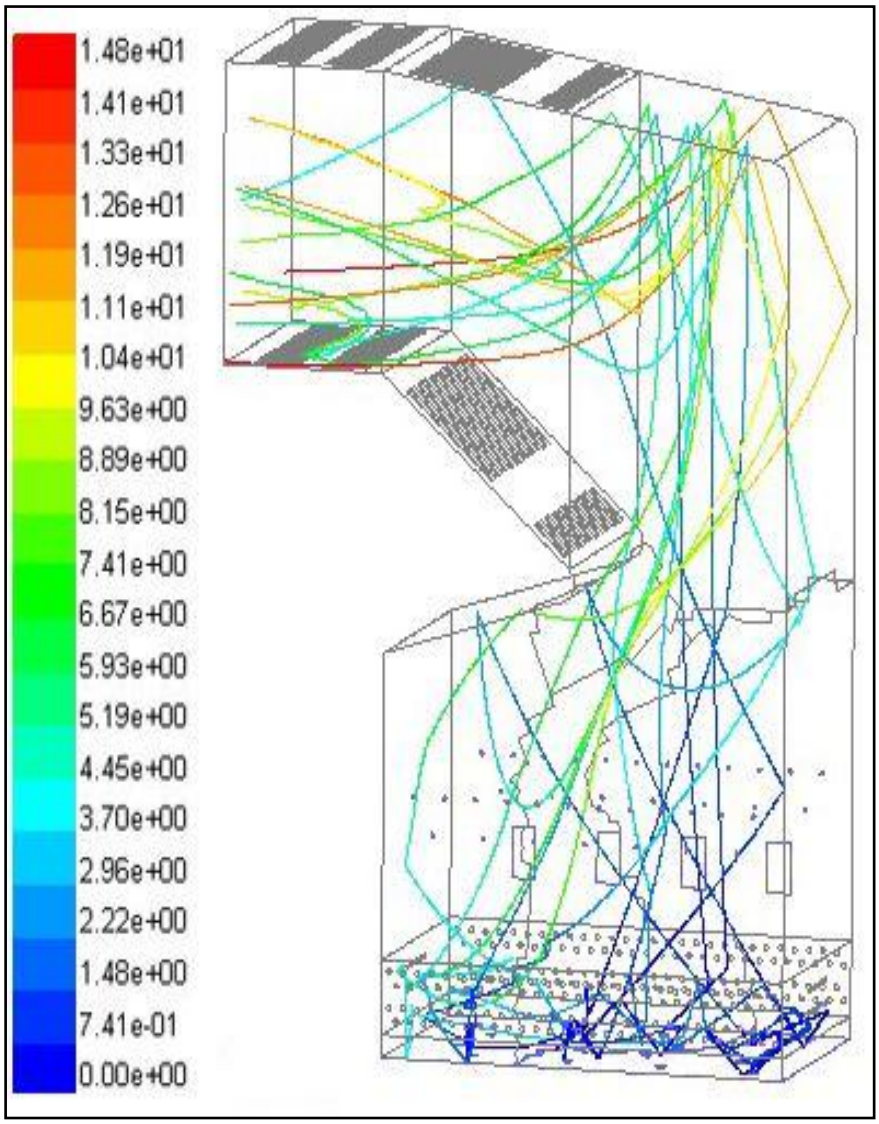

Fig.5.17: Particle traces shown by residence time(s) for coal

The trajectories are shown after selecting a required number of particles for presentation. DPM results give information about the mean residence time of the fuel particles in the lean zone and the efficiency of ignition. As coal and biomass have different inlet streams with underfeed and overfeed supplies, respectively, there is an inevitable difference in the mean residence time of fuel components, which is clearly more for coal than for biomass: 8.89s and 5.41s, respectively.

5.2.4 Char burnout and devolatilization

Efficiency of ignition is defined as how many fractions of volatiles and char are converted during combustion. Biomass inhibits fixed carbon less than 10%, compared with fixed carbon in coal which is 40–60%. On the contrary, the volatile matter in biomass is about 70–80%, which is quite higher than in coal.

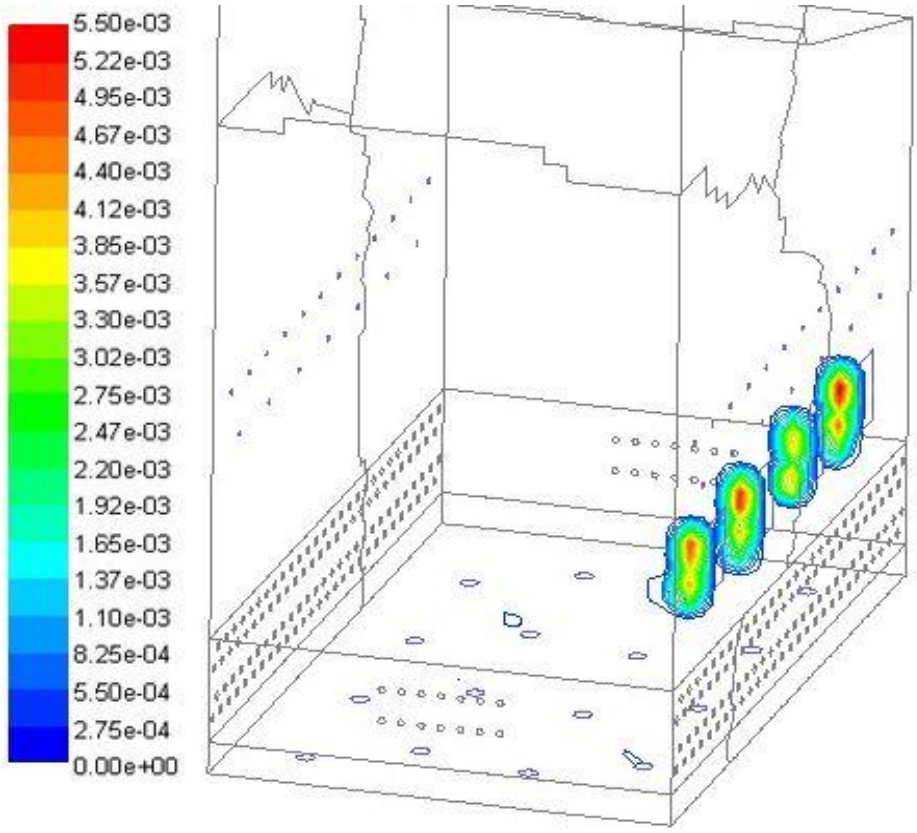

Fig. 5.18: Profiles of DPM devolatilization of biomass at planes x=1·2, 2·5, 4 and 5·4 m (kgs^{-1})

Consequently, the constituents of biomass diffuse thermally during the initial stage of ignition in the gas form instead of particle form, and the char combustion takes place during the final stage after the volatile matter has decomposed. This high-volatile nature of biomass and its fragile structure favour fast-activation volatile combustion. Fuel particles are broken into small fragments immediately after entering the furnace and accelerate the emission of volatiles from biomass; for that reason, the contours showing devolatilization are confined to very small regions (Fig. 5.18).

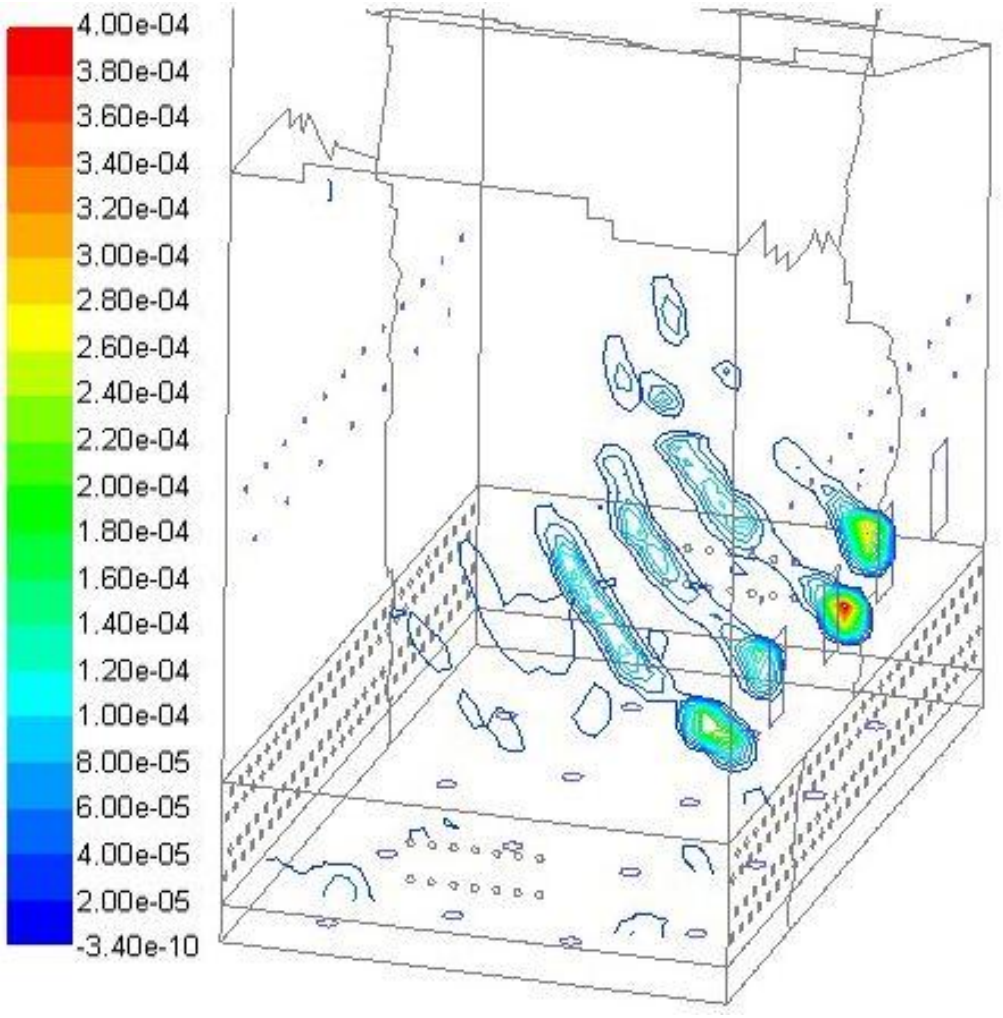

Fig.5.19: Contours of DPM burnout of biomass at planes x=1·2, 2·5, 4 and 5·4 m (kgs^{-1})

Fixed-carbon ignition starts after devolatilization and occurs in the splash zone and freeboard region, depending upon furnace operating conditions, as shown in Fig. 5.19. On the other hand, in the case of coal, owing to the high content of fixed carbon, there is heterogeneous char combustion and thus the mass flow rate is negligible in the splash zone, as shown in Fig. 5.20. In our study, the analysis is done, using input data, under full-load conditions. Under these conditions, our results show that the volatile and char conversions of both fuels are found to be nearly complete in terms of their mass flow rates and do not affect combustion efficiency. However, under partial-load conditions, the temperature of the flue gas which comes from the dense zone is not that much high to fire the ignition products completely and therefore fuel products may be entrained unburnt from the combustor, thus reducing the combustion efficiency.

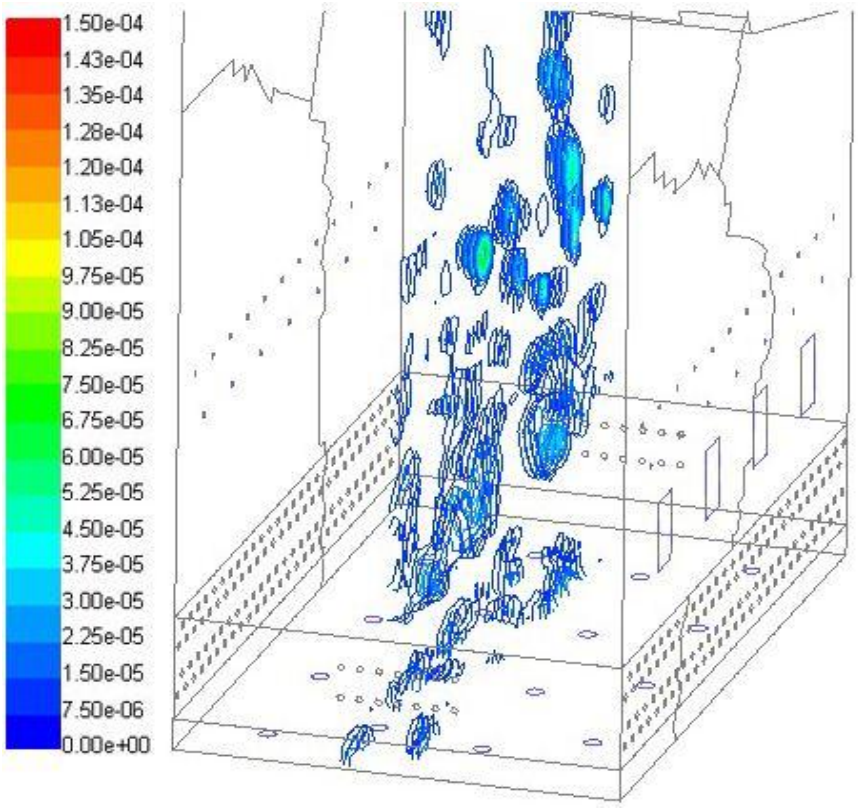

Fig. 5.20: Contours of DPM burnout of coal at planes z=2, 2·05, 2·1, 2·45 and 2·55 m (kgs^{-1})

5.2.5 Velocity vectors

Gas velocity vectors are shown in Fig. 5.21. The highest value was found at the bottom in the vicinity of the bed reaching up to 8 ms^{-1}. Then it showed another peak at a height above 5.5m where notch region was provided to accelerate the velocity. Gas then moves with an almost uniform velocity between 3 to 4 ms^{-1} up to superheater region. While passing through superheater region and convection bank tubes the velocity vectors show zig - zag trend due to obstructions faced in these regions and become difficult to measure as shown in Fig. 5.22. Adjacent to the walls of the combustor, the gas velocity remains lower between 2.42 to 3.02 ms^{-1}, owing to drag forces.

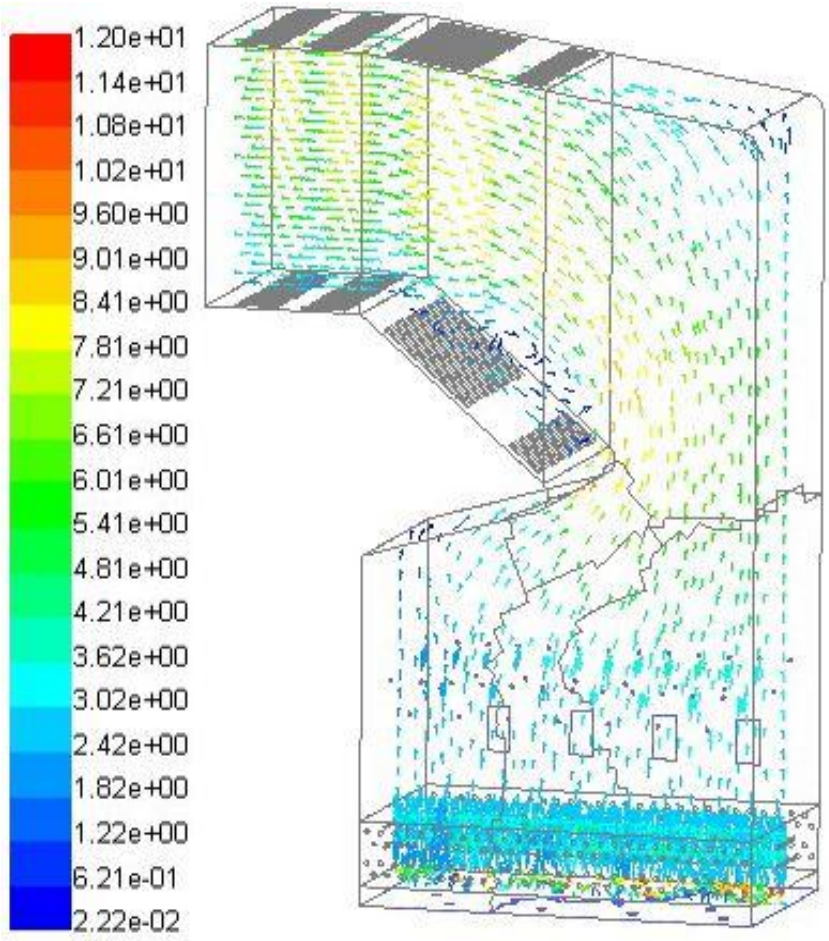

Fig. 5.21: Velocity vectors showing gas velocity (ms^{-1})

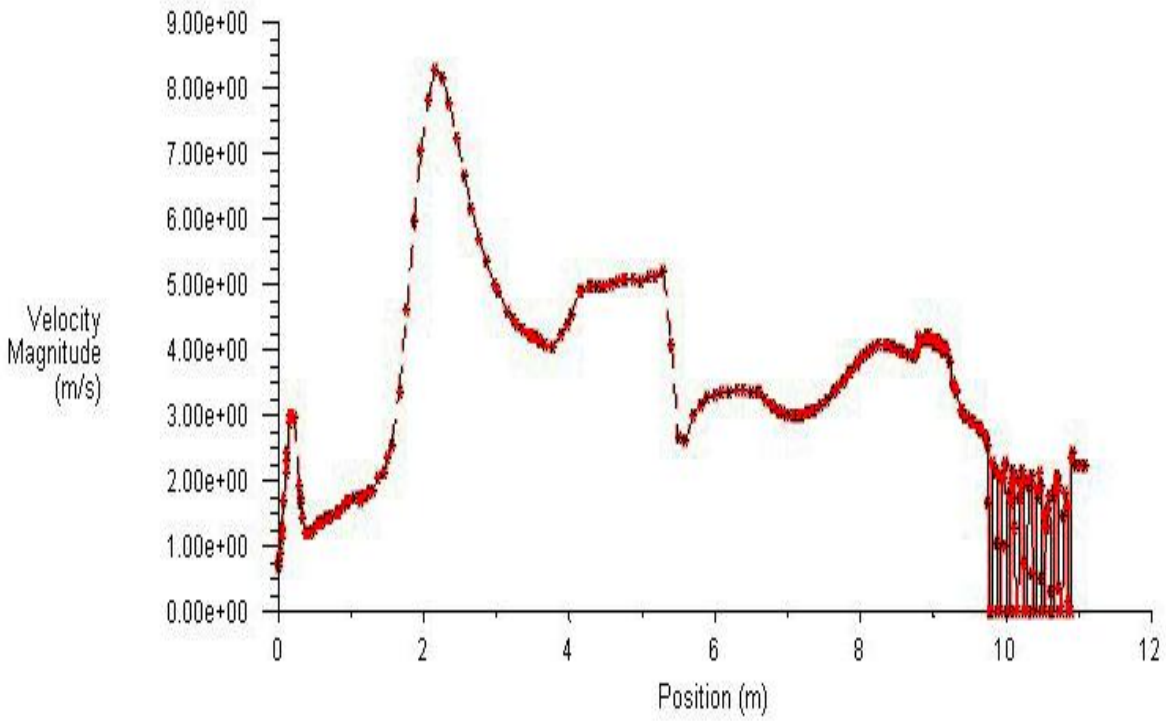

Fig. 5.22: Velocity magnitude along the height

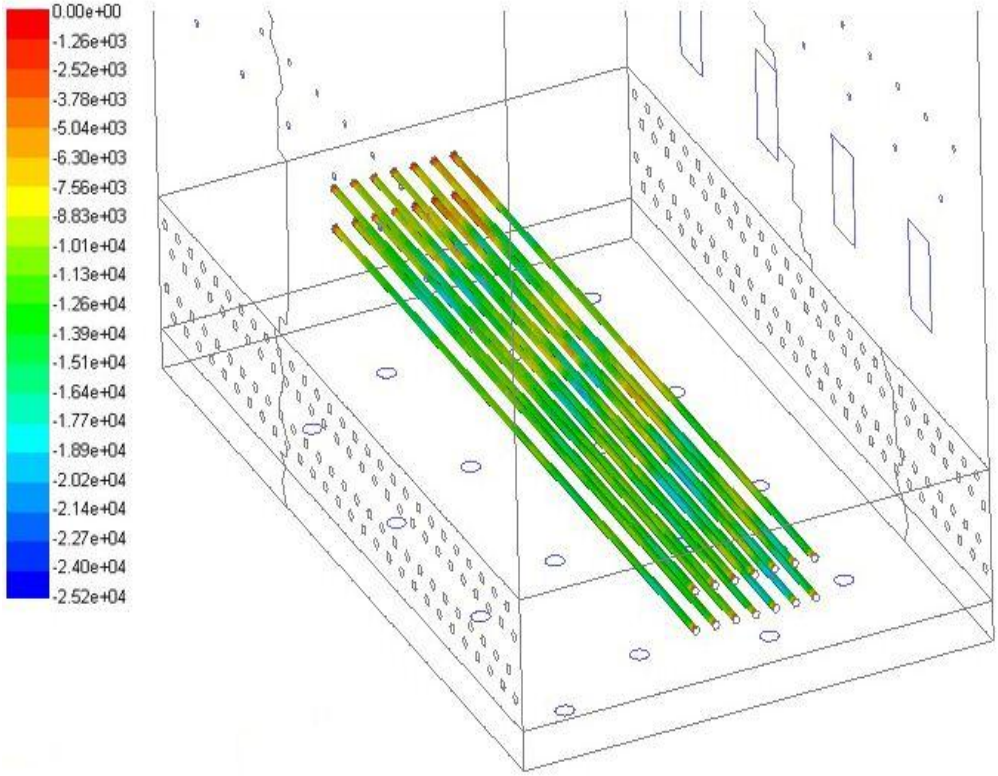

Fig. 5.23: Contours of heat flux of in-bed SH tubes (Wm^{-2})

5.2.6 Heat flux

Heat transfer from flue gases to in-bed superheater tubes is also taken into account, as in a fluidized bed combustor heat is primarily exchanged in the bottom portion of the furnace. The heat transfer coefficient of value 200$Wm^{-2}K^{-1}$ obtained from boiler design data and verified with Ravelli et al. [120] and steam temperature (500^{0}C) was defined at the surface to obtain heat flux. Heat flux contours from the in-bed superheater are shown in Fig.5.23.

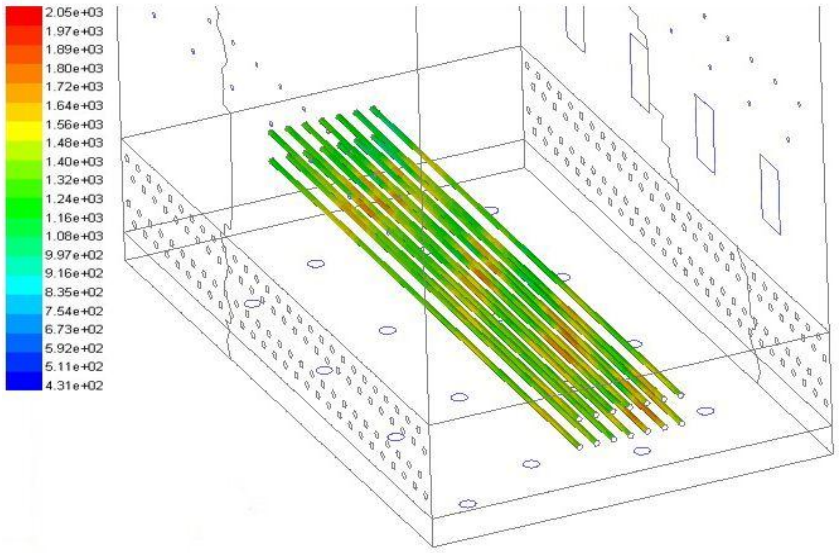

Fig. 5.24: Contours of static temperature of in-bed SH tubes (K)

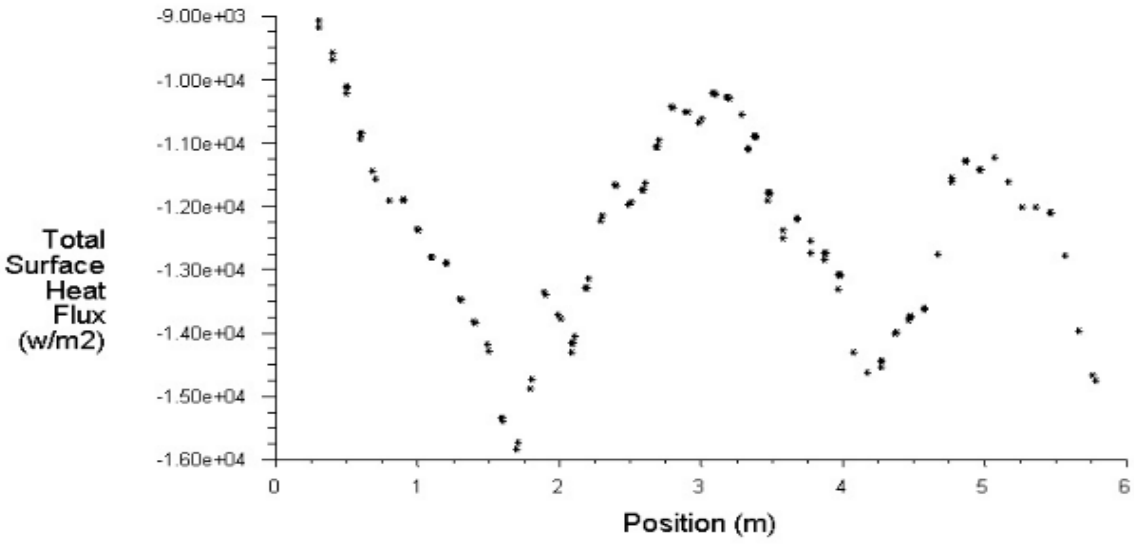

Fig. 5.25: Heat flux along the SH tubes (Wm^{-2})

The regions of the tubes close to the fuel ports attain the maximum temperature and ensure high heat exchange from flue gases to the SH tubes as shown in Fig.5.24. The heat fluxes from these regions are obtained between -1.40×10^4 Wm^{-2} to -1.50×10^4 Wm^{-2} at positions near 2m, 4m and 6m as shown in Fig. 5.25.

CHAPTER 6

CONCLUSIONS & FUTURE SCOPE

6.1 Conclusions

The present research was conducted in a large scale industrial boiler of Captive Power Plant of Ambuja Cement Limited, Ropar situated in the Punjab province of India. The CPP, Ambuja was opted for the study after keeping in mind the sustainable energy development approach and availability of large amount of surplus biomass in the Punjab region of India. The CFD code (Fluent 6.3) was used for conducting the performance analysis of the plant boiler of 45TPH capacity. The following conclusions were drawn from the study:

1. Maximum value of the CO_2 fraction was obtained at the regions where the flame generation took place due to instantaneous combustion of biomass fuel in the suspension at the highest range of temperature. CO_2 concentration was found minimum over the bed due to presence of primary air. During field study CO_2 concentration at the exit of the furnace was obtained to be 0.133. From simulation results it was found to be 0.14. The % age change in results was found to be 5.
2. O_2 concentration was found maximum in the vicinity of the bed due to supply of primary air from sixteen feed ports at 0.5 m/s. The O_2 concentration at the furnace exit was 0.105 and from model results it was obtained as 0.112. The % age change in the actual value and model results was found to be 6.25.
3. In the vicinity of the bed the temperature contours were obtained up to 1200K. The actual bed temperatures vary up to 1223K. The % age change in both the results was found 2.4. Flue gas temperature at the furnace exit was 1123K. The temperature

obtained from model results is 1140K. The change in the experimental value and model results was found to be 1.9%.

4. The trajectories of coal and biomass were plotted by selecting a desired number of streams for presentation. As coal and biomass have different inlet streams with underfeed and overfeed supplies, respectively, there was an inevitable difference in the average residence time of fuel products, which was higher for coal than for biomass: 8·89 and 5·41s, respectively.
5. Heat exchange from flue gases to in-bed superheater tubes was also taken into account, as in a fluidized bed combustor heat is primarily exchanged in the bottom portion of the furnace. The regions of the tubes close to the fuel ports attained the maximum temperature and ensured high heat exchange from flue gases to the SH tubes. The heat fluxes from these regions were obtained between -1.40×10^4 W m^{-2} to -1.50×10^4 W m^{-2}.
6. The simulation also provided the flow behavior of gas in terms of velocity. The highest value was found at the bottom in the vicinity of the bed reaching up to 8 ms^{-1}. Then it showed another peak at a height where notch region was provided to accelerate the velocity as compared with a uniform velocity of 3 to 4 ms^{-1} in the splash zone and a lower velocity in the range 2·42–3·02 ms^{-1} adjacent to the walls of the combustor because of drag forces.

6.2 Future Scope of the Work

- In the present research the combustion has been modeled, however hydrodynamic parameters like bubble formation and elutriation can be modeled in future.
- The freeboard reactions can be taken in account in further studies.
- Different heat rates during co-firing coal and biomass can be considered in further analysis of an industrial furnace.

REFERENCES

[1] Ladanai S, Vinterback J, "Global potential of sustainable biomass for energy", SLU, Swedish University of Agricultural Sciences Department of Energy and Technology, Uppsala, Sweden, 2009.

[2] Burnard k, Bhattacharya S, "Power generation from coal – ongoing developments and outlooks", International Energy Agency, Paris, France, 2011.

[3] Van Loo S, Koppejan j, "The handbook of biomass combustion and co-firing", Earthscan, London, UK, 2008.

[4] Gubba S R, Ingham D B, Larsen K J, Ma L , Pourkashanian M , Tan H Z, Williams A, Zhou H, "Numerical modeling of the co-firing of pulverized coal and straw in a 300 MW tangentially fired boiler", Fuel Proc. Technol., 104, 181-188, 2012.

[5] European Union, "Directive 2001/80/EC on the limitation of emissions of certain pollutants into the air from large combustion plants", Official Journal of the European Communities L, 309,1–21, 2001.

[6] Van Loo S, Koppejan J (Eds.), "The handbook of biomass combustion and co-firing", Earthscan, London, 2008.

[7] Kyoto Protocol. <http://unfccc.int/resource/docs/convkp/kpeng.pdf>

[8] Biomass Co-firing, A Renewable alternative for utilities, DOE, National Renewable Energy Laboratory, US, 2000.

[9] Srinath S, Reddy G V, "Combustion and emission characteristics of rice husk in a rectangular fluidized bed combustor", 2nd International Conference on Environmental Science and Technology, 6, Singapore, V2-343 – V2-346, 2011.

[10] Ekmann J M, Winslow J C, Smouse S M, Ramezan M, "International survey of co-firing coal with biomass and other wastes", Fuel Process Technol, 54,71–88, 1998.

[11] Harding N S, Adams B R, "Biomass as a reburning fuel—a specialized co-firing application", Biomass Bioenergy, 19, 29–45, 2000.

[12] Ross A B, Jones J M, "Measurement and prediction of the emission pollutants from the combustion of coal and biomass in a fixed bed furnace", Fuel, 2002, 81, 571–582.

[13] Sami M, Annamalai K, Wooldridge M, "Co-firing of coal and biomass fuel blends", Progr Energy Combust Sci, 27,7–23, 2001.

[14] Skodras G, Grammelis P, "Emission monitoring during coal waste wood co-combustion in an industrial steam boiler", Fuel, 81, 547–554, 2002.

[15] Battista J, Hughes EE, Tillman D A, "Biomass co-firing at Seward station", Biomass Bioenergy,19, 419–447, 2000.

[16] Changqing D, Baosheng J, Zhaoping Z, Jixiang L, "Tests on co-firing of coal and MSW in a circulating fluidized bed",Energy Convers Manage, 43,189–199, 2002.

[17] Hughes E, Tillman D A, "Biomass co-firing: status and prospects", Fuel Process Technol, 54, 27–42, 1996.

[18] Hus P J, Tillman D A, "Co-firing multiple opportunity fuels with coal at Baily generating station", Biomass Bioenergy,19, 385–394, 2000.

[19] Leckner B, "Emissions from fluidized bed combustion of Biomass", IEA workshop on FBC of unconventional fuels, 1999.

[20] Tillman D A, "Co-firing benefits for coal and biomass", Biomass Bioenergy, 19, 6, 2000.

[21] Tillman DA, "Biomass co-firing: the technology, the experience, the combustion consequences", Biomass Bioenergy, 19, 365 – 384, 2000.

[22] Karekezi S, Kithyoma W, "Bioenergy and agriculture: promises and challenges", Bioenergy and the Poor. In: 2020 Vision for Food, Agriculture, and the Environment. International Food Policy Research Institute, Washington DC, USA, 2006.

[23] Hashiramoto O, "Wood-product trade and policy issue", Cross-sectoral policy developments in forestry, 24-35, 2007.

[24] REN21 (Renewable Energy Policy Network for 21st Century) Renewables Global Status Report 2016.

[25] Bapat DW, Kulkarni SV, Bhandarkar VP, "Design and operating experience on fluidized bed boiler burning biomass fuels with high alkali ash", In: Preto FDS, editor. Proceedings of the 14th International Conference on Fluidized Bed Combustion, New York, ASME, 165–74, 1997.

[26] Hall DO, Rosillo-Calle F, Woods J, Biomass, its importance in balancing CO_2 budgets, In: Grassi G, Collina A, Zibetta H, editors. Biomass for energy, industry and environment, 6th E.C. Conference, London: Elsevier Science, 89–96, 1991.

[27] Sims R H, "Bioenergy Options for a cleaner environment: in developed and developing countries", Elsevier Ltd., Oxford, UK, 184, 2004.

[28] Hall D O, Rosillo-Calle F, "Biomass - other than wood", World Energy Council 1998, Survey of Energy Resources, 18th Edition, London, 227-241, 1998.

[29] Lashof D A, Tirpak D A, "Policy options for stabilizing global climate", United States Environmental Protection Agency, Hemisphere, New York, USA, 1990.

[30] Hall D O, Rosillo-Calle F, Williams R J, Woods J, "Biomass for energy: supply prospects", Renewable energy: sources for fuels and electricity, Earthscan, London, 593-651,1993.

[31] WEC, "New renewable energy sources. A guide to the future", World Energy Council/Kogan Page Ltd, London, UK, 1994.

[32] Fujino J, Yamaji K, Yamamoto H, "Biomass-balance table for evaluating bioenergy resources", Applied Energy, 63, 75–89, 1999.

[33] IPCC, "Special report on emissions scenarios", Inter governmental panel on climate change, Cambridge Univ. Press, Cambridge, UK, 2000.

[34] Rogner H H, "Energy resources", World Energy Assessment. J. Goldemberg, UNPD, Washington, District of Columbia, USA, 135–171, 2000.

[35] Fischer G, Schrattenholzer L, "Global bioenergy potentials through 2050", Biomass and Bioenergy, 20, 151–159, 2001.

[36] Hoogwijk M, On the global and regional potential of renewable energy sources. Ph.D thesis, Utrecht University, Utrecht, The Netherlands, 256, 2004.

[37] Berndes G, Hoogwijk M, Vanden Broek R, "The contribution of biomass in the future global energy supply: a review of 17 studies", Biomass and Bioenergy 25(1), 1-28, 2003.

[38] Hoogwijk M, Faaij A, Vanden Broek R, Berndes G, Gielen D, Turkenburg W, "Exploration of the ranges of the global potential of biomass for energy", Biomass and Bioenergy, 25, 119–133, 2003.

[39] Hoogwijk M , Faaij A, Eickhout B, De Vries B, Turkenburg W, Potential of biomass energy out to 2100, for four IPCC SRES land-use scenarios, 2005.

[40] Sørensen B, Long-term scenarios for global energy demand and supply: four global greenhouse mitigation scenarios. Energy & Environment Group, Roskilde University, Roskilde, Denmark,1999.

[41] Sørensen B, "Biomass for energy: how much is there", Proceedings of Hearing on biofuels and transportation, Danish Parliament, Danish Board of Technology Assessment, Roskilde, Denmark, 149–162, 2001.

[42] Hoogwijk M, Faaij A, Van den Broek R, Berndes G, Gielen D, Turkenburg W, "Exploration of the ranges of the global potential of biomass for energy", Biomass and Bioenergy, 25, 119–133, 2003.

[43] FAO, "Review of wood energy data in RWEDP member countries", Field Document No. 47, Bangkok, 1997.

[44] Central Electricity Authority of Government of India—general review, 2003.

[45] Coal Directory of India, Annual report, Ministry of coal, 2003–2004.

[46] Ministry of Non conventional energy sources, Government of India, Annual Report-2004–2005.

[47] Tata Energy Research Institute (TERI) Energy Data Directory and Year Book 2003–2004.

[48] Bhatnagar AP, Panesar BS, Gupta PK, Jain AK, "Collection, storage and preconditioning of paddy straw as fuel for 10mw power palnt in Patiala district, A special report prepared for Punjab State Electricity Board, 5, 1986.

[49] Baruah DC, Jain AK, "Distribution of agricultural crop residues in India", j Agr Eng, 35, 7 – 12, 1998.

[50] Ravindranath NH, Someshkar HI, Nagraja MS, Sudha P, Sangeetha G, Bhattacharya SC, Salam PA, " Assessment of sustainable non – plantation biomass resources potential for energy in India", Biomass and Bioenergy, 29, 178 – 190, 2005.

[51] Sudha P, Ravindranath NH, "Land availability and biomass production potential in India", Biomass and Bioenergy, 16, 207 – 221,1999.

[52] Narang HP, Parashar DC, Bhattacharya SC, Abdul SP, " A study of biomass as a source of energy in India, RERIC Inter Energy J, 21, 11 – 24,1999.

[53] http://biomasspower.gov.in/index.php

[54] IEA, "Bioenergy annual report", France, 2013.

[55] Biomass estimation and methodology, India, 2016.

[56] Official website of government of PEDA, http:// peda.gov.in

[57] Official website of government of Punjab, http:// punjabgovt.nic.in

[58] Aggarwal GC, "Crop residue management on mechanized farms in India", International Journal of Energy, 19, 957 – 960, 1994.

[59] Jenkins BM, Bhatnagar AP, "On the electric power potential from paddy straw in the Punjab and the optimal size of the power generation station", Intern J of Bioresourse Technol, 37, 35 – 40, 1991.

[60] Punjab government official gazette, 8, 906, 2006.

[61] Punjab State Electricity Regulatory Commission Notification no. 10/106/06 – STE (1)/5390, 2006.

[62] Frisch L E, "Reliable cogeneration utilizing wood as a primary fuel", ASME Power Conference, 1993.

[63] Davidson J F, Harrison D, Fluidized particles, Cambridge University Press, New York, 1963.

[64] Levenspiel O, "G/S reactor models-packed beds, bubbling fluidized bed, turbulent fluidized bed and circulating (fast) fluidized beds", Powder Technol, 122, 1–9, 2002.

[65] Toomey R, Johnstone H F, "Gas fluidization of solid particles", Chem Eng Prog, 48, 220–226, 1952.

[66] Kunii D, Levenspiel O, Fluidization Engineering, second edition, Butterworth-Heinemann, Stoneham, 1991.

[67] Werther J, "Hydrodynamics and mass transfer between the bubble and emulsion phases in fluidized beds of sand and cracking catalyst", Fluidization. New York: Engineering Foundation, 1983.

[68] Park D, Levenspiel O, Fitzgerald TJ, "Plume model for large particle fluidized-bed combustors", Fuel, 60, 295–306, 1980.

[69] De Kok JJ, Nieuwesteeg WCMA, Van Swaaij WPM, "An experimental evaluation of the plume model for atmospheric fluidized-bed combustors", In: Proceedings of the eighth international conference on fluidized bed combustion, 1985.

[70] Stubington JF, Chan SW, "On the phase location and rate of volatiles combustion in bubbling fluidized bed combustors", Trans IchemE, 68, 195–201, 1990.

[71] Fiorentino M, Marzocchella A, Salatino P, "Segregation of fuel particles and volatile matter during devolatilization in a fluidized bed reactor-I. Model development", Chem Eng Sci 52, 1893–1908, 1997.

[72] Fiorentino M, Marzocchella A, Salatino P, "Segregation of fuel particles and volatile matter during devolatilization in a fluidized bed reactor-II", Exp Chem Eng Sci, 52, 1909–1922, 1997.

[73] Avedesian MM, Davidson JF, "Combustion of carbon particles in a fluidized bed", Trans IchemE, 51,121–131, 1973.

[74] Adanez J, Abanades JC, de Diego LF, "Determination of coal combustion reactivities by burnout time measurements in a batch fluidized bed", Fuel, 73, 287–293, 1994.

[75] La Nauze RD, "Coal devolatilization in fluidized-bed combustors", Fuel, 61,771–4, 1982.

[76] Ross IB, f JF, "The combustion of carbon particles in a fluidized bed. Trans IchemE", 59,108–114, 1981.

[77] Chern JS, Hayhurst AN, "Does a large coal particle in a hot fluidized bed lose its volatile content according to the shrinking core model", Combust Flame, 139, 208–221, 2004.

[78] Stubington JF, "Comparisons of techniques for measuring the temperature of char particles burning in a fluidized bed", Chem Eng Res Des, 63,241–9, 1985.

[79] Yates JG, Walker PR, "Particle temperatures in a fluidized bed combustor", Cambridge: Cambridge University Press, 1978.

[80] Prins W, Fluidized bed combustion of a single carbon particle, PhD thesis, University of Twente, The Netherlands, 1987.

[81] Linjewile TM, Agarwal PK, "The product CO/CO_2 ratio from petroleum coke spheres in fluidized bed combustion", Fuel, 74, 5–11, 1995.

[82] Park D, "Estimation of temperature difference between char particles and the fluidized bed in char combustion", Fuel, 68, 1320–4, 1989.

[83] La Nauze RD, "Fundamentals of coal combustion in fluidized beds", Chem Eng Res Des 63, 3–33, 1985.

[84] Georgakis C, Congalidis J, Lee YY, "Physical interpretation of the feasibility region in the combustion of char by use of single and double film theories", Ind Eng Chem Fund, 19, 98–103, 1980.

[85] Brem G, Brouwers JJH, "A complete analytical model for the combustion of a single porous char particle incorporated in a AFBC system model", In: Proceedings of the 10th international conference on fluidized bed combustion, 37–47, 1989.

[86] Goel S, Lee CH, Longwell JP, Sarofim AF, "Modeling of ignition and CO oxidation in the boundary layer of a single char particle", Energy Fuel, 10,1091–8,1996.

[87] Hayhurst AN, Parmar MS, "Does solid carbon burn in oxygen to give the gaseous intermediate CO or produce CO_2 directly, Some experiments in a hot bed of sand fluidized by air", Chem Eng Sci, 53,427–438, 1998.

[88] Biggs MJ, Agarwal PK, "The CO/CO_2 product ratio for a porous char particle within an incipiently fluidized bed: a numerical study", Chem Eng Sci, 52, 941–252, 1997.

[89] Saxena SC, Jotshi CK, "Fluidized-bed incineration of waste materials", Prog Energy Combust Sci, 20, 281–324, 1994

[90] Anthony EJ, "Fluidized bed combustion of alternative solid fuels: status, success and problems of the technology", Prog Energy Combust Sci , 21, 239–268, 1995.

[91] Salatino P, Scala F, Chirone R, " Fluidized bed combustion of biomass char, the influence of carbon attrition and fines postcombustion on fixed carbon conversion", In: Proceedings of the 27th international symposium on combustion, 1998.

[92] Botteril JSM, Teoman Y, Yuregir KR, "Factors affecting heat transfer between gas-fluidized beds and immersed surfaces", Powder Technol 39,177–189, 1984.

[93] Andeen BR, Glicksman LR, "Heat transfer to horizontal tubes in shallow fluidized beds", In: Proceedings of ASME–AIchE heat transfer conference, Paper no. 76-HT-67, 1976.

[94] Decker Na, Glicksman LR, "Conduction heat transfer at the surface of bodies immersed in gas fluidized beds of spherical particles," AIChE Symp Ser, 77, 341–9, 1981.

[95] Scala F, Chirone R, "Fluidized bed combustion of alternative solid fuels", Exp Therm Fluid Sci, 28, 691–699, 2004.

[96] Sergio B, Paolo B, Campi MC, Antonio D M, Guido P, Walter Prandoni, "A model of a bubbling fluidized bed combustor oriented to char mass estimation", IEEE Transactions On Control Systems Technology, 8, 247- 258, 2000.

[97] Schmidt A, Renz U, "Eulerian computation of heat transfer," Chem Eng Sci, 54, 5515-5522, 1999.

[98] Armestoa L, Bahilloa A, Veijonenb K, Cabanillasa A, Oteroa J, "Combustion behaviour of rice husk in a bubbling fluidized bed". Biomass Bioenergy, 23, 171–9, 2002.

[99] Reddy GV, Mohapatra SK, "A mathematical model for exit gas composition in a 10 MW fluidized bed coal combustion power plant," Energy Convers Manage, 35(12), 1049–60, 1994.

[100] Reddy GV, Prashad S, Mohapatra SK, "Mathematical model for coal combustion in a fluidized bed combustor: particle size distribution effects," Ind J Eng Mater Sci, 2224–30, 1995.

[101] Zhou H, Flamant G, Gauthier D, "DEM-LES simulation of coal combustion in a bubbling fluidized bed part ii: coal combustion at the particle level," Chem Eng Sci, 59, 4205-4215, 2004.

[102] Campbell EK, Davidson JF, "The combustion of coal in fluidized beds," Inst Fuel Symp Ser 1, A2.1–9, 1975.

[103] Oka S, Fluidized bed combustion," New York, Marcel Dekker, 2004.

[104] Yang WC.Handbook of fluidization and fluidparticle systems, New York, Marcel Dekker, 2003.

[105] Wen CY, Yu YW, "Mechanics of fluidization", Eng. Progr.Symp, 100-125, 1966.

[106] Kato K, Wen CY "Bubble assemblage model for fluidized bed catalytic reactors", Chem. Eng. Sci., 24, 1351-1369, 1969.

[107] Galgano A, Salatino P, Crescitellis Scale F, Maffettone PL, " A model of the dynamics of a fluidized bed combustor burning bio-mass," Combust Flame, 140, 371–84, 2005.

[108] Yagi S, Aochi T, "Elutriation of particles from a batch fluidized bed,"Paper presented at soc chem engrs (Japan), Spring meeting, 1958.

[109] Zenz FA, Weil FA, "A theoretical–empirical approach to the mechanism of particle entrainment from fluidized beds," AIChE J, 4, 472, 1958.

[110] Wen CY, Harshinger RF, "Elutriation of solid particles from a dense-phase fluidized bed," AICHE, 6(2), 220, 1960.

[111] Geldart D, Baeyens J, Pope DJ, van de Wijer P, "Segregation in beds of large particles at high velocities," Powder Technol, 30(2), 195–205, 1981.

[112] Zenz FA, Weil FA, "A theoretical–empirical approach to the mechanism of particle entrainment from fluidized beds," AIChE J, 4, 472, 1958.

[113] Natrajan E, Nordin A, Rao AN, "Overview of combustion and gasification of rice husk in fluidized bed reactors," Biomass Bioenergy, 14, 533–546, 1998.

[114] Sergio B, Paolo B, Campi MC, Antonio D M, Guido P, Walter Prandoni, "A model of a bubbling fluidized bed combustor oriented to char mass estimation", IEEE Transactions On Control Systems Technology, 8, 247- 258, 2000.

[115] Dixon TF, Mann A, Hobson P, Plaza F, Pennisi S, Steind LR, "Application of CFD in sugar industry", Third International Conference on CFD in Minerals and Process Industry, CSIRO, Melbourne, Australia, 2013.

[116] Pennisi S, Liow JL, Schnieder PA, "CFD Model Development for Sugar Mill Evaporators," Third International Conference on CFD in Minerals and Process Industry, CSIRO, Melbourne, Australia, 2013.

[117] Ghenai C, Janajreh I, "CFD analysis of the effects of co-firing biomass with coal", Energy Conversion and Management, 51, 1694–1701, 2010.

[118] Zhou H, Flamant H, Gauthier D, **"**DEM-LES simulation of coal combustion in a bubbling fluidized bed part II: coal combustion at the particle level", Chemical Engg, Science, 59, 20, 4205-4215, 2004.

[119] Singh RI, Mohapatra SK,Gangacharyulu D, "Studies in an atmospheric bubbling fluidized-bed combustor of 10 MW power plant based on rice husk", Energy Conservation & Management, 49, 11, 3086- 3103, 2008.

[120] Ravelli S, Perdichizzi A, Barigozzi G, "Description, applications and numerical modeling of bubbling fluidized bed combustion in waste-to-energy plants," Prog Energy Combust Sci, 3, 224-253, 2008.

[121] Wankhede US, Adgulkar DD, "CFD simulations of heat transfer in a bubbling fluidized bed for different materials," Emerging Trends in Engineering and Technology, 1094 – 1098, 2008.

[122] Singh RI, Mohapatra SK, Gangacharyulu D, "CFD analysis of bubbling fluidized bed combustion using rice husk," Proceedings of 20th International Conference on FBC, 6, 857- 863, 2009.

[123] Wang S, Zhang X, Zhang Y, "Numerical calculation on fluidized property and flow field in small-scale fluidized bed", 20th International Conference on Bioinformatics and Biomedical Engineering, ICBBE, IEEE, Beijing, 2009.

[124] Rozainee M, Ngo SP, Salema AA, Tan KG, "Computational fluid dynamics modeling of rice husk combustion in a fluidized bed combustor," Powder Technol, 203, 331-347, 2010.

[125] Hamzehei M, Rahimzadeh H, Ahmadi G, "Computational and experimental study of heat transfer and hydrodynamics in 2-dimensional gas-solid fluidized bed reactor," Ind Eng Chem, 49, 5110–5121, 2010.

[126] Guodong L, Dan S, Huilin L, Bouillard J, Yinghua B, Shuai W, "Computations of fluid dynamics of a 50 MW circulating fluidized bed combustor", Ind. Eng. Chem. Res., 49, 5132–5140, 2010.

[127] Al-Abbas AH, Naser J, Dodds D, "CFD modeling of air-fired and oxy-fuel combustion in a large-scale furnace at Loy Yang A brown coal power station", Fuel, 102, 646–665, 2012.

[128] Staples J, Marshall L, In: Herman Resource Laboratories (HRL) Technology, Report No. HLC/2010/105.<http://www.hrl.com.au/>.

[129] Nikolopoulos N, Nikolopoulos A, Karampinis E, Grammelis P, Kakaras E, "Numerical investigation of the oxy-fuel combustion in large scale boilers adopting the ECO-Scrub technology", Fuel, 90, 198–214, 2011.

[130] Tan Y, Croiset E, Douglas MA, Thambimuthu V, "Combustion characteristics of coal in a mixture of oxygen and recycled flue gas", Fuel, 85, 507–12, 2006.

[131] Erfurth J, Toporov D, Forster M, Kneer R, "Numerical simulation of a 1200MW pulverized fuel oxy-firing furnace", In: Fourth international conference on clean coal technologies, CCT, 2009.

[132] Dixon TF, Mann AP, Plaza F, Gilfillan WN, "Development of advanced technology for biomass combustion—CFD as an essential tool", Fuel, 84, 1303–1311, 2005.

[133] Ma L, Jones JM, Pourkashanian M, Williams A, "Modeling the combustion of pulverized biomass in an industrial combustion test furnace", Fuel, 86, 1959–1965, 2007.

[134] Syred N, Kurniawan K, Griffiths T, Gralton T, Ray R, "Development of fragmentation models for solid fuel combustion and gasification as subroutines for inclusion in CFD codes", Fuel, 86, 2221–2231, 2007.

[135] Kurniawan KP, Studies of fundamental processes occurring in precalciners and cyclone pre-heater towers using CFD, Ph.D thesis Cardiff University, 2004.

[136] Werther J, Saenger M, Hartge E-U, Ogada T, Siagi Z, "Combustion of agricultural residues", Progress in Energy and Combustion Science, 26, 1–27, 2000.

[137] Sami M, Annamalai K, Wooldridge M, "Co-firing of coal and biomass fuel blends", Progress in Energy and Combustion Science, 27, 171–214, 2001.

[138] Hupa M, "Interaction of fuels in co-firing in FBC", Fuel, 84, 1312–1319, 2005.

[139] Janvijitsakul K, Kuprianov VI, "Similarity and modeling of axial CO and NO concentration profiles in a fluidized-bed combustor (co-)firing biomass fuels", Fuel, 87, 1574–1584, 2008.

[140] Kaushal P, Proll T, Hofbauer H, "Model development and validation: Co-combustion of residual char, gases and volatile fuels in the fast fluidized combustion chamber of a dual fluidized bed biomass gasifier", Fuel, 86, 2687–2695, 2007.

[141] Adanez J, Gayan P, de Diego LF, Garcia-Labiano F, Abad A, "Combustion of Wood Chips in a CFBC Modeling and Validation", Ind Eng Chem Res, 42, 987–99, 2003.

[142] Yan HM, Craig H, Zhang D, "Mathematical modeling of a bubbling fluidized bed coal gasifier and the significance of net flow", Fuel, 77,1067–79, 1998.

[143] Madhiyanon T, Sathitruangsak P, Soponronnarit S, "Co-combustion of rice husk with coal in a cyclonic fluidized-bed combustor (φ-FBC)", Fuel, 88, 132–138, 2009.

[144] Fletcher D F, Haynes B S, Christo F C, Joseph S D, "A CFD based combustion model of an entrained flow biomass gasifier", Applied Mathematical Modeling, 24, 165-182, 2000.

[145] Gerun L, Paraschiv M, Vijeu R, Bellettre J, Tazerout M, Gøbel B, Henriksen U, "Numerical investigation of the partial oxidation in a two-stage downdraft gasifier", Fuel, 87, 1383–1393, 2008.

[146] Xiu S N, Wang N N, Yi W M, Li B M, Shahbazi G, "Validation of kinetic parameter values for prediction of pyrolysis behavior of corn stalks in a horizontal entrained-flow reactor",Biosystems Engineering,100, 79-85, 2008.

[147] Yuen R K K, Yeoh G H, Davis G D, Leonardi E, "Modeling the pyrolysis of wet wood – I.Three-dimensional formulation and analysis", International Journal of Heat and Mass Transfer 50, 4371–4386, 2007.

[148] Yuen R K K, Yeoh G H, Davis G D, Leonardi E, "Modeling the pyrolysis of wet wood – II. Three-dimensional cone calorimeter simulation", International Journal of Heat and Mass Transfer, 50, 4387-4399, 2007.

[149] Yang Y B, Sharifi V N, Swithenbank J, "Converting moving-grate incineration from combustion to gasification-Numerical simulation of the burning characteristics", Waste Management, 27,645-655, 2007.

[150] Marklund M, Tegman R, Gebart R, "CFD modeling of black liquor gasification: Identification of important model parameters", Fuel, 86, 1918-1926, 2007.

[151] Sharma A K, "Modeling fluid and heat transport in the reactive, porous bed of down draft(biomass) gasifier", International Journal of Heat and Fluid Flow, 28, 1518-1530, 2007.

[152] Luo Z Y, Wang S R, Cen K F, "A model of wood flash pyrolysis in fluidized bed reactor", Renewable Energy, 30, 377-92, 2005.

[153] Kaer S K, "Numerical modeling of a straw-fired grate boiler", Fuel, 83, 1183-1190, 2004.

[154] Kaer S K, Rosendahl L A, Baxter L L, "Towards a CFD-based mechanistic deposit formation model for straw-fired boilers", Fuel, 85, 833-848, 2006.

[155] Kaer S K, Rosendahl L, "Extending the modeling capacity of CFD codes applied to biomass-fired boilers", In Proc. ECOS, Copenhangen, Denmark, 251-264, 2003.

[156] Kaer S K, Rosendahl L A, Baxter L L, "Extending the capability of CFD codes to assess ash related problems in biomass fired boilers. In Proc. 227th ACS Annual Meeting¸ Anaheim California, Division of Fuel Chemistry, No. 12, 2004.

[157] Shanmukharadhya K S, "Simulation and thermal analysis of the effect of fuel size on combustion in an industrial biomass furnace", Energy & Fuels, 21, 1895-1900, 2007.

[158] Marias F, "A model of a rotary kiln incinerator including processes occurring within the solid and the gaseous phases", Computers & Chemical Engineering, 2003, 27, 813-825, 2003.Int. J. Mol. Sci. 2008, 9, 1130

[159] Shanmukharadhya K S, Sudhakar K G, "Effect of fuel moisture on combustion in a bagasse fired furnace", Journal of Energy Resources Technology-Transactions of the Asme,129, 248-253, 2007.

[160] Dixit C S B, Paul P J, Mukunda H S, "Part II: Computational studies on a pulverised fuel stove", Biomass & Bioenergy, 30, 684-691, 2006.

[161] Goddard C D, Yang Y B, Goodfellow J, Sharifi V N, Swithenbank J, Chartier J, Mouquet D, Kirkman R, Barlow D, Moseley S, "Optimisation study of a large waste-to-energy plant using computational modeling and experimental measurements", Journal of the Energy Institute, 78(3), 106-116, 2005.

[162] Abbas T, Awais M M, Lockwood F C, "An artificial intelligence treatment of devolatilization for pulverized coal and biomass in co-fired flames" Combustion and Flame, 132, 305-318, 2003.

[163] Backreedy R I, Fletcher L M, Jones J M, Ma L, Pourkashanian M, Williams A, "Co-firing pulverised coal and biomass: a modeling approach", Proceedings of the Combustion Institute, 30, 2955-2964, 2005.

[164] Syred N, Kurniawan K, Grifths T, Gralton T, Ray R, "Development of fragmentation models for solid fuel combustion and gasification as subroutines for inclusion in CFD codes", Fuel, 2007, 86, 2221-2231, 2007.

[165] Tan C K, Wilcox S J, Ward J, "Use of artificial intelligence techniques for optimization of co-combustion of coal with biomass", Journal of the Energy Institute, 79, 19-25, 2006.

[166] Gera D, Mathur M P, Freeman M C, Robinson A, "Effect of large aspect ratio of biomass particles on carbon burnout in a utility boiler", Energy & Fuels, 16, 1523-1532, 2002.

[167] Miltner M, Miltner A, Harasek M, Friedl A, "Process simulation and CFD calculations for the development of an innovative baled biomass-fired combustion chamber", Applied Thermal Engineering,27, 1138-1143, 2007.

[168] Zarnescu V, Pisupati S V, "An integrative approach for combustor design using CFD methods", Energy & Fuels, 16, 622-633, 2002.

[169] Saario A, Oksanen A, "Comparison of global ammonia chemistry mechanisms in biomass combustion and selective noncatalytic reduction process conditions", Energy & Fuels, 22, 297-305, 2008.

[170] Norstrom T, Kilpinen P, Brink A, Vakkilainen E, Hupa M, "Comparisons of the validity of different simplified NH3-oxidation mechanisms for combustion of biomass", Energy & Fuels, 14, 947-952, 2000.

[171] Weydahl T, Bugge M, Gran I R, Ertesvag I. S, "Computational modeling of nitric oxide formation in biomass combustion," Applied Mechanics and Engineering, 7, 125-142, 2002

[172] Rogerson J W, KentJ H, Bilger R W, "Conditional moment closure in a bagasse-fired boiler," Proceedings of the Combustion Institute, 31, 2805-2811 , 2007.

[173] Mueller C, A. Brink, M. Hupa, "Numerical simulation of the combustion behavior of different biomasses in a bubbling fluidized bed boiler," in: Proceedings of 18th

International conference on Fluidized bed combustion, Toronto, Ontario, Canada, 2005.

[174] Black S, Szuhánszki J, Pranzitelli A, Ma L, Stanger PJ, Ingham DB, Pourkashanian M, "Effects of firing coal and biomass under oxy-fuel conditions in a power plant boiler using CFD modeling," Fuel 113 , 780–786, 2013.

[175] Zhang X, Ghamari M, Ratner A, "Numerical modeling of co-firing a light density biomass, oat (Avena sativa) hulls, and chunk coal in fluidized bed boiler", Biomass and Bioenergy, 56, 239 – 246, 2013.

[176] Singh RI, Brink A, Hupa M , "CFD modeling to study fluidized bed combustion and gasification", App Thermal Engg, 52, 585-614, 2013.

[177] Hirsch C, "Numerical computation of internal and external flows", Butterworth–Heinemann, USA, 2007.

[178] Gera D, Gautam, Tsuji M, Kawaguchi Y, Tanaka T, "Computer simulation of bubbles in large-particle fluidized beds," Powder Technology, 98, 38–47, 1998.

[179] Ergun S, "Fluid flow through packed columns," Chemical Engineering Progress, 48, 89–94, 1952.

[180] Gidaspow D, Bezburuah R, Ding J, "Hydrodynamics of circulating fluidized beds, kinetic theory approach," Fluidization VII Proceedings of the 7th Engineering Foundation Conference on Fluidization, Gold Coast (Australia),75–82, 1992.

[181] Ranganathan P, Sai Gu, "Computational fluid dynamics modeling of biomass fast pyrolysis in fluidized bed reactors, focusing different kinetic schemes", Bioresource Technology, 213, 333–341, 2016.

[182] Tsuji Y, Kawagushi T, Tanaka T, "Discrete particle simulation of two-dimensional fluidized bed," Powder Technology, 77, 79–87, 1993.

[183] Hoomans BPB, Kuipers JAM, Briels WJ, Van Swaaij WPM, "Discrete particle simulation of bubble and slug formation in a two-dimensional gas-fluidized bed: A hard-sphere approach", Chemical Engineering Science, 51, 99–118, 1996.

[184] Kobayashi N, Yamazaki R, Mori S, "A study on the behavior of bubbles and solids in bubbling fluidized beds", Powder Technology, 113, 327–344, 2000.

[185] Kaneko Y, Shiojima T, Horio M, "DEM simulation of fluidized beds for gas-phase olefin polymerization", Chemical Engineering Science, 54, 5809–5821, 1999.

[186] Van der Hoef MA, M. Van Sint Annaland M, Kuipers JAM, Computational fluid dynamics for dense gas–solid fluidized beds: a multiscale modeling strategy", China Particuology, 3, 69–77, 2005.

[187] Blasi CD, "Modeling chemical and physical processes of wood and biomass pyrolysis", Progress in Energy and Combustion Science,34, 47-90, 2008.

[188] Moghtaderi B, "The state-of-the-art in pyrolysis modeling of lignocellulosic solid fuels", Fire and Materials, 30, 1-34, 2006.

[189] Wurzenberger JC, Wallner S, Raupenstrauch H, Khinast JG, "Thermal conversion of biomass: Comprehensive reactor and particle modeling", Aiche Journal, 48, 2398-2411, 2002.

[190] Corella J, Sanz A, "Modeling circulating fluidized bed biomass gasifiers.A pseudo-rigorous model for stationary state", Fuel Processing Technology**,** 86, 1021-1053, 2005.

[191] Fluent Inc. FLUENT 6.1 User's Guide, 2003.

[192] Kobayashi H, Howard JB, Sarofim AF, "Coal devolatilization at high temperatures", In Proc.16th International Symposium on Combustion, 1976.

[193] Eaton AM, Smoot LD, Hill SC, Eatough CN, "Components, formulations, solutions, evaluation, and application of comprehensive combustion models", Progress in Energy and Combustion Science,25, 387-436, 1999.

[194] Pallares J, Arauzo I, Williams A, "Integration of CFD codes and advanced combustion models for quantitative burnout determination", Fuel, 86, 2283–2290, 2007.

[195] Bakul CEJ, Gershtein VY, Xianming L, "Computational Fluid Dynamics in Industrial Combustion", CRC Press, New York, 2001.

[196] Sau D C, Mohanty S, Biswal K C, "Minimum fluidization velocities and maximum bed pressure drops for gas–solid tapered fluidized beds", Chemical Engineering Journal, 132, 151–157, 2007.

[197] Baum M M, Street P J, "Predicting the combustion behavior of coal particles", Combust. Sci. Tech., 3, 231–243, 1971.

[198] Field M A, "Rate of combustion of size-graded fractions of char from a low rank coal between 1200K-2000K", Combustion and Flame, 13, 237–252, 1969.

[199] Indian Network for Climate Change Assessment (INCCA), Greenhouse gas emissions, Ministry of Environment & Forests, India, 2010.

[200] Bell S, Measurement good practice guide no. 11 (Issue 2) - A beginner's guide to uncertainty of measurement, National Physical Laboratory, Middlesex, UK, ISSN 1368-6550, 2001.

[201] Freitas CJ, "The issue of numerical uncertainty", Applied Mathematical Modelling, 26, 237–248, 2002.

APPENDIX

A 1 Proximate Analysis of fuel [Test method IS: 1350 (Part 1)]

In this analysis the percentage of moisture content, volatile matter, ash and fixed carbon are determined.

A 1.1 Determination of moisture

Moisture is defined as the difference in weight of sample of fuel when the same is heated at 108 ± 2°C for one hour under specified conditions.

A 1.1.1 Procedure

Silica crucible is taken, cleaned and dried in an oven at 108 ± 2°C for one hour. It is cooled for 15 minutes and then weighed accurately. Approximately one gram of sample of fuel is weighed and put into the silica crucible. Then crucible is kept in an air-dried oven which is maintained at 108 ± 2°C for one hour. After one hour crucible is removed from the oven, cooled and then weighed accurately.

A 1.1.2 Calculations

Weight of dried and empty crucible with lid x gm

Weight of sample and crucible with lid = y gm

Weight of sample and crucible after heating = z gm

Therefore, weight of sample before heating = (y-x) gm

Weight of Moisture loss due to heating = (y-z) gm

Percentage of Moisture $\{(y-z) / (y-x)\} \times 100$

A 1.2 Determination of volatile matter

Volatile matter is defined as the loss of weight of sample when the same is heated under specified conditions in the absence of air at 900 ± 10°C for a period of seven minutes.

A 1.2.1 Procedure

For the determination of volatile matter, a crucible with lid is taken and then weighed accurately. Now one gram of fuel sample is weighed accurately into the crucible and spread evenly in the crucible by gentle tapping. The crucible with the lid is transferred in the furnace at 900 ± 10°C for seven minutes. After seven minutes, the crucible is removed from the furnace and placed on a cooled iron plate to ensure rapid cooling. Then the crucible is placed in a desicator for 15 minutes for further cooling and then weighed accurately.

A 1.2.2 Calculations

Weight of dried and empty crucible with lid = x gm

Weight of sample and crucible with lid = y gm

Weight of sample and crucible after heating = z gm

Therefore, weight of sample before loss of weight = (y-x) gm

Loss of weight (y-z) gm

Percentage of volatile matter = {(y-z) / (y-x)} × 100

A 1.3 Determination of ash

Ash is defined as the weight of residue left when a known weight of sample is burnt at 815 ± 10°C for one hour under specified conditions.

A 1.3.1 Procedure

For the determination of ash, a silica dish is taken, heated at 815 ± 10°C for one hour. Then the dish is cooled for 20 minutes and then weight of empty dish is taken. Now one gram of sample is weighed accurately into the crucible and spread evenly in the crucible by gentle tapping the crucible with the lid. The silica dish is transferred in the furnace at 500°C for half an hour. Then the temperature of the furnace is raised to 815 ± 10°C. The

dish is kept at this temperature for another one hour. The crucible is removed from the furnace, cooled and then weighed accurately.

A 1.3.2 Calculations

Weight of dried and empty crucible = x gm

Weight of sample and crucible = y gm

Weight of sample and crucible after heating = z gm

Therefore, weight of sample before heating = (y-x) gm

Weight of ash = (z-x) gm

Percentage of ash = {(z-x) / (y-x)} × 100

A 1.4 Determination of fixed carbon

The percentage of the fixed carbon can be found by subtracting the percentage of moisture content, volatile matter and ash content from 100.

A 2 Data Monitoring of Bed Temperatures, O/L Temperatures of Flue Gas, %age Of O_2 and CO_2 at O/L

Table A 2.1: Day – 1(Data collected in March 2012)

Time (hr.)	Bed temperature (K)								Air and flue gas temp. (K)	O_2 (% vol) at O/L	CO_2 (% vol) at O/L
	Bed – 1 Temp.L	Bed – 1 Temp.R	Bed – 2 Temp.L	Bed – 2 Temp.R	Bed – 3 Temp.L	Bed – 3 Temp.R	Bed – 4 Temp.L	Bed – 4 Temp.R	Boiler bank O/L		
15.00	1214	1239	1239	1237	1239	1234	1229	1221	1134	9.6	9.1
14.00	1211	1235	1234	1233	1234	1236	1226	1218	1139	9.7	9
13.00	1189	1224	1222	1210	1236	1231	1204	1202	1109	9.9	9.1
12.00	1206	1209	1214	1224	1214	1204	1206	1199	1129	9.4	9.2
11.00	1194	1219	1219	1218	1216	1214	1204	1202	1104	9.8	8.6
10.00	1219	1214	1219	1228	1199	1204	1229	1194	1125	9.7	8.8
9.00	1229	1234	1229	1223	1229	1234	1228	1219	1114	9.8	8.6
8.00	1194	1218	1218	1219	1226	1227	1220	1193	1124	9.7	8.8
AVG	1207	1224	1224	1224	1224	1223	1218	1206	1123	9.7	8.9

Table A 2.2: Day – 2 (On full load conditions)

Time (hr.)	Bed temperature (K)								Air and flue gas temp. (K)	O_2 (% vol) at O/L	CO_2 (% vol) at O/L
	Bed – 1 Temp.L	Bed – 1 Temp.R	Bed – 2 Temp.L	Bed – 2 Temp.R	Bed – 3 Temp.L	Bed – 3 Temp.R	Bed – 4 Temp.L	Bed – 4 Temp.R	Boiler bank O/L		
15.00	1214	1229	1245	1240	1238	1240	1223	1214	1144	10	9.6
14.00	1212	1234	1236	1234	1231	1233	1218	1193	1154	9.7	9
13.00	1209	1238	1233	1226	1231	1227	1214	1201	1144	9.9	8
12.00	1196	1218	1219	1219	1217	1215	1207	1205	1098	9.5	8.9
11.00	1214	1213	1218	1223	1226	1214	1210	1203	1131	9.8	8.6
10.00	1220	1211	1226	1219	1206	1209	1218	1201	1114	9.9	8.8
9.00	1222	1232	1233	1239	1229	1238	1224	1206	1124	9.9	9
8.00	1207	1215	1222	1220	1214	1216	1210	1191	1107	9.7	8.9
AVG	1211	1223	1229	1227	1224	1224	1215	1201	1127	9.8	8.85

Table A 2.3: Day – 3 (On full load conditions)

Time (hr.)	Bed temperature (K)								Air and flue gas temp.(K)	O_2 (% vol) at O/L	CO_2 (% vol) at O/L
	Bed – 1 Temp.L	Bed – 1 Temp.R	Bed – 2 Temp.L	Bed – 2 Temp.R	Bed – 3 Temp.L	Bed – 3 Temp.R	Bed – 4 Temp.L	Bed – 4 Temp.R	Boiler bank O/L		
15.00	1212	1224	1242	1234	1234	1234	1222	1219	1139	9.8	9.3
14.00	1209	1239	1233	1229	1229	1237	1230	1199	1144	9.9	9
13.00	1197	1230	1228	1222	1232	1229	1209	1199	1141	9.9	8.2
12.00	1198	1219	1215	1218	1219	1210	1204	1208	1104	9.7	8.9
11.00	1204	1209	1214	1224	1217	1209	1209	1193	1124	9.6	8.8
10.00	1210	1209	1221	1217	1197	1208	1224	1199	1108	9.8	9
9.00	1221	1229	1234	1231	1224	1237	1223	1214	1129	10	9
8.00	1199	1214	1219	1221	1224	1224	1215	1195	1105	9.7	9
AVG	1206	1221	1225	1224	1222	1223	1217	1203	1124	9.8	8.9

Table A 2.4: Day – 4 (On full load conditions)

Time (hr.)	Bed temperature (K)								Air and flue gas temp. (K)	O_2 (% vol) at O/L	CO_2 (% vol) at O/L
	Bed – 1 Temp.L	Bed – 1 Temp.R	Bed – 2 Temp.L	Bed – 2 Temp.R	Bed – 3 Temp.L	Bed – 3 Temp.R	Bed – 4 Temp.L	Bed – 4 Temp.R	Boiler bank O/L		
15.00	1214	1239	1239	1237	1239	1234	1229	1221	1144	10	8.9
14.00	1211	1235	1234	1233	1234	1236	1226	1218	1134	9.9	9
13.00	1189	1224	1222	1210	1236	1231	1204	1202	1139	9.8	8.5
12.00	1206	1209	1214	1224	1214	1204	1206	1199	1109	9.5	8.9
11.00	1194	1219	1219	1218	1216	1214	1204	1202	1129	9.6	8.7
10.00	1219	1214	1219	1228	1199	1204	1229	1194	1104	10	9.1
9.00	1229	1234	1229	1223	1229	1234	1228	1219	1125	10	9
8.00	1194	1218	1218	1219	1226	1227	1220	1193	1114	9.6	9
AVG	1207	1224	1224	1224	1224	1223	1218	1206	1124	9.8	8.88

Table A 2.5: Day – 5 (On full load conditions)

Time (hr.)	Bed temperature (K)								Air and flue gas temp. (K)	O_2 (% vol) at O/L	CO_2 (% vol) at O/L
	Bed – 1 Temp.L	Bed – 1 Temp.R	Bed – 2 Temp.L	Bed – 2 Temp.R	Bed – 3 Temp.L	Bed – 3 Temp.R	Bed – 4 Temp.L	Bed – 4 Temp.R	Boiler bank O/L		
15.00	1219	1244	1234	1244	1244	1239	1234	1224	1139	9.8	9.2
14.00	1209	1239	1239	1234	1229	1234	1229	1211	1132	10	8.8
13.00	1199	1219	1229	1204	1232	1229	1199	1194	1138	9.7	8.5
12.00	1214	1204	1204	1229	1224	1214	1214	1208	1094	9.8	8.9
11.00	1189	1224	1214	1224	1227	1224	1209	1209	1134	9.6	9
10.00	1220	1222	1229	1222	1193	1196	1224	1189	1114	10	9
9.00	1224	1229	1234	1219	1219	1237	1234	1188	1129	9.9	8.8
8.00	1204	1213	1204	1224	1224	1221	1219	1201	1112	9.7	8.9
AVG	1209	1224	1223	1225	1224	1224	1220	1203	1124	9.812	8.887

Table A 2.6: Day – 6 (On full load conditions)

Time (hr.)	Bed temperature (K)								Air and flue gas temp. (K)	O_2 (% vol) at O/L	CO_2 (% vol) at O/L
	Bed – 1 Temp.L	Bed – 1 Temp.R	Bed – 2 Temp.L	Bed – 2 Temp.R	Bed – 3 Temp.L	Bed – 3 Temp.R	Bed – 4 Temp.L	Bed – 4 Temp.R	Boiler bank O/L		
15.00	1214	1242	1239	1239	1239	1242	1239	1229	1140	10	9.3
14.00	1210	1236	1234	1235	1234	1229	1224	1219	1134	9.8	8.9
13.00	1194	1224	1224	1201	1235	1228	1194	1199	1134	9.5	8.5
12.00	1213	1210	1202	1234	1219	1224	1217	1211	1099	9.8	8.9
11.00	1184	1219	1217	1220	1229	1219	1204	1214	1129	9.8	8.9
10.00	1224	1229	1234	1226	1199	1199	1219	1194	1119	9.9	9
9.00	1219	1234	1232	1221	1211	1229	1234	1189	1124	9.8	8.9
8.00	1208	1202	1212	1222	1229	1222	1225	1209	1114	9.8	8.9
AVG	1208	1224	1224	1224	1224	1224	1219	1208	1124	9.8	8.912

A 3 Geometry Modeling and Mesh Generation

The model was initially generated in Solid Works which provides a user friendly platform for geometry generation. The grid formation of the CPP boiler for analysis has been done in the pre – processor of the Fluent 6·3 commercial code which is known as GAMBIT. The geometry of the boiler with dimensions and inside components is shown in Fig. A 3.1. There are four feed ports, with 380 mm×680 mm of dimensions available for biomass supply over the bed and sixteen feed ports under the bed for supply of coal. There are twelve upper secondary airports and seven lower secondary airports available, each of

diameter 50 mm, for supplying excess air to allow complete combustion. Three superheaters are installed inside the combustor. One is an in-bed superheater with seven coils, and the others are primary and secondary superheaters installed at the upper portion of the combustor. The primary superheater coils are of 45 mm diameter and 5 mm thickness. The in-bed superheater coils are of 51 mm outer diameter and 6·5 mm thickness. After the superheaters, there are convection bank tubes, which also work as a heat sink. The grid contains a total of 6,39,798 elements, of which 2,62,644 are hexahedral, 3,54,612 tetrahedral and 22,542 pyramidal.

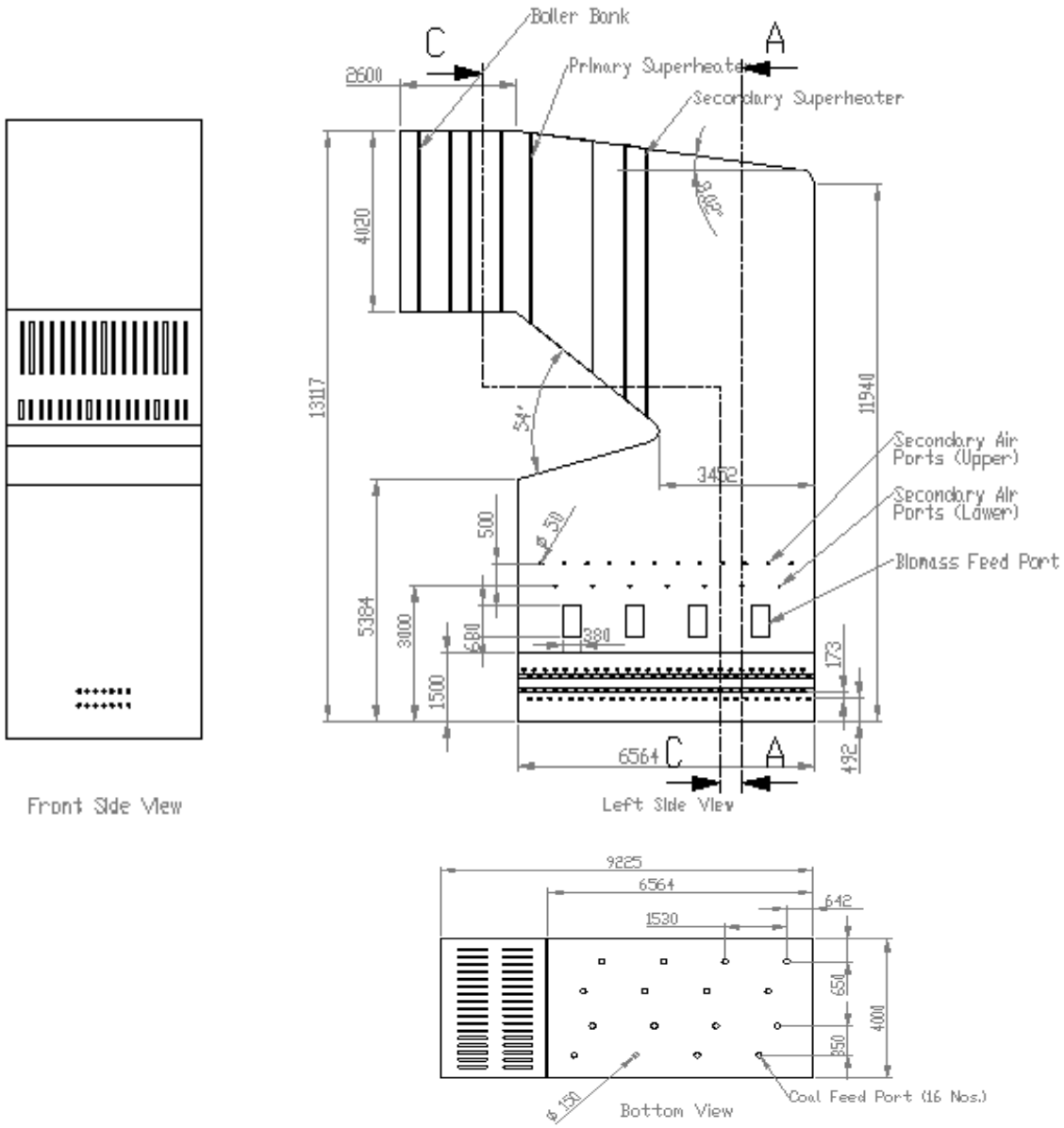

Fig A 3.1: CPP boiler geometry

Steps for performing CFD analysis

1. The geometry volume was imported to GAMBIT.
2. Since the volume to be meshed was large and complex. The volume was split into 5 volumes considering Geometry decomposition techniques. The aim was to generate hexahedral elements wherever possible to reduce the total number of elements as shown in Fig. A 3.2.

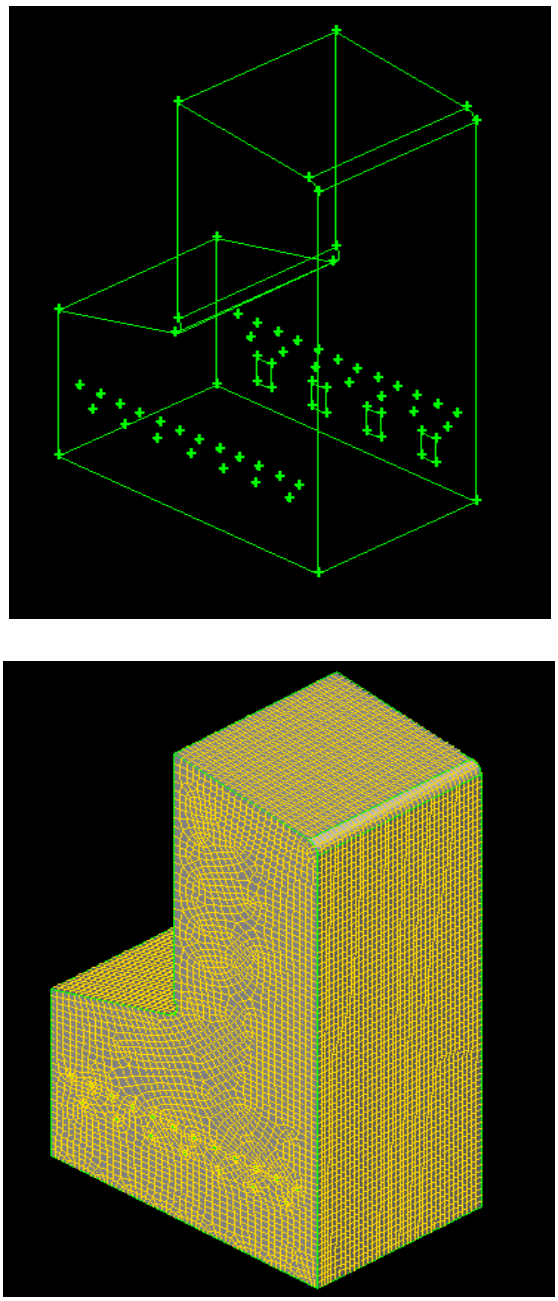

Fig A 3.2: Freeboard region with hexahedral elements

3. The free-board region was first meshed (Fig. A 3.3). A curvature sizing function was attached to the circular edges of the secondary air ports with angle of 36^0 so that each circular edge was meshed with 10 elements. A maximum size of 150 was assigned to the source faces with a growth rate of 2.

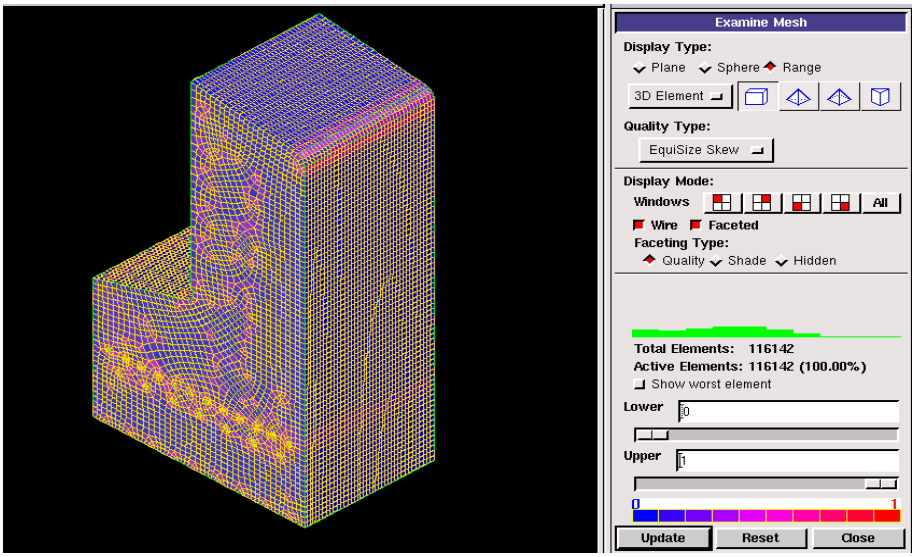

Fig A 3.3: Freeboard region showing total number of elements

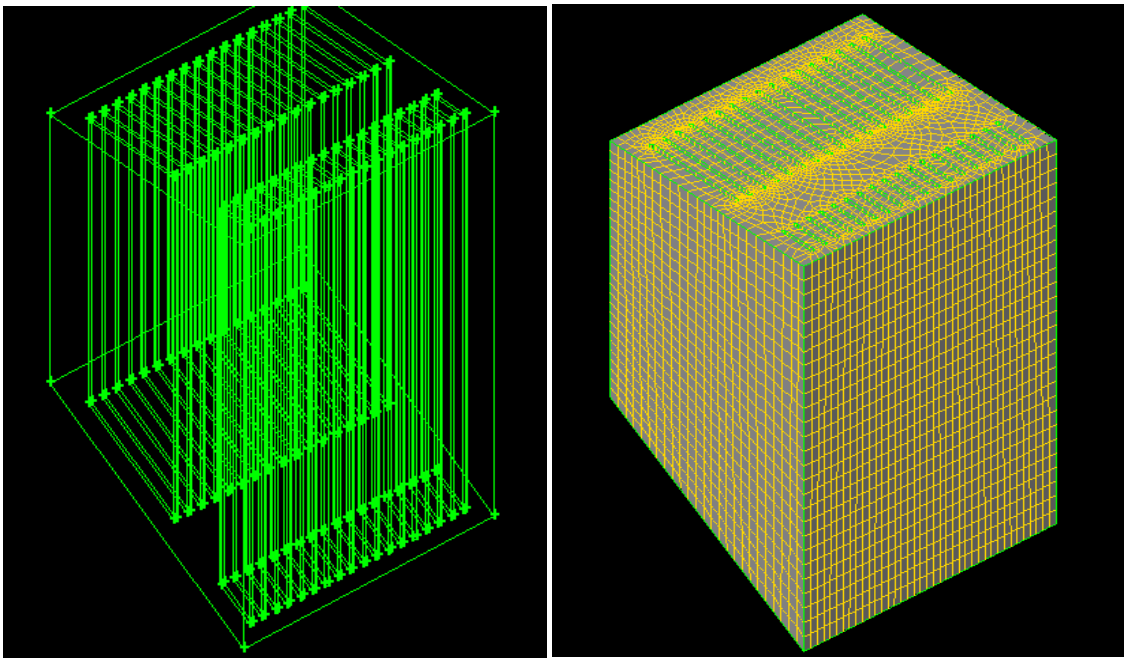

Fig A 3.4: Volume consisting primary and secondary superheaters

4. Next the volume consisting primary & secondary super heaters was meshed as shown in Fig. A 3.4. A curvature sizing function was assigned to the top edges of the super-heater with angle of 36^0 so that each circular edge was meshed with 10 elements. A maximum size of 150 was assigned to the source faces with a growth rate of 1.4 specified. The volume was meshed using Cooper meshing scheme and all hexahedral element mesh was generated as shown in Fig. A 3.5

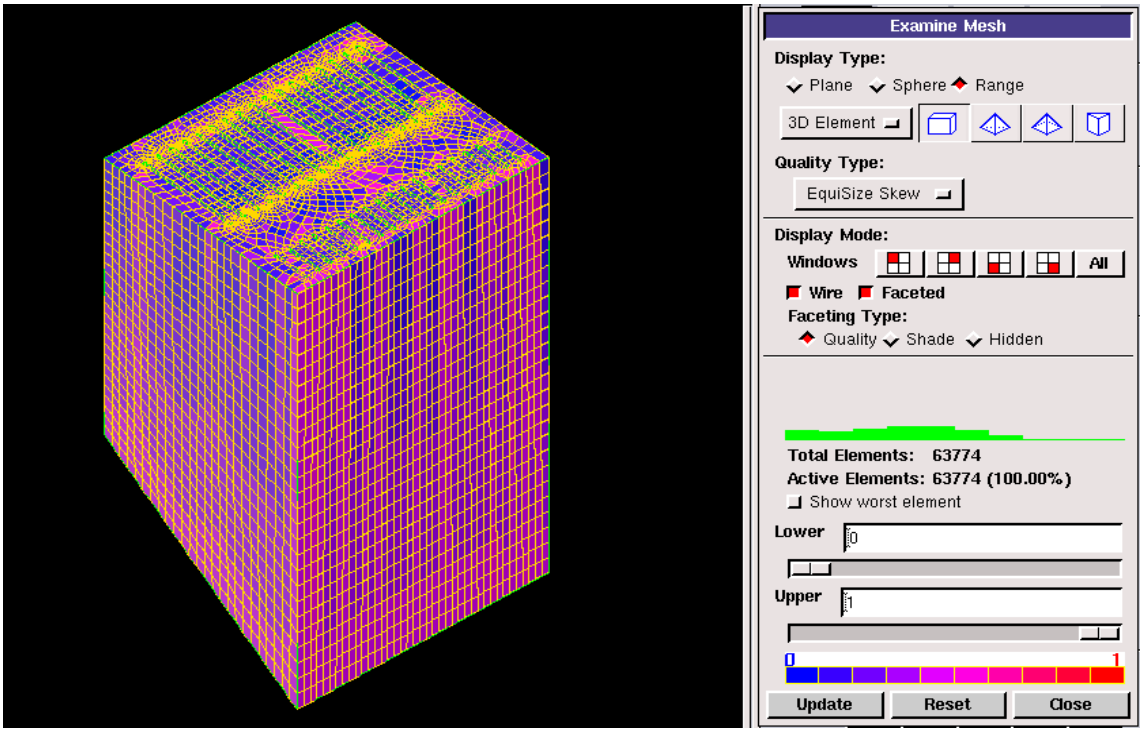

Fig A 3.5: Superheater region showing hexahedral elements

5. Next the volume consisting boiler bank was meshed (Fig. A 3.6). A curvature sizing function was assigned to the top edges of the boiler bank tubes with angle of 36^0 so that each circular edge was meshed with 10 elements. A maximum size of 150 was assigned to the source faces with a growth rate of 1.4 was specified. The volume was meshed using Cooper Meshing Scheme and all hexahedral element mesh was generated as shown in Fig. A 3.7.

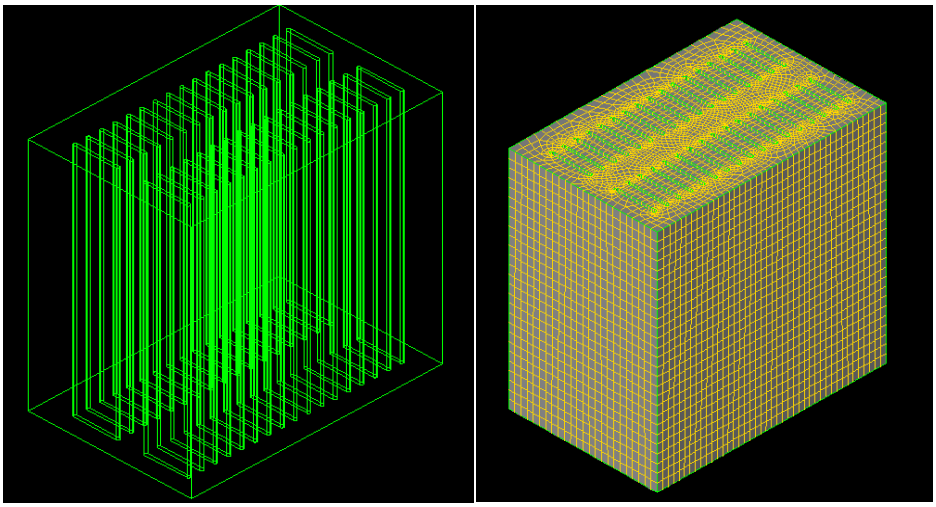

Fig. A 3.6: Boiler bank tubes

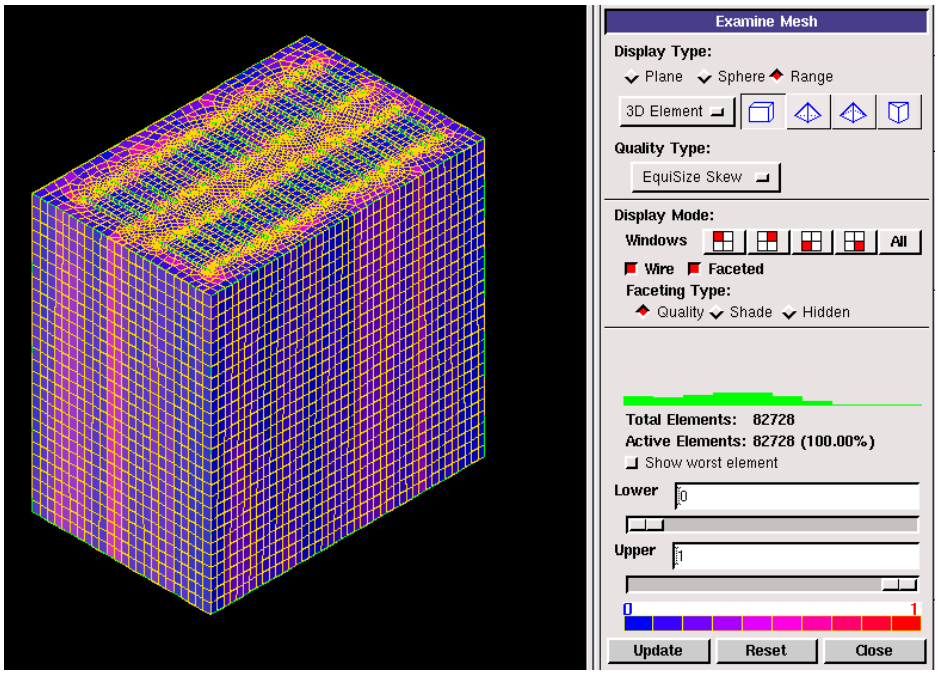

Fig. A 3.7: Boiler bank region showing hexahedral elements

6. Finally the lowest volumes representing inbed superheater, evaporating coils (Fig. A 3.8) and coal feed ports were meshed (Fig. A 3.9). Circular edges of inbed evaporating coils and inbed superheater were pre-meshed to generate six elements on the edge (Fig. A 3.10). Faces representing the coal inlet ports were meshed to

get 16 elements on the edge of the ports. Then the volume mesh was generated with 100mm element size using Tet/Hybrid scheme. Pyramid elements were created at the junction of tetraheadral & hexahedral elements as shown in Fig. A 3.11.

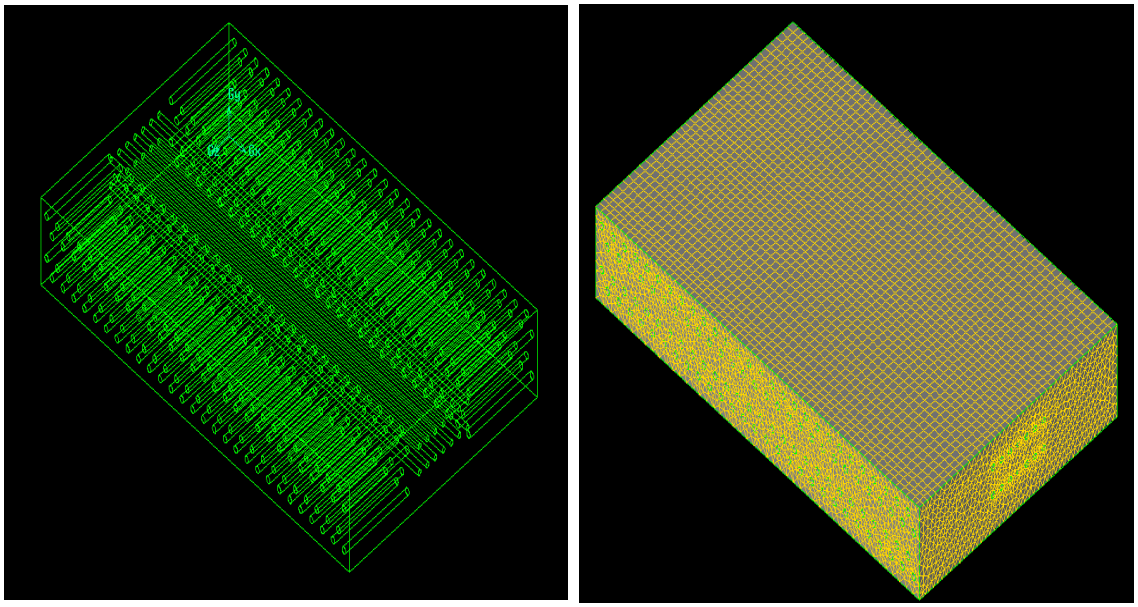

Fig. A 3.8: Volume consisting inbed superheater and evaporating coils

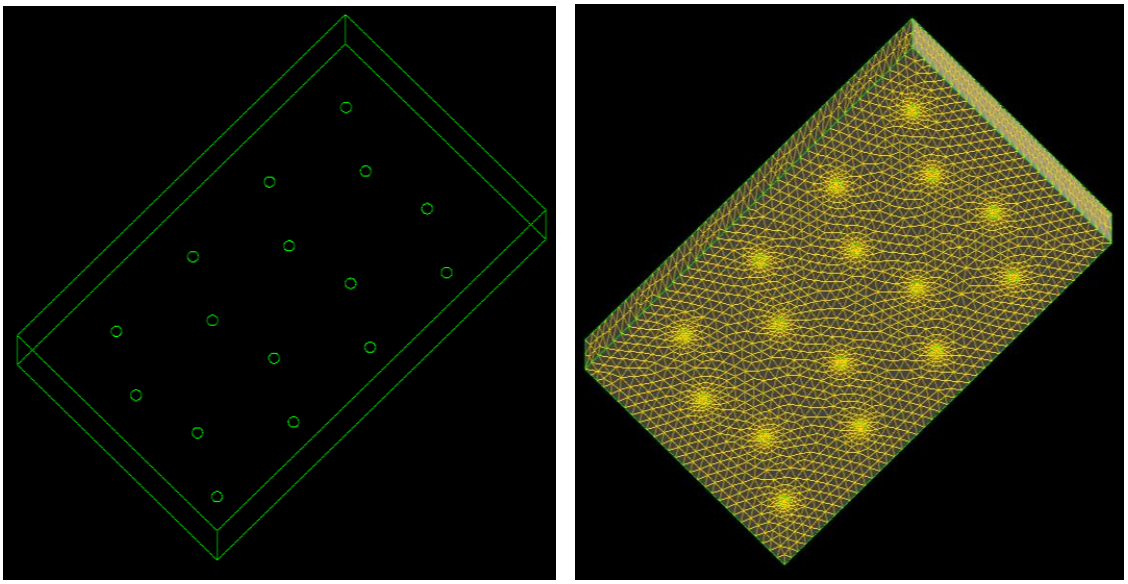

Fig. A 3.9: Geometry and mesh of coal feed ports

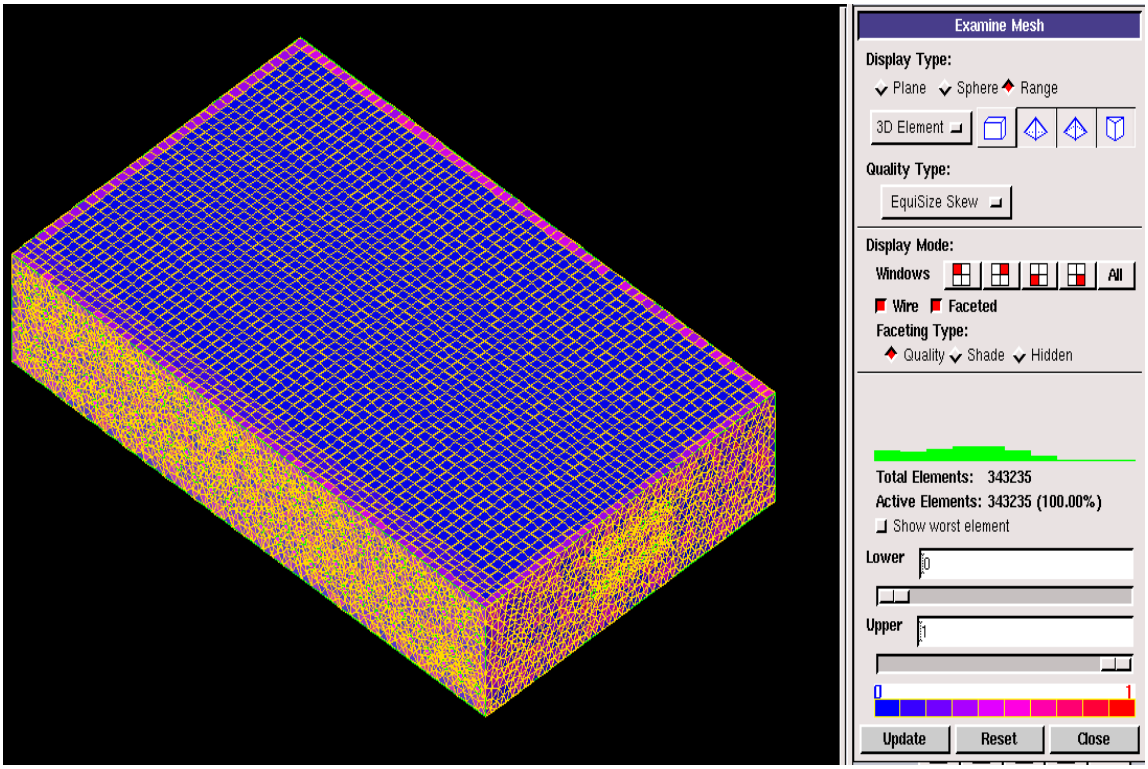

Fig. A 3.10: Total number of elements in inbed superheater and evaporating coils region

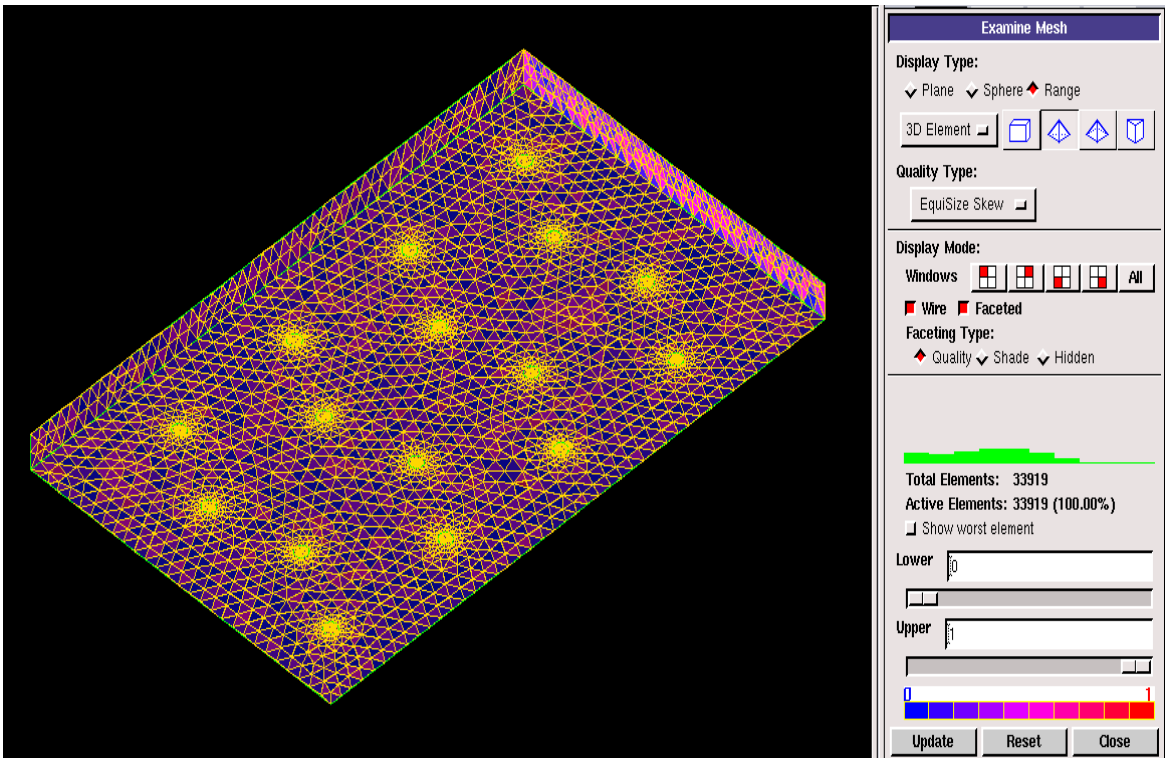

Fig. A 3.11: Volume consisting coal feed ports

7. Once the mesh was generated, then boundary types were specified to various faces. Recognizable names were specified to the boundary types so that the specified boundary conditions can be given. The mesh generate was then exported to Fluent (Fig. A 3.12)

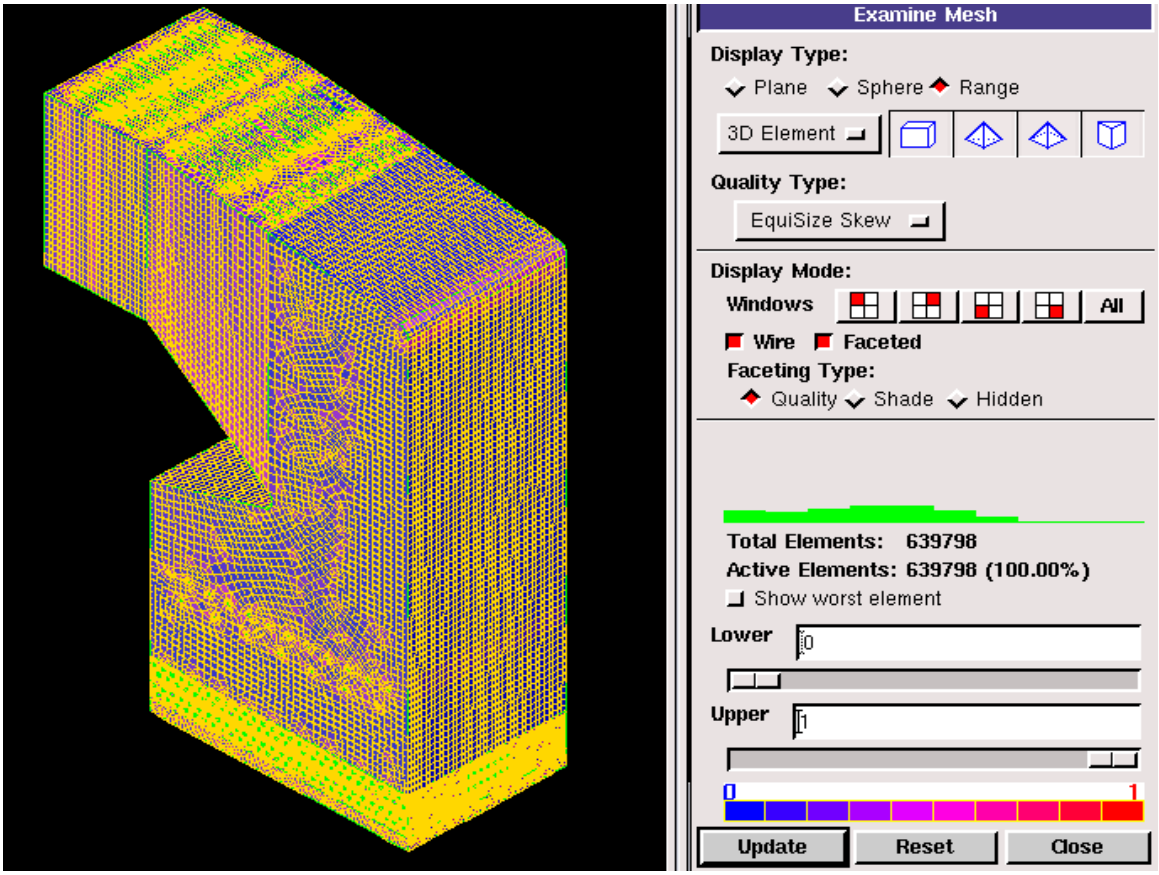

Fig. A 3.12: CPP boiler mesh

A 4 Analysis in Fluent

1. Importing the Mesh

The mesh file exported from GAMBIT is read into Fluent. As a general practice, the mesh is checked in Fluent for inverted volume and highly skewed elements *(this check can also be done in GAMBIT).*

2. Selecting the models

    a. Energy equation is turned on

b. K-epsilon (2-eqn) model with standard wall function is selected for turbulence modeling
c. Non-Premixed combustion is selected from species model. Using coal calculator, empirical fuel stream is defined by giving the proximate & ultimate analysis of the coal. Coal particle is automatically created and DPM model is switched on.
d. Second fuel stream is defined in boundary tab by providing proximate analysis of biomass.
e. The PDF (probability density function) table is calculated.

3. Defining the discrete phase model and injection
    a. Interaction with continuous phase is switched on.
    b. Injection is created with injection-type as surface from coal-inlet surface.
    c. Particle type combusting and coal-particle is selected. Velocity, diameter, temperature and mass flow rate of the particle is defined.
    d. Discrete random walk model with 2 particles ejecting from each cell face of the surface is defined.
    e. Another combusting particle for biomass is created by specifying the relevant particle properties.
    f. One more injection is created for the biomass particle releasing from biomass-inlet surface.
    g. Particle type combusting and biomass-particle is selected. Velocity, diameter, temperature and mass flow rate of the particle is defined.
4. Defining the materials
    a. When PDF table is calculated, a pdf-mixture of specific components is automatically defined. The related properties like density, molecular

weight, enthalpy and specific heat of the components is already built in Fluent software.

b. The properties of the coal-particle are also automatically created and defined using coal calculator values while defining Non-Premixed Model (NPM).

c. Biomass-particle is created and all the particle properties namely density, Specific heat, thermal conductivity, vaporization temperature, volatile component fraction, swelling coefficient, stoichiometric ratio, volatile fraction, combustible fraction, devolatilization model and combustion model is defined.

5. Defining the boundary conditions

   a. Boundary conditions such as velocity, mass flow inlet, temperature and turbulence are defined at all the relevant boundary faces of the domain. The details of the relevant conditions are summarized in Table no. 5.2.

   b. Heat Transfer coefficient is defined for the wall boundaries of the domain.

   c. Outlet condition is specified for the outlet boundary face of the domain.

6. Defining the solution methods

   a. SIMPLE scheme is selected for Pressure -Velocity coupling *(default)*

   b. Default first order upwind method is selected for spatial discretization of the parameters like density, momentum, turbulence kinetic energy and fuel mixture fraction.

7. Initializing and running the calculation

   a. Solution is initialized using hybrid initialization.

   b. A surface monitor is created for average temperature at the outlet boundary.

c. Case and data files are saved.

d. Calculation is run and temperature is monitored for convergence of the solution.

A 5 Experimental and Numerical Uncertainty

Experimental uncertainty is a quantification of the doubt about the measurement of result [200]. The experimental measurements involve uncertainty in spite of all care and precautions to eliminate all possible sources of errors from the measurements. This error may be due geometrical in-accuracy of the test apparatus and measuring instruments. In view of the fact that absolute accuracy can never be achieved in any experimentation, it is essential to estimate accuracy achieved in the measurements.

The uncertainty in the apparatus used in the plant for proximate analysis was:

Hot air oven: $\pm 0.8^0$C (with 95% level of confidence at coverage factor, k=2)

Muffle furnace: $\pm 3^0$C (with 95% level of confidence at coverage factor, k=2)

Numerical uncertainty is originated from input uncertainty and model uncertainty [201]. Input uncertainty is eliminated by using well defined input parameters. For example input materials, their flow rate and others relevant properties (refer Table no. 5.2). Model uncertainty may be eliminated by reducing the skewness of elements less than one (0.9 in this study), by applying relevant model and finally by the process of validation of the model results. The results of the present study have been validated with real process plant data.

PUBLICATIONS FROM RESEARCH WORK

Journal Publications

1) Hemant Kumar, S.K. Mohapatra, Ravi Inder Singh (2015), "Three-dimensional CFD modeling of a fluidized bed combustor fuelled by biomass and coal", *Materials Research Innovations (SCI)*, vol. 19, 8, pp. 118-124.

2) Hemant Kumar, S.K. Mohapatra, Ravi Inder Singh (2015), "Study of a 30 MW bubbling fluidized bed combustor based on co-firing biomass and coal", *Sadhana – Academy Proceedings in Engineering Sciences (SCI),*vol. 40, Part 4, pp. 1283–1299.
3) Hemant Kumar, S.K. Mohapatra, Ravi Inder Singh, "Review on CFD Modeling of Fluidized Bed Combustion Systems based on Biomass and Co – firing", *Journal of the Institutions of Engineers (India) – Series C* (DOI :10.1007/s40032-017-0361-2).

International Conference

1) Hemant Kumar, S.K. Mohapatra, Ravi Inder Singh, "CFD analysis of a fluidized bed combustor based on co-firing", Proceedings of the ASME International Mechanical Engineering Congress & Exposition (IMECE 2015), November 13-19, 2015, Hoston, USA.